Macromolecular Design: UV-Curable Thiol–Ene Networks Based on Renewable Resources

MAURO CLAUDINO

KTH Chemical Science
and Engineering

Doctoral Thesis in Polymer Technology
Stockholm, Sweden 2013

KTH Chemical Science
and Engineering

Macromolecular Design: UV-Curable Thiol–ene Networks Based on Renewable Resources

Mauro Claudino

Doctoral Thesis

Kungliga Tekniska högskolan, Stockholm 2013

AKADEMISK AVHANDLING

Akademisk avhandling som med tillstånd av Kungliga Tekniska högskolan i Stockholm, framlägges till offentlig granskning för avläggande av teknologie doktorsexamen torsdagen den 03 oktober 2013, kl. 14.30 i sal F3, Lindstedtsvägen 26, KTH, Stockholm. Avhandlingen försvaras på engelska. Fakultetsopponent: Professor Dr. Michael A. R. Meier från Karlsruhe Institute of Technology (KIT), Germany.

TRITA-CHE Report 2013:36
ISSN 1654-1081
ISBN 978-91-7501-845-4

To my parents

Eduardo e Mariana

Eles não sabem que o sonho
é uma constante da vida
tão concreta e definida
como outra coisa qualquer,

Eles não sabem, nem sonham,
que o sonho comanda a vida.
Que sempre que um homem sonha
o mundo pula e avança
como bola colorida
entre as mãos de uma criança.

– António Gedeão
(Rómulo de Carvalho, 1906-2006)

Excertos de
Poema "Pedra Filosofal",
In Movimento Perpétuo, 1956

Abstract

Plant oils and terpenes are ubiquitous natural renewable compounds. The double bonds contained in most of these monomers can be utilized *via* the photo-induced free-radical thiol–ene reaction to create novel bio-derived polymer thermosets representing a valuable '*green*' alternative to petrochemical olefins and resulting synthetic plastic materials. Nevertheless, there are several factors limiting their applicability, the first one being the relatively slow reaction rates towards thiol–ene coupling and many times the need to modify these natural olefins to make them more reactive. The latter process necessarily introduces additional pre-synthesis steps which has implications related both to cost and synthetic routes employed thereafter, those of which may or may not follow the principles of *Green Chemistry*. Therefore, this thesis intends to gain primary insight about the thiol–ene mechanism, kinetics and reactivity involving these multi-substituted olefins and then use the resulting knowledge to design semi-synthetic thermosets by incorporating these natural monomers into thiol–ene networks in the most environmentally friendly way possible. Mechanistic kinetic results show that internal 1,2-disubstituted enes found in mono-unsaturated vegetable oils and some macrolactones undergo a fast reversible *cis*/*trans*-isomerization process in favour of *trans*-isomer formation coupled with the thiol–ene mechanism. The slow reactivity of these enes has been accredited not just to the isomerization itself, but predominantly to the chain-transfer hydrogen-abstraction step. This rate-limiting step, however, does not seem to compromise their use in the creation of thiol–ene networks as demonstrated by photopolymerization in the melt of a series of linear globalide/ε-caprolactone-based copolyesters differing in amount of unsaturations along the backbone crosslinked with a tri-functional thiol propionate ester monomer. The resulting thermoset films were amorphous elastomers exhibiting different thermal and mechanical properties depending on the comonomer feed ratio. *D*-limonene, a renewable diolefinic substrate, proved to be an important terpene in free-radical thiol–ene additions. Empirical results show that the 1,1-disubstituted *exo*-vinylidene bond is about 6.5 times more reactive than the endocyclic 1,1,2-trisubstituted 1-metyl-cyclohexene moiety when reacting with mercapto propionate esters in organic solution conditions. Kinetic modeling results suggest that the differences in double bond reactivity are partially ascribed to steric impediments coupled with differences in electron-density controlling thiyl-radical insertion onto the two unsaturations but predominantly to differences in relative energy between the two tertiary insertion carbon-centered radical intermediates. Off-stoichiometric manipulations in the thiol–limonene mole ratio, assisted by numerical model simulations, offer a convenient method to visualize and assess the overall reaction system kinetics irrespective of time, thus being regarded as an important guiding tool for organic and polymer chemists aiming at designing thiol–ene reaction systems based on limonene. Multifunctional limonene-terminated thiol–ene macromonomer resins were synthesized in ethyl acetate solution and then reacted in different combinations with polyfunctional mercapto propionate esters to afford semi-synthetic thiol–ene networks with different thermo-viscoelastic properties depending on functionality, crosslink density, homogeneity and excess of thiol occluded into the networks. The bulky cycloaliphatic ring structure of limonene locked between thioether linkages introduce a certain degree of rigidity to the final networks and increase the glass-transition temperature when compared to more standard thiol–allyl systems. In all cases evaluated, high thiol–ene conversions were achieved with minimum or no side-reactions such as chain-growth homo-polymerization and at reasonable reaction rates.

Sammanfattning

Växtoljor och terpener är vanligt förekommande förnybara substanser. Dubbelbindningen i de flesta av dessa monomerer kan användas med hjälp av fotoinducerade friradikal tiol-en-reaktioner för att skapa nya biobaserade härdplaster som ett '*grönt*' alternativ till fossilbaserade syntetiska plaster. Det är dock flera faktorer som begränsar deras användning där den främsta är den relativt låga reaktionshastigheten som dessa monomerer uppvisar i tiol-en reaktionen. I många fall måste man modifiera råvaran i ett första steg för att öka reaktiviteten. En modifiering medför extra syntessteg vilket påverkar både kostnaden och följande reaktionssteg med möjliga implikationer på principerna för *Grön Kemi*. Målet med denna avhandling är att öka förståelsen för reaktionsmekanismen för tiol-en kemi, kinetiken och reaktiviteten hos multisubstituerade alkener och tillämpa denna förståelse i design av semi-syntetiska härdplaster genom att introducera dessa naturliga monomerer i ett tiol-en nätverk på det miljömässigt bästa sättet. Mekanism och kinetikstudier visar att 1,2-disubstituerade alkener som finns i omättade vegetabiliska oljor och vissa makrolaktoner genomgår en snabb och reversibel *cis/trans*-isomerisation till fördel för *trans*-isomeren kopplat till tiol-en-mekanismen. Den låga reaktiviteten hos dessa alkener är inte enbart kopplad till isomerisationen utan i huvudsak till kedjeöverföringsteget med väteabstraktion. Detta hastighetsbestämmande steg hindrar dock inte bildandet av ett tiol-en-nätverk vilket kan bekräftats med fotopolymerisation i smälta av en serie linjära polyglobalide/ε-kaprolaktonbaserade sampolyestrar med olika mängd omättnad tvärbundna med en trifunktionel tiolmonomer. Det bildade härdplastmaterialet blev amorfa elastomerer med olika termiska och mekaniska egenskaper beroende på ingående monomerförhållanden. *D*-Limonen, som en difunktionell förnyelsebar monomer, har visats vara en viktig terpen i tiol-en sammanhang. Empiriska resultat visar att den 1,1-disubstituerade alkengruppen reagerar 6.5 gånger snabbare en den 1,1,2-trisubstituerade alkengruppen i ringen när den reagerar med en merkaptopropionatester i lösning. Kinetiska modelleringsresultat visar att skillnaden i reaktivitet mellan dubbelbindningarna delvis kan tillskrivas steriska effekter i kombination med skillnader i elektrontäthet vilket styr tiylradikalens addition till dubbelbindningarna men att det i huvudsak är det skillnaden i relativ energi mellan de två tertiära kolcentrerade radikalintermediärer som har betydelse. Variationer i stökiometrin mellan limonen och tiolen tillsammans med numeriska modellsimuleringar har visats vara en bra metod för att visualisera och utvärdera den totala reaktionskinetiken oberoende av tid. Detta blir alltså ett viktigt verktyg för organ- och polymerkemister med avseende på design av tiol-en-system baserade på limonen. Multifunktionella makromonomerer med terminala limonengrupper syntetiserades i etylacetat och reagerades i kombination med olika polyfunktionella merkaptopropionatestrar för att bilda semi-syntetiska härdplaster. Härdplasterna uppvisade olika termiska och mekaniska egenskaper beroende på funktionalitet, tvärbindningstäthet, homogenitet och eventuellt överskott av tiol i systemet. Den cykloalifatiska ringstrukturen mellan tio-eter-bindningarna introducerar ett visst mått av styvhet i den slutliga nätverksstrukturen och därmed ett högre T_g jämfört med traditionella tiol-allyl-system. I samtliga utvärderade fall kunde en relativt hög reaktionshastighet och hög omsättning av tiol-en-reaktionen uppnås med ett minimum av sidoreaktioner som exempelvis homopolymerisation av alken-monomeren.

Preface

The search of valuable compounds from renewable resources in replacement of petroleum-derived ones is seen nowadays as one of the greatest challenges in polymer science on grounds of increased environmental awareness and issues of sustainable development. Also, the fact that crude-oil reserves are globally diminishing at increasing rate, coupled with the incessant market fluctuations in oil-prices showing a clear tendency to rise as result of escalated geopolitical instability, is pushing the quest of these natural (or bio-based) fossil-substituents as new important building-blocks. To meet the demands of the new approaching '*Era*' – *which will inevitably strike us!* – novel and highly efficient synthesis processes following the principles of *green chemistry* must be devised and integrated (if possible) within already existing industrial infrastructures, saving energy and reducing the emission of potentially toxic pollutants.

Driven by these important considerations, the scope of this thesis was to find and examine different classes of renewable alkene monomers with potential applicability in the creation of semi-synthetic thermosetting polymers, as film-forming materials, by means of the free-radical thiol–ene reaction as leading chemistry route.

The marriage between renewable feedstocks and *green* synthetic chemistries brings enormous benefits in terms of sustainability. In first place, all the biosynthetic power of *Nature* is fully exploited in a straightforward manner directly from its extensive sources (trees, plants, fruits, seeds, etc.) making the resulting renewable compounds abundant and, therefore, cheap. Second, these monomers are shown, in most cases, to bear biodegradable chemical moieties, a feature seldom encountered in polymers derived from their fossil-counterparts. Third, the thiol–ene reaction, with use of photopolymerization, is probably one of the few efficient chemistries with simple industrial implementation which directly incorporates renewable alkene monomers into polymer networks, representing this way a real innovative solution to the synthesis of specialty materials not easily accessible *via* petrochemistry (say, for instance, chirality). Therefore, within the realm of polymers from renewable resources and using an integrated approach as sustainable as possible, this thesis intends to investigate two major groups of unsaturated compounds: *1,2-disubstituted enes* (**Papers I** and **II**) and *terpenes* (**Paper III and IV**) in combination with the thiol–ene reaction, and assess their overall feasibility in the design of crosslinked thiol–ene networks as bio-based macromolecular materials aimed at end-use applications such as organic coatings.

Stockholm, 29th of August, 2013
Mauro Claudino

List of Publications

This thesis is an extensive summary of the following articles, which are referred to in the text by Roman numerals and appended at the end of the thesis:

Paper I (published)

Thiol–Ene Coupling of 1,2-Disubstituted Alkenes: the kinetic effect of *cis*/*trans*-isomer structures. Claudino, M.; Johansson, M.; and Jonsson, M. *European Polymer Journal*, 2010 46(12), p. 2321–2332.

Paper II (published)

Photoinduced Thiol–Ene Crosslinking of Globalide/ε-caprolactone Copolymers: curing performance and resulting thermoset properties. Claudino, M.; van der Meulen, I.; Trey, S.; Jonsson, M.; Heise, A.; and Johansson, M. *Journal of Polymer Science Part A: Polymer Chemistry*, 2011 50(1), p. 16–24.

Paper III (published)

Thiol–Ene Coupling Kinetics of *D*-Limonene: a versatile '*non-click*' free-radical reaction involving a natural terpene. Claudino, M.; Jonsson, M.; and Johansson, M. *RSC Advances*, 2013 3, p. 11021–11034.

Paper IV (manuscript)

Utilizing Thiol–Ene Coupling Kinetics in the Design of Renewable Thermoset Resins based on *D*-Limonene and Polyfunctional Thiols. Claudino, M.; Jonsson, M.; and Johansson, M. (2013).

Other scientific publications not included in this thesis:

UV-Curable Acrylate Based Nanocomposites: effect of polyaniline additives on the curing kinetics. Jafarzadeh, S.; Johansson, M.; Sundell, P.-E.; Claudino, M.; Pan, J.; and, Claesson, P. E. *Polymers for Advanced Technology*, 2013 24(7) p. 668–678. (published)

Contribution to the Papers

The contribution of the author to the appended papers goes as follows:

Paper I. All of the experimental work and measurements, all numerical kinetic simulations (modeling) and data analysis, and most of the preparation of the manuscript.

Paper II. Half of the experimental work and measurements, a large part of the data analysis and writing of the manuscript.

Paper III. Most of the experimental work and measurements, a large part of the data analysis and modeling and all of the preparation of the manuscript.

Paper IV. Most of the experimental work, all of the measurements and numerical kinetic simulations and all the writing of the manuscript.

List of Abbreviations and Terms

4MeCL	4-methyl caprolactone
$A^{\bullet}$	Intermediary Carbon-Centered Radical Adduct
$A^{\bullet}_{E}$	Intermediary *trans*-isomer Carbon Radical Adduct (conformer *E-trans*)
$A^{\bullet}_{Z}$	Intermediary *cis*-isomer Carbon Radical Adduct (conformer *Z-cis*)
AIBN	Azobisisobutyronitrile (thermal radical initiator)
Am	Ambrettolide
ATR	Attenuated Total Reflectance
BDE	Bond Dissociation Energy (kJ mol^{-1})
BP	Benzophenone
C(t)	Molarity (mol L^{-1})
C_0	Initial Molarity (mol L^{-1})
$C^{\bullet}_{1,2}$	Intermediary Carbon-Centered Radical(s)
CALB	*Candida antarctica* Lipase B
$CDCl_3$/*d*-chloroform	Deuterated Chloroform
CL (or ε-CL)	ε-caprolactone
C–S	Thioether Covalent Bond
D	Di-addition Product
Da	Dalton (g mol^{-1})
DCP	Dicumyl Peroxide
DI (or Đ)	*Dispersity Index* (according to IUPAC)
DMF	Dimethylformamide
DMPA	2,2-dimethoxy-2-phenylacetophenone (Irgacure 651©, photoinitiator)
DMTA	Dynamic Mechanical Thermal Analysis
DP	Degree of Polymerization
DSC	Dynamic Scanning Calorimetry
DXO	1,5-dioxepan-2-one
E	*trans*-isomer
E'	Storage (Elastic) Modulus (Pa)
E''	Loss (Viscous) Modulus (Pa)
E_a	Activation Energy (J mol^{-1})
EDA	Electron-Donor/-Acceptor Complex
ene	*exo*, *endo* or C=C double bonds
ENE_T	Total Ene (*exo* + *endo*)
E'_{rubb}	Storage Modulus at the Rubbery Plateau Region (Pa)
EtOAc	Ethyl Acetate
FA	Fatty Acid
FAME	Fatty Acid Methyl Ester
f	Chemical Group Functionality Number
f_c	Fractional Conversion
f_{ene}	Ene Functionality Number
f_{thiol}	Thiol Functionality Number
f_{mol}	Mole Fraction
FT	Fourier Transform
FTIR	Fourier Transform Infrared Spectroscopy
fwhm	Full-Width-at-Half-Maximum Peak Height

GI	Globalide
GPC	Gel Permeation Chromatography (analogous to SEC)
$I^{\bullet}$	Primary Initiating Free-Radical / or Iodide Radical
IH	Protonated Initiator Fragment
In	Initiator
$k_{1,2}$	Second-Order Overall Coupling Rate Coefficients (cycles **I** and **II**) ($M^{-1}\,s^{-1}$)
k_{add}	Thiyl-Ene Elementary Addition Rate Coefficient ($M^{-1}\,s^{-1}$)
${k_a}^E$	Thiyl-*trans*-Ene Elementary Addition Rate Coefficient ($M^{-1}\,s^{-1}$)
${k_a}^Z$	Thiyl-*cis*-Ene Elementary Addition Rate Coefficient ($M^{-1}\,s^{-1}$)
k_c	Second-Order Coupling Parameter ($M^{-1}\,s^{-1}$)
k_{CT}	Elementary Chain-Transfer Hydrogen-Abstraction Rate Coefficient ($M^{-1}\,s^{-1}$)
k_d	First-Order Photodecomposition Rate Coefficient (s^{-1})
$k_{Z\to E}$	Overall *cis*-to-*trans* Conversion Rate Parameter (s^{-1})
$k_{E\to Z}$	Overall *trans*-to-*cis* Conversion Rate Parameter (s^{-1})
k_{elim}	Elimination Rate Coefficient (s^{-1})
K_{eq}	Chemical Equilibrium Constant of the Propagation Step with Limonene (M^{-1})
${k_f}^E$	Fragmentation Rate Coefficient with respect to *trans*-isomer (s^{-1})
${k_f}^Z$	Fragmentation Rate Coefficient with respect to *cis*-isomer (s^{-1})
k_{hp}	Second-Order Homopropagation Rate Coefficient ($M^{-1}\,s^{-1}$)
k_{obs}	Overall (Observed) Second-Order Rate Parameter ($M^{-1}\,s^{-1}$)
k_{RSH}	Second-Order Elementary Hydrogen-Abstraction Rate Coefficient ($M^{-1}\,s^{-1}$)
k_t	Thiyl-Radical Self-Termination Rate Coefficient ($M^{-1}\,s^{-1}$)
Lim	Limonene
LSODA	*"Livermore Solver for Ordinary Differential Equations"*
M1	Macromonomer 1
M2	Macromonomer 2
$m_{1,2}$	Fractional Reactivity Coefficients
m_{polym}	Mass of Polymer (g)
$m_{trithiol}$	Mass of Trithiol (g)
MAH	Molecular Assisted Homolysis
MCT	Mercury Cadmium Telluride (photoconductive detector)
ME	Methyl Elaidate (*trans*-isomer of Methyl Oleate)
M_n	Average Molecular Number ($g\,mol^{-1}$)
MO	Methyl Oleate (*cis*-isomer of Methyl Elaidate)
mRSH (or C13MP)	Monothiol (*iso*-tridecyl 3-mercapto propionate)
M_t	Molecular Weight of Trithiol (TMPMP) ($g\,mol^{-1}$)
MW	Molecular Weight ($g\,mol^{-1}$)
NIR	Near Infrared
NMR	Nuclear Magnetic Resonance
ODE	Ordinary Differential Equation
OSTE	Off-Stoichiometry Thiol–Ene
P	Thiol–Ene Coupled C–S Product
P(GI-*co*-CL)	Poly(globalide-caprolactone) Copolymer
$P_{1,2}$	Mono-Addition Coupled Products
PAm	Polyambrettolide
PCL	Poly(ε-caprolactone)
PETMP	Pentaerythritol tetra(3-mercapto propionate)
PGI	Polyglobalide

PI	Photoinitiator
PS	Polystyrene
r	Thiol–Ene Molar Ratio (based on functional groups)
r_{C}	Global Coupling Rate (mol L^{-1} s^{-1})
$r_{C\text{-}S}^{app}$	Apparent Rate of Coupled Product Formation (mol L^{-1} s^{-1})
$r_{1,2}$	Overall Coupling Rate(s) of Cycles **I** and **II** (mol L^{-1} s^{-1})
$r_{CT1,2}$	Individual Chain-Transfer Rate(s) (mol L^{-1} s^{-1})
$r_{p1,2}$	Individual Propagation Rate(s) (mol L^{-1} s^{-1})
$r_{P1,2}$	Coupled Product(s) Formation Rate(s) (mol L^{-1} s^{-1})
r_{P}	Total Rate of Formation of Mono-Addition Product(s) (mol L^{-1} s^{-1})
r_{Lim}	Consumption Rate of Limonene (mol L^{-1} s^{-1})
r_{RSH}	Consumption Rate of Thiol Functional Groups (mol L^{-1} s^{-1})
R	Ideal Gas Constant (8.314510_{70} J mol^{-1} K^{-1})
REDOX	Oxidation-Reduction
ROP	Ring-Opening (Co)Polymerization
$RS^{\bullet}$	Thiyl Radical
RSH	Thiol Functional Group
RSSR	Dissulfide Product
RT-FTIR	Real-Time Fourier Transform Infrared Spectroscopy
RTIR	Real-Time Infrared Spectroscopy
SD	Standard Deviation
SEC	Size-Exclusion Chromatography (analogous to GPC)
S_{m}	Double Bond Selectivity (Relative Reactivity) based on the Mechanism
S_{exp}	Empirical Double Bond Selectivity (Relative Reactivity)
STM	Starting Thiol–Ene Mixture
T	Temperature (°C or K)
T3	Trithiol (TMPMP)
T4	Tetrathiol (PETMP)
Tan δ	Damping Parameter
TBD	Triazabicyclodecene (1,5,7-triazabicyclo[4.4.0]dec-5-ene) (organocatalyst)
TE	Thiol–Ene
T_{g}	Glass Transition Temperature (°C)
T_{m}	Melting Point Temperature (°C)
TGS	Triglycine Sulfate (piroelectric detector)
THF	Tetrahydrofurane
TMP	2-ethyl-(hydroxymethyl)-1,3-propanediol
TMPMP	Trimethylolpropane Trimercaptopropionate
TMS	Tetramethylsilane
UV	Ultraviolet
UVA	Ultraviolet-A
UV-Vis	Ultraviolet-Visible Range of Electromagnetic Spectrum
W_{f}	Mass *After* Swelling (g)
W_{s}	Mass *Before* Swelling (g)
x_{0}	Normalized C═C ^{1}H Integrations or FT-Raman Band Heights *Before* Reaction
x_{f}	Normalized C═C ^{1}H Integrations or FT-Raman Band Heights *After* Reaction
x_{c}	Critical Fractional Conversion
Z	*cis*-isomer
α	Scaling Exponent of Ene (Partial Reaction Order)
β	Scaling Exponent of Thiol (Partial Reaction Order)

δ	Delta ($=E''/E'$) or ^{1}H NMR Chemical Shift (ppm)
ΔE_a	Difference in Activation Energy (J mol^{-1})

Nomenclature of the polymers and films

Composition	Polymer P(GI-*co*-CL)	Homopolymerized film	Thiol–ene film
G:C 100:0	P(G:C) 100:0	f-H(G:C) 100:0	f-TE(G:C) 100:0
G:C 50:50	P(G:C) 50:50	f-H(G:C) 50:50	f-TE(G:C) 50:50
G:C 40:60	P(G:C) 40:60	f-H(G:C) 40:60	f-TE(G:C) 40:60
G:C 30:70	P(G:C) 30:70	f-H(G:C) 30:70	f-TE(G:C) 30:70
G:C 20:80	P(G:C) 20:80	f-H(G:C) 20:80	f-TE(G:C) 20:80
G:C 10:90	P(G:C) 10:90	f-H(G:C) 10:90	f-TE(G:C) 10:90

G: globalide (GI); C: ε-caprolactone (CL); f-H: homopolymerized film; f-TE: thiol–ene film.

Table of Contents

1 Introduction 1

1.1 Objective and Outline of the Thesis 2

2 Background 4

2.1 Free-Radical Induced Thiol–Ene Reaction 4

2.1.1 Brief historical perspective 4

2.1.2 Basic chemistry, reaction mechanisms and kinetics 5

2.1.3 Thermosets in relation to thiol–ene chemistry 12

2.1.4 Interface with *Green Chemistry* 14

2.1.5 Renewable monomers for thiol–ene additions 15

3 Experimental 18

3.1 Chemicals 18

3.2 Instrumentation 19

3.3 Preparative, Synthetic and Analytical Procedures 20

3.3.1 Sample preparation 20

3.3.2 Initiator photolysis 21

3.3.3 Photo-RTIR measurements 21

3.3.4 Evaluation of reactivity 22

3.3.5 Thiol–ene conversions 22

3.3.6 Product identification 23

3.3.7 Simulation software and kinetic modeling 23

3.3.8 Film-formation and UV-curing 24

3.3.9 Dynamic Scanning Calorimetry (DSC) 25

3.3.10 Dynamic Mechanical Thermal Analysis (DMTA) 25

3.3.11 Sol-content determination 25

4 Results and Discussion 27

4.1 Thiol–ene Addition of 1,2-disubstituted Alkenes 27

4.1.1 *Z*/*E*-isomerization mechanism and kinetics 27

4.1.1.1 Thiol–ene reaction dynamics 27

4.1.1.2 Product formation 30

4.1.1.3 Kinetic modeling 30

4.1.2 Globalide/ε-caprolactone-based thermosets 33

4.1.2.1 Thiol–ene curing kinetics and conversion 35

4.1.2.2 Characterization of thermosets 38

4.2 Terpene-based Renewable Thermosets 43

4.2.1 Thiol–ene coupling kinetics of *D*-limonene: model studies, mechanism and selectivity 43

4.2.1.1 Relative reactivity: kinetic analysis and modeling 43

4.2.1.2 Effect of stoichiometry 49

4.2.2 Synthesis and characterization of multifunctional resins 57

4.2.3 Photo-crosslinking and network characterization 61

4.2.3.1 Thiol–ene photopolymerization 62

4.2.3.2 Thermo-mechanical properties 65

5 Conclusions 69

6 Future Work 71

7 Acknowledgements 73

8 References 75

Appendix

It doesn't matter how beautiful your theory is, it doesn't matter how smart you are. If it doesn't agree with experiment, it's wrong.

– Richard P. Feynman

1 Introduction

Nowadays, virtually all commodity plastic materials are made from petroleum-derived chemicals. To give an ominous perspective of the overall volumes produced, between 2009 and 2011 the manufacture of plastics worldwide upraised by 25 million tonnes (9.5%) to about 280 million tonnes, confirming the long-lasting growth trend of almost 5% annually over the past 20 years.[1] Yet, the fast dwindling of crude-oil fossil reserves coupled to a growing emergent awareness for the negative environmental impacts of petroleum processing and concomitant emission of greenhouse gases – *let's not forget an ever growing oil-supply instability!* – is thrusting more than never the polymer community toward the rational design of '*green*' polymeric materials based on renewable feedstocks, hopefully leading to a gradual reduction of our dependence from oil and help contribute to a better and sustainable future. The benefits of this transition are obvious, nevertheless challenging, and can be easily traced from the origin to the final materials *via* a life-cycle assessment analysis.[2]

To start with, most renewable resources are ubiquitous, *i.e.*, they exist abundantly throughout *Nature* or, to some extent, can be obtained as by-products from current industrial activities. This means that direct extraction from the source, taking full advantage of the biosynthetic capabilities of the *Natural World*, eliminates the necessary petrochemical steps required to create the synthetic monomers as starting materials for the manufacture of polymers. Alongside, such shift will help reduce drastically the carbon footprint so adversely associated with their industrial production. Another important attribute is that most renewable monomers hold chemical moieties susceptible to cell or enzymatic attack which makes them perfect candidates to produce recyclable and/or biodegradable materials desirable for certain applications. This avoids the serious issue of solid-waste disposal, a problem that plagues our societies from increased build-

up of inert plastics. At last, by integrating effective and eco-friendly synthesis routes that mediates the source and end-material completes the cycle towards the development of highly sustainable renewable polymers.

Within this context, the route of synthesis represents one of the key elements in the global linking chain and must, therefore, meet some important demands. Preferably it should go well along the lines with the postulates of *Green Chemistry* [3] not only involving clean technologies and improved reaction efficiency but also show integrative potential into already existing industrial facilities. One kind of chemistry which excels to meet most of these requirements is the so-called '*free-radical thiol–ene reaction*' and throughout this thesis will be used as the main synthesis procedure used in the formation of semi-synthetic thermoset materials derived from a selected set of renewable alkene feedstocks. The utilization of enzyme biocatalysis will be also stressed as important preliminary step to synthesize bio-based aliphatic alkene polyesters leading to novel thiol–ene networks.

1.1 Objective and Outline of the Thesis

The major focus of this work highlights the use of a chemically simplistic approach aimed at the synthesis of bio-based thiol–ene networks derived from two major groups of renewable alkene monomers: (1.) *mono-unsaturated vegetable oils* (*e.g.*, fatty-acids and/or triglycerides) and *macrolactones* (*e.g.*, globalide), both of which contain internal main-chain 1,2-disubstituted double-bonds; and, (2.) *monoterpenic dienes* such as *D*-limonene. It was not the prime goal here to develop '*per se*' novel highly advanced (tailor-made) organic materials from such natural monomers but rather to demonstrate from a '*proof-of-concept*' perspective that is possible to use and integrate them into polymer networks using chemically green and highly efficient synthesis routes. The knowledge gained can later on be transferred to design new photocurable thiol–ene systems aiming at real materials and coating applications which are usually much more demanding in terms of final specifications.[4]

Two principal lines of study were thus pursued. The first consists in performing reactivity studies using selected thiol and alkene model compounds to assess the feasibility of thiol–ene radical additions that could result in the formation of thermosetting polymers. The second utilizes this knowledge to synthesize polymeric film coatings – mainly in the form of elastomers – with use of UV-light, which are then characterized with respect to the physicomechanical properties (thermal and viscoelastic), including crosslink density and homogeneity of the final networks.

Therefore, with the aim of widespreading the use of renewable resources in the synthesis of thermosetting polymers, this work was initially focused on model reaction studies involving *mono-unsaturated oil derivatives*, as typical representatives of 1,2-dialkyl substituted olefins and a trithiol propionate ester crosslinker,

in order to expand the current knowledge on the reactivity, reaction mechanism and kinetics of these internal C=C bonds toward free-radical thiol–ene additions (**Paper I**). The validity of this concept was subsequently demonstrated in **Paper II** using *globalide* as characteristic unsaturated macrolactone copolymerized with *ε-caprolactone* to form thermosetting aliphatic polyesters owning different crosslink densities. Some monoterpenic dienes, such as *limonene*, also bear intrinsic double-bond functionality useful to be explored directly in thermoset synthesis *via* the thiol–ene reaction. In this case, unmodified *D*-limonene was employed as intermediary crosslinking unit between polyfunctional ester mercaptans to prepare UV-curable chiral networks (results to be published). A systematic kinetic study on the evaluation of the relative reactivity (selectivity) with respect to the two unsaturated structures in *D*-limonene and the effect of co-reactant stoichiometry on the overall reaction kinetics were conducted in **Papers III** and **IV**, respectively.

2 Background

The primary goal of this chapter is to introduce the reader to the topic of free-radical thiol–ene chemistry at the fundamental and applied levels and its advantages in the synthesis of thermosets. Its interface with *green chemistry* will also be emphasized as well as the most promising classes of renewable alkene monomers for free-radical thiol–ene additions.

2.1 Free-Radical Induced Thiol–Ene Reaction

2.1.1 Brief historical perspective

Historically, the thiol–ene reaction dates back to 1839 when Charles Goodyear discovered the thermal crosslinking of natural rubber, 1,4-poly(*cis*-isoprene), with elemental sulphur, a process which later became known as vulcanization and that up to this date is extensively used by the tyre industry.[5] Yet, this process – *in its simplest form* – is anthropologically known to exist far way back to the ancient Mesoamerican Aztec and Maya civilizations (1600 B.C.) who used natural latex extracted from the *Castilla elastica* tree combined with the sulphur rich sap of certain native plants to produce artifacts and bouncing rubber balls used in the religious and ritual ballgame '*Ullamaliztli*'.[6, 7]

The thiol–ene reaction was already observed in 1905 by the German chemist Posner showing that enes and thiols could react spontaneously with each other or in the presence of an acid.[8] In 1926 was presented for the first time as a polymer forming reaction where it was discovered that allyl mercaptan 'spontaneously gelled' upon heating.[9] However, its basic mechanistic formulation as a free-radical 'mediated' polymerization, including the elementary reaction steps, was only accomplished in 1938 by Kharasch, essentially laying the foundation for this type of chemistry.[10] The early work involving the coupling of thiols to olefins was concisely described in 1970 by Griesbaum[11] and in 1993 Jacobine reviewed extensively all the aspects of thiol–ene photopolymerizations[12]. Since then, this unique reaction has attracted significant attention especially in the fields of organic[13] and polymer syntheses[14, 15].

In the past, the main large-scale applications of free-radical thiol–ene chemistry included the manufacture of relief printing plates (also known as the Latterflex process), wear layers for floor tiles (based on UV-curable resins) and coatings for electronics.[16] However, the use of thiol–ene systems had been restricted to some extent due to issues of bad odour and difficulties in stabilizing the systems

leading to short pot-life of formulated monomer mixtures. It was not until very recently (2012) that the mechanistic cause of this instability was clarified by Metzger *et al.* based on the early works by Pryor *et al.*, Nuyken *et al.*, and Klemm and Sensfuß.[17] Moreover, the erroneous impression that all thiol–ene coatings were subject to rapid yellowing (caused by residues of photoinitiator) and discoloration upon weathering, in part ascribed to the large usage of benzophenone (BP) as photoinitiator, as well as introduction of cheap, readily-available, acrylate monomers made the popularity of thiol–ene photopolymerization decrease severely and in alternative gave way to acrylate-based photocurable systems. The revival of this chemistry was attributed mainly to the development of efficient cleavage-type photoinitiators to initiate the thiol–ene photopolymerization (eliminating the problem of yellowing) and the incorporation of thiols into acrylate formulations to decrease oxygen inhibition and improve the final network properties. Over the last 10–15 years most of the research in thiol–ene chemistry has been focused on the development of new materials and applications, namely: substrate surface modifications, formation of networks with unique properties, polymer functionalization and photocuring, high-impact energy absorbing materials, among very many others.[16, 18] Given its high efficiency, the term ('click') was recently coined to this reaction (2008)[19-21] and there are already a vast number of excellent reviews on the subject covering a broad range of scientific fields and applications.[12, 14, 16, 18, 22, 23]

2.1.2 Basic chemistry, reaction mechanisms and kinetics

The lability of thiol hydrogens differentiates thiol–ene polymerizations from conventional free-radical polymerizations. The thiol–ene reaction takes advantage of the easily abstractable hydrogen atom of the thiol group due to the relatively weak sulphur-hydrogen (S–H) covalent bond. This abstraction ability is independent of the alkyl moiety (R = Me, Et, Pr, etc.) connected to the sulphur atom (bond-dissociation energy (BDE) of MeS–H = 368.44 kJ·mol^{-1}).[24, 25] It happens because the electron-poor hydrogen is bonded to the less electronegative sulphur atom ($RS^{\delta-}$–$H^{\delta+}$) if compared with a more electronegative oxygen from an alcohol group where this is more difficult to accomplish (BDE, MeO–H = 435.43 kJ·mol^{-1}). The cleavage of S–H bonds can be promoted either by direct photolysis/thermolysis or indirectly *via* hydrogen-transfer from heat- or light-generated nucleophilic carbon-centered radicals derived from the cleavage of initiators which abstract the hydrogen atom. The reaction can also be initiated *via* a REDOX mechanism[26], in the simple case by oxidation of a metal cation (*e.g.*, RSH + Ce^{4+} → $RS^{\bullet}$ + H^{+} + Ce^{3+})[24], and self-initiated through a complex MAH/EDA mechanism.[17, 23] The resulting electrophilic thiyl radicals ($RS^{\bullet}$), despite of being very poor hydrogen abstracting agents, can easily add to a wide variety of unsaturated compounds (both electron-rich/poor C=C bonds) to form new carbon–carbon linkages. This addition reaction (also termed hydrothiolation of C=C bonds) is exothermic[18] and energetically favoured as a new strong σ C–C

bond (~370 kJ·mol^{-1}) is formed at the expense of a weaker alkene π-bond (~235 kJ·mol^{-1}).[27] However, the overall rate of addition is strongly dependent on the chemical structure of the thiol and ene (internal, isolated, conjugated, non-conjugated, and substituted), with thiyl radicals adding generally faster to electron-rich α-olefins (terminal and monosubstituted) and norbornenes than to electron-deficient ones (*e.g.*, (meth)acrylates) and sterically hindered multi-substituted olefins.[28] This difference in ene reactivity drastically affects the ('click') character of free-radical thiol–ene additions and explains why most thiol–ene coupled products bearing β-thioether linkages are predominantly primary in structure exhibiting less exothermicities than secondary β-thioether products despite of the latter being energetically more stable (more exothermic).[29] With respect to the thiol it has been reported that the mercapto propionate ester is the most reactive moiety, this being attributed to a weakening of the S–H bond by intermolecular hydrogen bonding with the ester carbonyl group.[16] An accurate summary of the general trends in reactivity involving thiols and enes is given by Hoyle *et al.*[14, 16] and Northrop and Coffey.[29]

The thiol–ene reaction proceeds as a typical radical chain process with *initiation*, *propagation* and *termination* steps. The characteristic two-step mechanism for the hydrothiolation of an isolated unsaturation is represented in Scheme 1. At first, the reaction starts *via* initiation (often UV-induced) which promotes hydrogen transfer from the thiol to one of the initiating free-radicals generated, for instance, *via* the cleavage of a photoinitiator. The resulting thiyl radical then reversibly adds across any accessible C=C double-bond (labelled propagation step **i.**) yielding an intermediate β-thioether carbon-centered radical followed by chain-transfer to a second thiol group (labelled propagation step **ii.**) to give the final thiol–ene addition product with *anti*-Markovnikov orientation. The mechanism continuously regenerates the RS$^{\bullet}$ radical, thus there is no net consumption of thiol groups, allowing the polymerization to be propagated incessantly in a cyclic sequence until an equal amount of thiol–ene reactants are exhausted. Termination reactions are frequently considered unimportant when compared with the rates of propagation/chain-transfer and usually involve bimolecular (re)combination of the intervening radical species (β-carbon or thiyl radicals); although, other yet unidentified mechanisms may also be involved.[30]

Ideally, the concentration of the final β-thioether coupled product should be equal to the initial concentration of the limiting thiol–ene reactant leading to a theoretical coupling efficiency of 100%. This indication strongly suggests that the reaction rate kinetics might be first order with respect to the individual thiol and ene concentrations and second-order overall for the thiol–ene mechanism:

$$\frac{d[ene]_t}{dt} = \frac{d[\mathrm{RSH}]_t}{dt} = -k_c[ene]_t[\mathrm{RSH}]_t \qquad (1)$$

where, k_c, denotes an overall coupling rate coefficient (in $M^{-1}{\cdot}s^{-1}$). However, in a series of experimental kinetic studies, Bowman and co-workers[16, 31, 32] have shown that the reaction follows first-order rate kinetics of the form:

$$rate \propto [ene]_t^{\alpha}[\mathrm{RSH}]_t^{\beta} \tag{2}$$

with the scaling exponents: $\alpha + \beta = 1$. By consecutively holding the thiol and ene concentrations constant and changing the concentration of the second constituent the authors were able to determine the partial reaction orders with respect to thiol and alkene functional groups. Relation (2) implies that depending on the thiol–ene system considered the exponents may take distinct values and, therefore, the overall reaction rate becomes more heavily dependent on the concentration of one component than the other.[31] They have also determined that the key element governing the overall kinetics of thiol–ene polymerizations and rate-limiting step is the *propagation*-to-*chain-transfer* coefficient ratio (k_{add}/k_{CT}) of the corresponding elementary reactions. In general, the relationship between k_{add}/k_{CT} and reaction order derived from experimental measurements has been defined by the following first-order kinetic dependences:[29]

$$\frac{k_{add}}{k_{CT}} = \frac{[\mathrm{RC}^{\bullet}]_t}{[\mathrm{RS}^{\bullet}]_t} \begin{cases} \gg 1 \;\Rightarrow\; rate \propto [\mathrm{RSH}]_t^1 \\ \approx 1 \;\Rightarrow\; rate \propto [ene]_t^{0.5}[\mathrm{RSH}]_t^{0.5} \\ \ll 1 \;\Rightarrow\; rate \propto [ene]_t^1 \end{cases}$$

That is, when $k_{add} \gg k_{CT}$, the chain-transfer reaction is the rate-limiting step and the overall rate is dependent only on the concentration of thiol (*e.g.*, thiol–allyl ether systems). In this case, increasing the concentration of ene does not alter the reaction rate which is controlled by the hydrogen-abstraction step (*i.e.*, the slowest step). In cases where $k_{add} \approx k_{CT}$ (and $[ene]_t = [\mathrm{RSH}]_t$)[32] the overall rate is half-order with respect to both thiol and alkene concentrations and there is no rate-limiting step since both propagation and chain-transfer reactions contribute equally to the kinetics (*e.g.*, thiol–norbornene and thiol–vinyl ether systems). When, $k_{add} \ll k_{CT}$, the propagation step is rate-determining and the overall rate is first-order only with respect to the ene concentration (*e.g.*, thiol–vinyl silazane systems). A summary of the values obtained for the kinetic ratio, polymerization rate scaling factors, and maximum polymerization rates is given in Table 1 for different olefinic structures.

One of the most prominent competing reactions to thiol–ene additions is the propensity of the ene to homopolymerize *via* a pure chain-wise radical growth mechanism. In this case the choice of the alkene structure will affect the progress and outcome of the polymerization as one route is favoured over the other resulting in a mixed polymerization process with different structure build-up patterns

occurring simultaneously in multifunctional monomer systems. For example, enes such as acrylates, prone to rapid homopropagation ($k_{hp} \gg k_{add}$), will to some extent polymerize even in the presence of thiol whereas monomers such as allyl ethers to a significantly less extent will do this ($k_{hp} \ll k_{add}$) (Scheme 2).[18] In this particular case, the ratio of the consumption rates of ene to thiol functional groups deviates from unity according to the steady-state relationship[33-35]:

$$\frac{d[ene]_t}{d[\mathrm{RSH}]_t} = 1 + \frac{k_{hp}}{k_{CT}} \frac{[ene]_t}{[\mathrm{RSH}]_t} \tag{3}$$

where, k_{hp} represents the homopropagation rate coefficient defining the addition of the carbon-centered radical to the ene (in $M^{-1} \cdot s^{-1}$). This feature has allowed the adjustment of the overall reaction sequence in systems based on more than two monomers to create novel polymeric structures with exclusive properties as described by Bowman *et al.*[36-38] A thiol–ene system is, therefore, to larger extent affected by the reaction kinetics for the different competing reactions than conventional radical chain-growth polymerizations.

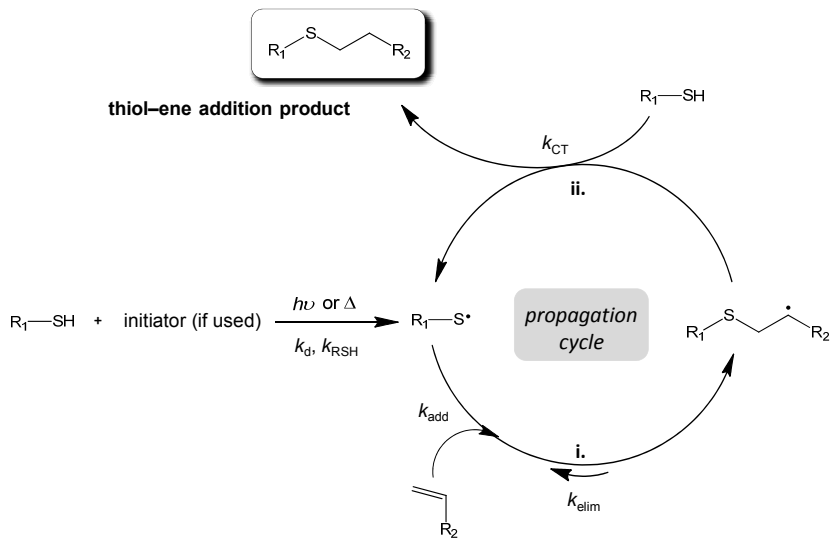

Scheme 1. Step-wise growth mechanism of the free-radical thiol–ene coupling involving a terminal ene with alternating *propagation (insertion–elimination)* (i.) and *chain-transfer* (ii.). Under ideal stoichiometry and absence of competing reactions, such as homopolymerization of the alkene monomer (*i.e.*, chain growth), a single thiol group couples with an alkene functionality to yield the final β-thioether product (C–S linkage).

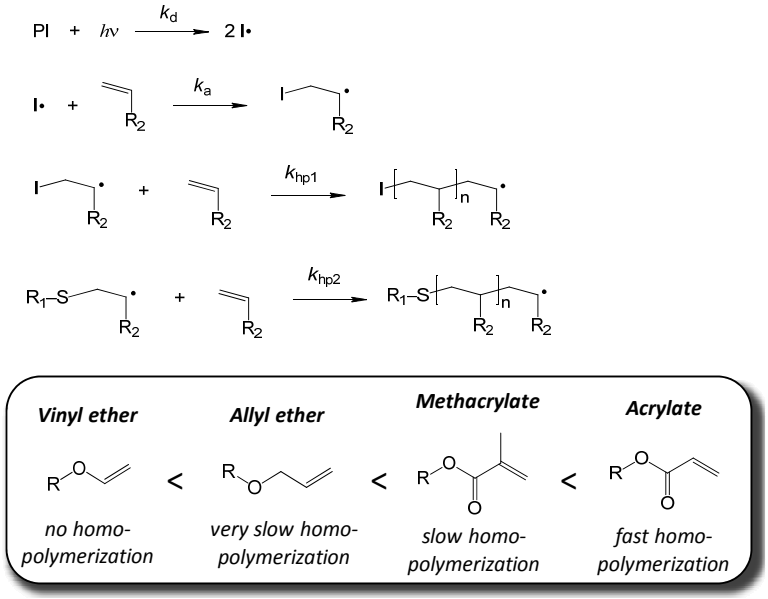

Scheme 2. Chain-wise radical growth mechanism showing the different degrees in homo-polymerization of the ene-monomer.

Table 1. Kinetic '*propagation*-to-*chain-transfer*' ratio, scaling exponents, and maximal polymerization rates attained for different multifunctional thiol–ene systems.[16, 29, 32]

Alkene moiety	k_{add}/k_{CT}	$r \propto [RSH]^{\alpha} \times [ene]^{\beta}$ α	β	r_{max} [b]
Allyl ether [a,b]	10	1.0	0	1.0
Acrylate [a,b]	13	0.4	0.6	2.1
Vinyl ether [a,b]	1.2	0.5	0.5	4.8
Norbornene [a,b]	1.0	0.5	0.5	6.0
Vinyl silazane [b]	0.2	0	1.0	3.3
Styrene [a]	8.0×10^5	—	—	—
Butadiene [c]	1.5×10^6	—	—	—
Pentene [a]	43	—	—	—

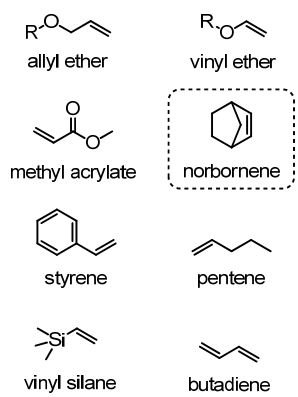

Note: values of the scaling exponents are valid only for 1:1 stoichiometric ratio systems with respect to concentrations of thiol and ene functional groups. [a] from ref.[16], [b] from ref.[32]; and, [c] from ref.[29]. All alkenes evaluated are mono-substituted except for norbornene which is 1,2-disubstituted (row shaded in grey). Propagation step was assumed irreversible in all cases (*i.e.*, $k_{elim} = 0$).

Although internal 1,2-disubstituted olefins generally show much lower reactivity towards the hydrothiolation of unsaturations than singly substituted ones, this is not uniquely due to an increased degree of substitution of the double-bonds (causing steric hindrance effects for the approaching thiyl radical) but also because of the existence of an isomerization process. One exception to this is the double-bond of norbornene which exhibits an exceptionally high reactivity toward thiol–ene coupling attributed to bond angle distortion in association with ring strain relief.[16] When internal 1,2-dialkyl substituted enes are involved, for instance those present in fatty acids and some macrolactones, isomerization further reduces the rate at which this occurs due to interchangeability between *cis/trans* configurations (cf. Scheme 3). Additionally, the intermediate alkyl radical formed between the two isomeric forms has a rather short lifetime and poor resonance stability which further hampers its reaction with the thiol. This reduces the rate of reaction of the second hydrogen-transfer step due to the inherently low hydrogen-abstraction rate constant.[11] Two common ways used to speed-up this process is by increasing the concentration of thiol in the reaction system or by lowering the reaction temperature; although these approaches are often impractical.[11, 39] For example, when equimolar thiol–ene ratios are required, such as formation of pure stoichiometric networks, the thiol concentration cannot be increased and the reaction temperature should be elevated to the molten state in order to prevent crystallization of the aliphatic chain segments and reduce viscosity during cure. The contribution of all these factors has made internal main-chain alkenes less desirable for thiol–ene additions, especially concerning polymer synthesis. Common routes used to circumvent this problem include derivatization of the 1,2-disubstituted moiety *via* catalytic olefin metathesis[2] to afford a more reactive (terminal) ene in thiol–ene additions and functionalization of the double bonds (*e.g.*, thiol–ene grafting[23, 40, 41], epoxidation[42, 43], acrylation[44-46] and ozonolysis[2, 47]) to subsequently employ more standard polymerization chemistries.

From a pure physical or thermodynamic perspective, the *cis*-to-*trans* conversion of unsaturations is a temperature driven process, which can also be induced chemically by reversible addition with thiyl radicals ($RS^{\bullet}$) using the thiol–ene coupling reaction.[48, 49] The mechanism conceived involves the abstraction of an hydrogen atom from the thiol group *via* one of the initiation mechanisms described, the insertion of the generated thiyl radical to the *cis* unsaturation of an oleate '1,2-disubstituted' moiety to form the intermediary radical adduct ($A^{\bullet}_{Z}$) immediately followed by half-rotation about the C_9–C_{10} bond to give the radical adduct ($A^{\bullet}_{E}$) and subsequent ejection of the thiyl radical by β-fragmentation (regeneration) (cf. Scheme 4). Mechanistically, the reaction scheme shows essentially the same elementary sequence steps as for terminal enes except the existence of isomerization. The formation of either *cis*- or *trans*-isomers depends on the conformational state of the intermediary fragmentation adduct at the instant of thiyl radical loss.[50] This event changes the double-bond geometry leading to the thermodynamically more stable *trans*-isomer. The energy difference between the two geometrical isoforms based on the catalysis of 2-butene by $HOCH_2CH_2S^{\bullet}$

has been determined to be 1.0 kcal·mol^{-1} at 20°C.[48] Chatgilialoglu *et al.*[39, 48] showed that thiyl radicals are amongst the most effective agents known to catalyze the *cis/trans*-isomerization because even a small amount of radical species is capable of making the reaction to proceed.[49, 51] Constitutional isomers cannot be obtained as reaction products since the mechanism does not allow positional migration of the double-bond.[51] Also, the location of the unsaturation along the aliphatic main-chain, together with tail length, has proven to have no relevant effect on the isomerization itself although it affects the reactive character of the C=C bond as a result of steric hindrance effects.[50] It was shown, for instance, that 1-hexene (a mono-substituted terminal ene) is 13-times more reactive than *trans*-2-hexene and 25-times more reactive than *trans*-3-hexene based on equally balanced C=C/RSH mole ratios.[52] Many other free-radicals (*e.g.*, $RSO_2^{\bullet}$, $R_3Sn^{\bullet}$, $RSe^{\bullet}$, $NO_2^{\bullet}$, or $(Me_3Si)_3Si^{\bullet}$) and elementary radicals (such as $Br^{\bullet}$ or $I^{\bullet}$) are known to induce *cis/trans*-isomerization through an *insertion–elimination* sequence, although with different efficiency than with thiyl radicals.[49, 51, 53, 54] There is also supporting evidence that oxygen (<0.3 mM) does not seem to play a strong influential role in the effectiveness of *cis/trans*-isomerization if internal *cis*-alkenes are employed.[55, 56]

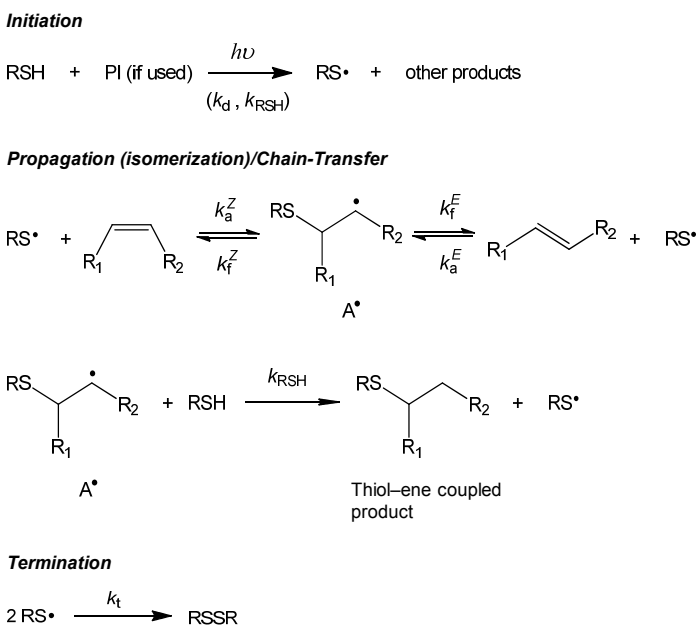

Scheme 3. Thiyl-radical mediated *cis/trans*-isomerization of internal double-bonds. The species ($A^{\bullet}$) denotes the equilibrium radical structure of the intermediary fragmentation adduct.

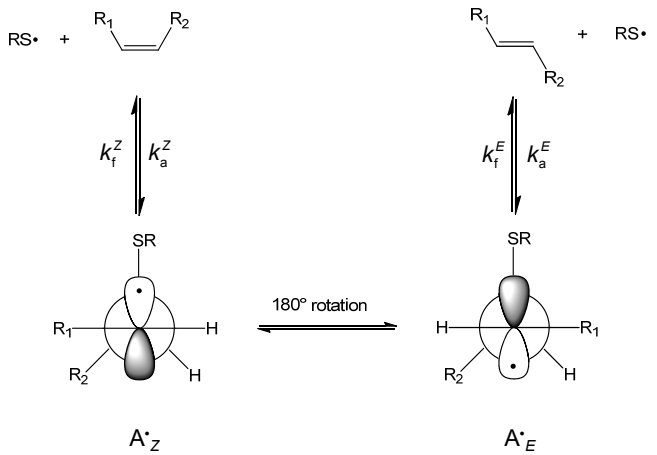

Scheme 4. Proposed reversible addition mechanism of the thiyl radical to a 1,2-disubstituted ene at position C_9–C_{10} (adapted partially from ref.[55]). The conformers ($A^{\bullet}_Z$ and $A^{\bullet}_E$) denote intermediary fragmentation states of the carbon-centered radical adduct.

2.1.3 Thermosets in relation to thiol–ene chemistry

By definition, a thermoset plastic – *as opposed to a thermoplastic* – is a polymeric material which once cured (*i.e.*, covalently crosslinked) cannot flow, be dissolved, be molded or melted within the same range of temperature; although it may undergo deformation (vulcanised rubber is an example). This is attributed to the tridimensional network structure, when contrasted to the linear or branched configuration found in thermoplastic polymers. Thermosets are formed when two components co-react in such a way that one of them has a functionality $f \geq 2$ and the other has $f > 2$. The two components may be linear oligomers or polymers of high functionality along the main chain (pendant functional groups or contained within the backbone), branched polymers or multi-arm (macro)monomers. From a manufacturing perspective, thermosets are shaped during the crosslinking process and once cured they become 'set', and cannot be reprocessed again. They retain improved physicochemical properties such as stability toward elevated temperatures and physical stress and are dimensionally stable under a variety of conditions owed to the network structure. Because they are chemically crosslinked, thermosets usually exhibit higher residual stress, shrinkage and cure-induced defects such as formation of cracks and other irregularities when compared to thermoplastics. Their main application areas include: packaging, composites, adhesives, dental materials and protective coatings.

One of the oldest kinds and most common thermosets are alkyd-based paints. Alkyd coatings are generally prepared by condensation polymerization of three

types of monomers: polyalcohols (*e.g.*, glycerol), polybasic acids (*e.g.*, phthalic anhydride) and unsaturated fatty acids or triglyceride oils, to obtain fatty-acid containing polyesters. When applied to a surface they are slowly cured through a free-radical auto-oxidation mechanism (chemical drying) in which atmospheric oxygen adds to the unsaturated fraction of the resin leading to its crosslinking and the paint hardens.[57, 58]

One of the key advantages offered by thiol–ene chemistry over classical free-radical polymerizations is the high ability to overcome oxygen inhibition. Besides acting as quenching agent of photoexcited states of molecules, oxygen also stops the polymerization by its reaction with radicals.[59] In the case of free-radical polymerization using (meth)acrylates, if oxygen adds to a polymeric propagating carbon-radical terminus, that chain will end immediately because the formed alkyl peroxy radical will have insufficient reactivity to add to a new ene monomer. This results in short chain fragments, a loose network structure and reduced crosslink density.[60] For a thiol–ene polymerization system this does not happen since the peroxy radical is still able to abstract the hydrogen from a thiol monomer producing a new thiyl radical that propagates the polymerization with only minimum impact on the main reaction route (Scheme 5). Since thiols act as strong hydrogen donors, they can be added (even in small amounts) to acrylic formulations to suppress the inhibitory effect of oxygen through trapping of peroxy radicals during cure.[61]

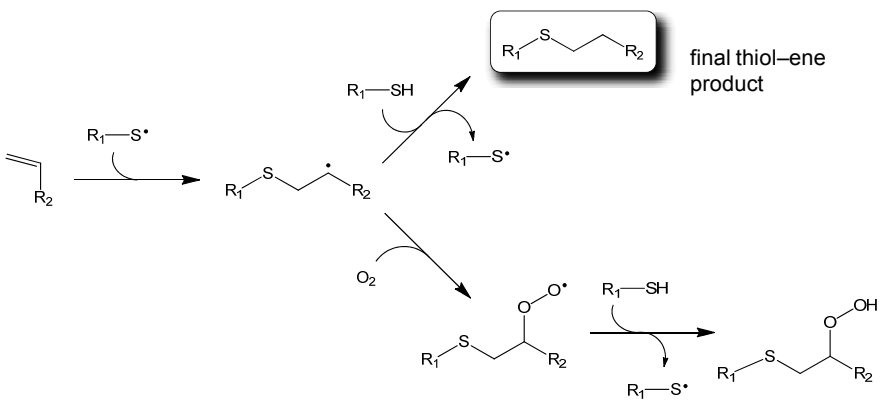

Scheme 5. Hydrogen abstraction *vs.* oxygen-scavenging routes for the free-radical-mediated thiol–ene reaction involving terminal enes.

Concerning network formation of thermoset polymers for organic film-coating applications, principal attributes of the thiol–ene reaction are summarized as follows:

- *Initiation without the need of photoinitiator*. Since the RS–H bond of thiols excite at ~254 nm light, irradiating with a UV-lamp emitting primarily at this wavelength allows fast and direct generation of thiyl radicals without utilization of a photoinitiator.[34, 61, 62] This enables the polymerization of very thick geometries since UV-light is able to penetrate throughout the thickness of the film without attenuation resulting in homogeneous cure. Alongside, it also minimizes occurrence of termination reactions by homocoupling of thiyl radicals since disulphides absorb essentially at the same wavelength as thiols.[63] As a consequence, the photo-crosslinked polymers formed are less prone to degradation/yellowing, without generation of coloured or volatile by-products, and fast aging during prolonged exposure to sunlight.[62] If a photoinitiator is to be employed, then it must be ensured that the main emission peak of the UV-light source overlaps with the absorption peaks of the initiator for maximum thru-cure efficiency.

- *Step-wise mechanism of radical growth*. This mode of assembly enables high level of control of the polymerization process since the build-up in molecular weight (viscosity) associated to the development of the network structure occurs geometrically keeping the reaction system in the liquid phase throughout cure until very high monomer conversions are finally achieved. This gradual ('slow') growth of the network minimizes the influence of diffusional effects in the polymerization kinetics until very late in the reaction, resulting in a delayed gel-point, minimal amount of unreacted thiol–ene functional groups, high crosslink densities with narrow glass-transition temperatures and significantly lower stresses and volume shrinkage than in conventional thermosets (*e.g.*, acrylates).

- *High uniformity in the network crosslink density*. This results in materials with homogeneous thermo-mechanical properties across all spacial dimensions as a consequence of free-radical two step-growth mechanism which ensures optimal mechanical performances and tendency for extensive sub-T_g relaxation processes related with physical aging (enthalpy and volume relaxation).[18, 64]

2.1.4 Interface with *Green Chemistry*

'Green or Sustainable Chemistry' is a relatively recent concept in organic and polymer syntheses developed by Anastas and Warner at the end of the twentieth century.[65, 66] Its twelve guidelines[3] orient and direct chemists to develop chemical and biochemical processes not only more environmentally friendly but also safer without recurring to nasty toxic chemicals, reagents and solvents which endanger human operators and sometimes make the chemical processes more complex and unfavourable economically because of these inherent hazards. Some of the green chemistry principles include essentially:[67] energy efficiency, safer or no use of organic solvents, atom and molecular economy, less harmful chemical synthesis

and resulting products, use of renewable feedstocks over petrochemical ones, recoverable and reusable catalysts, enzyme biocatalysis, reduced derivatives and minimization of waste. Within this context, the free-radical thiol–ene reaction is considered to be a simple and environmentally benign tool that proceeds without the need of organic solvents when both monomers are miscible and under clean and mild reaction conditions (if photochemically induced), and that rejects potentially toxic metal catalysts so commonly employed in other ('click') reactions.[14, 22] The fact that the reaction can be triggered by UV-light is also relevant industrially since it is has relatively low energy requirements compared to more intensive synthesis processes and the possibility to use currently available industrial infrastructures.

2.1.5 Renewable monomers for thiol–ene additions

One remarkable feature inherent to the thiol–ene reaction is that virtually any alkene functional group can participate.[11] As already mentioned, the chemical nature of the double-bond affects, to a large or small extent, the efficiency of the reaction and this much often dictates which ene monomers can be effectively selected for a particular application. So far terminal enes and norbornenes have gained preferential choice due to their highly reactive character. Yet, they are derived mostly from petrochemical feedstocks and viable green alternatives to these alkene moieties are urgently needed. Many good examples of natural alkene compounds are reported in the literature as building-blocks in polymer science using a wide variety of chemistries[68-71]; however, only 'a handful' are actually utilized in the thiol–ene reaction. The large majority of these include unsaturated vegetable oils or their derivatives[23] and to far less extent macrocyclic lactones such as ambrettolide (and globalide)[72-74] as well as monoterpenes such as (*R*)-(+)- and (*S*)-(−)-limonene and β-pinene.[75-77] Frequently, these renewable monomers need to be transformed first (*e.g.*, ring-opening (co)polymerization of macrolactones *via* lipase biocatalysis) and/or functionalized *via* thiol–ene chemistry to introduce new chemical groups; and, subsequently utilized in a second step as 'bio-derived' platform chemicals in the synthesis of linear polymers *via* polycondensation using more standard organic chemistries (*e.g.* transesterification). Direct use of these monomers in combination with thiol–ene coupling solely to prepare linear polymers or thermosets is very limited. Also, the narrow availability of natural thiol compounds (*e.g.*, 2-furfurylmethanethiol[78]) hampers the synthesis of such polymers and/or thermosets by means of thiol–ene chemistry exclusively.

D-limonene constitutes about 90–96% of orange peel essential oil and therefore is available in large scale as by-product of the citrus processing industry.[79] This monoterpene contains in its chemical structure two non-conjugated electron-rich double bonds with different degrees of substitution susceptible to radical polymerization: a terminal (exocyclic) 1,1-disubstituted alkene functionality (*i.e.*, vinylidene or isopropenyl moiety) and an internal (endocyclic) 1,1,2-

trisubstituted alkene group (*i.e.*, 1-methyl-cyclohexene moiety). Significant efforts have been conducted throughout the years to polymerize limonene either by itself or with other monomers using a variety of chemistries.[70, 79-81] Since the two unsaturations remain virtually unreactive towards free-radical homopolymerization, they constitute the ideal alkene moieties for the thiol–ene reaction. Very recently, Meier and co-workers (2012) have demonstrated the efficient thiol–ene coupling of cysteine hydrochloride to the two limonenes in the preparation of new diamine functionalized renewable monomers which served as platform precursors for polyamide and polyurethane synthesis.[77] In an early report, the authors developed optimal conditions for the selective functionalization of the terminal vinylidene group with methyl thioglycolate as model compound further allowing the synthesis of a diversity of monomers and ensuing polymers.[75] Direct polymerization of limonene with dithiols was also reported in this proceeding. In another paper[76], the authors also described the attachment of alcohol and ester functionalized thiols to the two enantiomers of limonene *via* thiol–ene coupling affording mono-functional, homo-difunctional and hetero-difunctional terpene-modified monomers. The difunctional addition products were subsequently homo- and co-polymerized with short-chain diols using cyclo guanidine 1,5,7-triazabicyclododecene (TBD) as polycondensation organocatalyst because of its high transesterification activity. The same strategy was employed to synthesize high molecular weight polyesters (from 9 up to 25 kDa) based on limonene and fatty-acid methyl ester derivatives. These three recent studies illustrate the extreme versatility of the thiol–ene reaction in the design of new linear polymers issued from limonene in combination with distinct classes of renewable monomers (natural or modified) and chemistries.

Some other prospective alkene-based monomers worth exploring in free-radical thiol–ene additions include (Figure 2.1):

(a) *Aliphatic and cyclic terpenes* (*e.g.*, myrcene and α-pinene);

(b) *Plant triterpenoids(ols)* (*e.g.*, betulin or betulinic acid, stigmasterol and brassicasterol);

(c) *Rosin acids* (*e.g.*, pimaric and isopimaric acids);

(d) *Itaconates* (*e.g.*, itaconic acid);

(e) *Allicin*, a diene organosulphur compound extracted from garlic;

(f) *Thioterpineol* (*p*-menth-1-en-8-thiol), a monoterpenoid commonly known as grapefruit mercaptan;

(g) *Valencene*, an aliphatic terpene-based compound found in the essential peel oil of Valencia oranges.

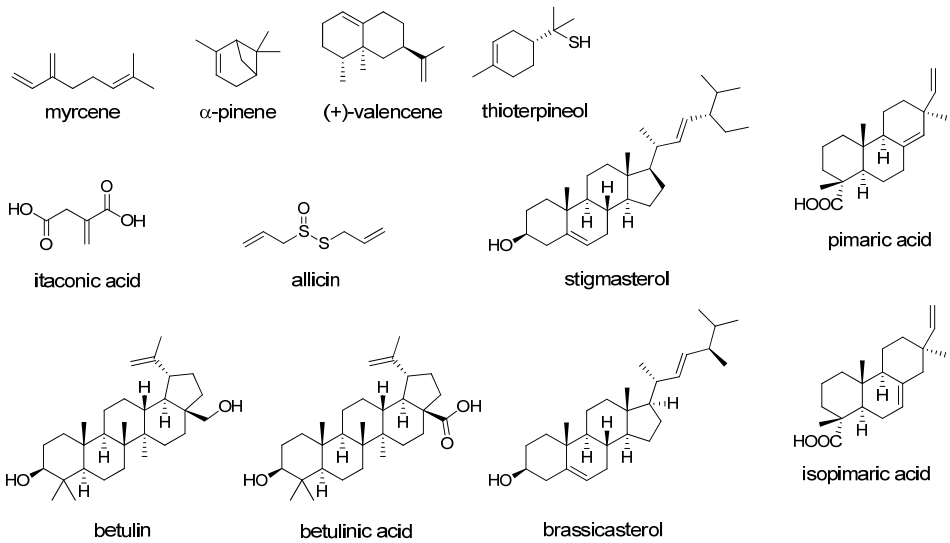

Figure 2.1 Some renewable alkene structures with potential for thiol–ene additions.

3 Experimental

3.1 Chemicals

The multifunctional thiols trimethylolpropane tris(3-mercaptopropionate) (TMPMP, 398.56 g·mol^{-1}) and pentaerythritol tetra(3-mercapto propionate (PETMP, 488.6 g·mol^{-1}) and mono-functional thiol *iso*-tridecyl 3-mercapto propionate (C13MP, 288.1 g·mol^{-1}) were kindly supplied by Bruno Bock Chemische Fabrik GmbH & Co (Marschacht, Germany). Methyl oleate (MO, 99%, 296.49 g·mol^{-1}), methyl elaidate (ME, 99%, 296.49 g·mol^{-1}), ε-caprolactone (ε-CL, 99% 114.14 g·mol^{-1}), (*R*)-(+)-limonene (Lim, 97% 136.24 g·mol^{-1}) and tetrahydrofuran (THF) were purchased from Sigma-Aldrich (Stockholm, Sweden) and the photoinitiators 1-hydroxy-cyclohexyl-phenyl-ketone (Irgacure 184®, 204.3 g·mol^{-1}) and 2,2-dimethoxy-2-phenylaceto-phenone (Irgacure 651®/DMPA, 256.3 g·mol^{-1}) were obtained from Ciba Specialty Chemicals Inc. (Switzerland). Globalide (GI, 240.38 g·mol^{-1}) was a kindly gift of Symrise (Holzminden, Germany). Deuterated chloroform ($CDCl_3$, 99.8%) was provided by CIL (Cambridge Isotope Laboratories, Inc., USA). Ethyl acetate (EtOAc, 99%) was acquired from Merck (Darmstadt, Germany). Novozyme 435 (*Candida antarctica* lipase B immobilized on crosslinked polyacrylate beads) was purchased from Novozymes A/S (Bagsvaerd, Denmark). All chemicals were commercial products, used as received without further purification (Figure 3.1).

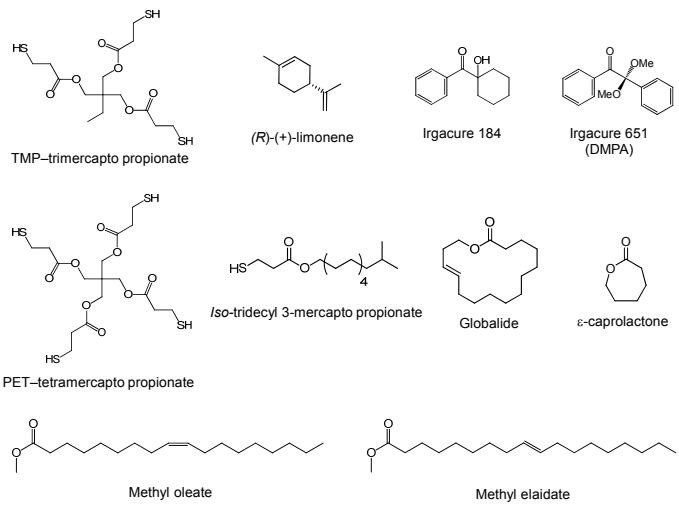

Figure 3.1 List of chemical compounds used in the thesis.

3.2 Instrumentation

NMR Spectroscopy. ^{1}H and ^{13}C NMR spectra of the samples were recorded on a 400 MHz Bruker Aspect NMR spectrophotometer (Karlsruhe, Germany). $CDCl_3$ containing 0.05 vol.% of tetramethylsilane (TMS) was used as *d*-solvent. Chemical shifts (δ) were reported in parts per million (ppm) relative to the tetramethylsilane internal standard (TMS, δ=0.00 ppm). Spectral analysis was made using the Mestrec® Software.

FT–IR Spectroscopy. RT–FTIR spectra were recorded in the mid-region with a Perkin-Elmer Spectrum 2000 (Norwalk, CT) using an MCT detector cooled with liquid N_2. The FTIR instrument was equipped with a heat-controlled Golden Gate single reflection ATR-accessory from Graseby Specac Ltd. (Kent, England). The horizontal ATR-sampling unit was modified in order to accommodate a vertical UV-light cable. All FTIR measurements were performed in the reflection mode *via* the single-bounce diamond ATR crystal. Conventional ATR–FTIR measurements were performed on a Perkin-Elmer Spectrum 2000 equipped with a TGS detector using the Golden Gate setup. Each spectrum collected was based on 32 scans averaged at 4.0 cm^{-1} resolution in the range of 600–4000 cm^{-1}. Data were recorded and processed using the software Spectrum from Perkin-Elmer.

FT–Raman Spectroscopy. Spectra were acquired using a Perkin-Elmer Spectra 2000 NIR-Raman instrument with Spectrum software. Each spectrum collected was based on 16- or 32-scans using a laser power of 800–1000 mW.

UV/Vis-spectrophotometry. Ultraviolet–visible spectrometry was conducted on a double-beam Cary E1 UV–Vis spectrophotometer. The scan resolution of the UV–Vis spectrometer was 1.0 nm.

UV–light Sources. A Hamamatsu L5662 equipped with a standard medium-pressure 200W L6722-01 Hg–Xe lamp and provided with optical fibers was used as the UV-source for the photo-RTIR measurements and discontinuous kinetic studies. A condenser lens adapter, model A4093 from Hamamatsu, was employed to focus the UV-beam. Neutral density filters with optical densities of 0.2, 0.4, 0.6, 1.0 and 2.0 from CVI Laser Corp. LCC were used to obtain a constant irradiance of 5.0 $mW{\cdot}cm^{-2}$. The UV-intensity was measured using a Hamamatsu UV-light power meter (model C6080-03) calibrated for the main emission line centred at 365 nm. An UV Fusion Conveyor MC6R equipped with Fusion electrodless bulbs standard type BF9 (UV-fusion lamp) was employed for network formation issued from P(GI-*co*-CL) copolymers. The UV-light intensity was determined with a UVICURE®Plus from ET, Sterling, VA. The light source used for synthesis of limonene-based resins was a Blak Ray B-100AP (100 W, λ=365 nm) Hg UV-lamp delivering an irradiance of ~25 $mW{\cdot}cm^{-2}$ as determined with an UVICURE Plus High Energy UV Integrating Radiometer (EIT, USA), measuring UVA at $320 \leq \lambda \leq 390$ nm.

Size-Exclusion Chromatography. SEC measurements were a TOSOH EcoSEC HLC-8320GPC system equipped with an EcoSEC RI detector and three columns (PSS PFG 5 μm; Microguard, 100 Å and 300 Å) (MW resolving range: 300–1.0×10^5 Da) from PSS GmbH. Measurements were carried out at 50°C using DMF solvent supplemented with 0.01 M LiBr as mobile phase (isocratic elution, 0.2 ml·min^{-1}). A conventional calibration method was created using narrow linear poly(methyl methacrylate) standards. Corrections for flow rate fluctuations were made using toluene as an internal standard. PSS WinGPC Unity software version 7.2 was used to process and analyse the data. For THF–SEC measurements see details in **Paper II** appended.

3.3 Preparative, Synthetic and Analytical Procedures

Bellow follows a summary of the general methods and experimental procedures used for the presented results. For more complete details the reader is referred to the appended papers.

3.3.1 Sample preparation

Two different reaction mixtures containing TMP-trimercapto propionate (89.6 mg) and mono-unsaturated oil (MO or ME, 200 mg) in a molar ratio of 1:1 with respect to thiol–ene functionalities were prepared. Irgacure 184 (2.0 wt.%, ~2.8 mg) was added to each mixture. The approximate molarities of trithiol, FAMEs and PI in the samples were 0.74, 2.21 and 0.045 M, respectively. The initial bulk mixtures had to be heated slightly prior to the analysis in order to mix all the components completely.

Thiol–ene mixtures of the different unsaturated P(GI-*co*-CL) copolymers were prepared by dissolving the copolymer in 5.0 ml of THF solvent and then mixing equimolar amounts of trithiol with respect to thiol and ene functionalities so that all groups could react theoretically with each other at the same stoichiometry. The samples were supplemented with a small amount of the UV-initiator Irgacure 184 (~2.0 wt.%) and then kept at 4°C protected from light until further use. A typical formulation is as follows: 525 mg of P(GI-*co*-CL) 47/53, 190 mg of TMP-trimercapto propionate and 14.3 mg of Irgacure 184. The same recipe and amounts were used, with omission of the thiol reactant, for the homopolymerized samples. For the thiol–ene films, the mass ratio necessary for equimolar reaction of thiol–ene functional groups was calculated using the expression:

$$\frac{m_{\text{trithiol}}}{m_{\text{polym.}}} = \frac{f_{\text{mol}} \cdot DP \cdot M_{\text{t}}}{3 \cdot M_{\text{n}}} \tag{4}$$

where, f_{mol}, is the mole fraction of ene in the copolymer, DP is the degree of polymerization, M_t is the molecular weight of the trithiol (TMPMP) and M_n the number-average molecular weight of the copolymer. The number of ene functionalities per copolymer chain is given by $f \cdot DP$. Copolymer synthesis details can be found in **Paper II** appended.

Stock solutions of terpene and monothiol (C13MP) or trithiol (TMPMP) based on a composition ratio of 1:0.5 with respect to thiol–ene functional groups were prepared by mixing equivalent mole amounts of each reactant in 50 wt.% of $CDCl_3$ solvent and the resulting solution added with 1.0 wt.% of DMPA. For reactions performed in liquid bulk conditions, both the monothiol and limonene were first mixed to obtain two individual thiol–ene stoichiometries of 1:0.5 and 1:1 and the resulting mixture supplemented with 2.0 wt.% of DMPA. A volume of 2.0 ml from each mother solution was transferred to corresponding small glass vessels of cylindrical shape (40×12 mm) used as mini photochemical reactors.

3.3.2 Initiator photolysis

To obtain a rough estimate for the production rate of primary free-radicals, a diluted solution of Irgacure 184 in methyl oleate was prepared (0.02 wt.%, ~0.86 mM). The sample was sealed inside a 1-mm thick quartz cuvette and then irradiated intermittently in the presence of air at ~20°C with an UV-intensity of 5.0 $mW \cdot cm^{-2}$. The absorbance was measured in the range 190–600 nm. The decomposition of photoinitiator with time was monitored by following the decrease of the main absorption peak at 247 nm until there was no significant change in the absorption spectrum. All spectra were subtracted from a blank sample containing only methyl oleate in order to eliminate spectral contribution of the solvent (background spectra). Concentrations over time were calculated from the Lambert–Beer law.

3.3.3 Photo-RTIR measurements

For RT–FTIR measurements of photoinduced reactions, the heat-controller was set to 60°C and the system left to equilibrate for 10 min. Two drops of the monomers/photoinitiator mixture (~75 μl) were then applied onto the surface of the ATR diamond probe connected *in-situ* to a circular heater plate and the measurements were started immediately. The photoreaction and photopolymerizations were initiated by vertically irradiating UV-light from the Hamamatsu lamp. IR-runs were conducted in the presence and absence of air (by covering the liquid samples with a thin quartz lamella) over a period of 30 min using independent samples. RT–FTIR continuously recorded the chemical changes over the range of 4000–600 cm^{-1}. Spectroscopic data were collected at an optimized scanning rate of 1 scan per 1.67 seconds with a spectral resolution of 4.0 cm^{-1} using the Time-

Base® software from Perkin-Elmer. The course of the reaction was followed by monitoring the peaks corresponding to the *cis*- and *trans*-unsaturation C=C bonds occurring at ~3010 and 968 cm^{-1}, respectively. Figure 3.2 illustrates the custom-made RTIR setup utilized in the experiments. Aliquot samples for ^1H NMR analysis were taken before and after the reaction in order to estimate the final conversion of double-bonds (photoreaction system only).

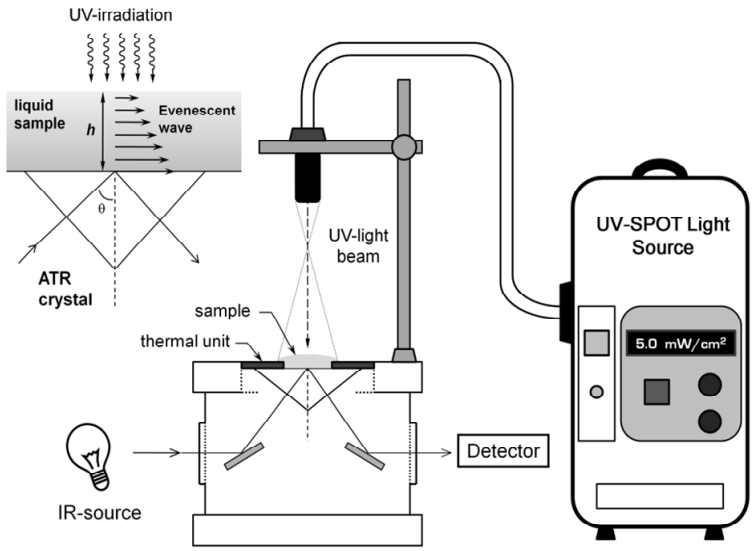

Figure 3.2 Experimental RT–FTIR setup equipped with an ATR-accessory for single reflection with a fixed incidence angle of 45°.

3.3.4 Evaluation of reactivity

Assessment of thiol–ene reactivity in limonene-based mixtures was performed by exposing the separate samples to different doses of polychromatic UV-light delivering ~4.2 $mW{\cdot}cm^{-1}$ of irradiance in the presence of air at room-temperature and constant stirring (10^3 rpm). The resulting photoproduct mixtures were dissolved in 1.0 ml of $CDCl_3$ after each kinetic run was finished and 800 µl of the diluted samples were analysed by ^1H NMR spectroscopy to determine double bond conversion over time.

3.3.5 Thiol–ene conversions

FT–Raman and ^1H NMR spectroscopies were used for the discontinuous evaluation of thiol and ene conversions. Analysis of the R–SH peak occurring at ~2576 cm^{-1} and alkene functional groups located at 3010 cm^{-1} and 1652 cm^{-1} (*cis*-ene),

~1670 cm^{-1} (*trans*-ene), 1645 cm^{-1} (*exocyclic*, vinylidene), and 1678 cm^{-1} (*endocyclic*, trisubstituted) was performed by normalizing the individual spectra against the band characteristic of the ester carbonyl group centered at ~1735 cm^{-1}. Thiol–ene conversions were calculated using the ratio of peak heights to the peak height prior to the reactions. ^{1}H NMR integration signals corresponding to the C═C bonds of the two mono-unsaturated oils (*vinylic*: 5.05–5.54 ppm and *allylic*: 2.0 ppm) were used to estimate the extent of the reaction using the integral areas of two conserved signals: (*i.*) the methyl ester protons at 3.66 ppm, and (*ii.*) the aliphatic protons at 2.29 ppm adjacent to the ester group; whereas, integral areas for the unsaturation proton signals of limonene located at 4.7 ppm (*exocyclic*, vinylidene) and 5.4 ppm (*endocyclic*, trisubstituted) were normalized against the areas of the ethyl protons from the thiol compounds located at 4.1 ppm. The degree of conversion into C–S bonds was expressed as the cross-average of the values obtained from both unchanged signals (only for the final mixtures issued from mono-unsaturated oils). Percent conversions of each chemical group into β-thioether (C–S) bonds were determined from the formula:

$$\text{Conversion } (\%) = \left(1 - \frac{x_f}{x_0}\right) \times 100 \tag{5}$$

where x denotes either normalized double-bond ^{1}H integrations or FT-Raman band heights before (x_0) and after reaction (x_f). The sum of individual double-bond conversions (*exo*+*endo*) over time provided an estimation of the extent of reacted limonene as a species (considering only primary coupling reactions, **Paper III**) and/or total ene conversion (**Paper IV**). The kinetic conversion data were subsequently changed into the corresponding chemical species (or functional group) concentrations by means of the simple relation: $C(t)=C_0\times(1-f_c)$ (eqn. 6); with the symbol $C(t)$ representing the molar concentration at time t, C_0 is the initial molarity, and $0 \leq f_c \leq 1$ denotes the fraction of total conversion at each time.

3.3.6. Product identification

Identification of reaction products and characterization of the chemical structures was accomplished *via* proton and carbon NMR.

3.3.7. Simulation software and kinetic modeling

Kinetic simulations of the mechanistic reactions (Tables 2, 6 and Scheme 9) were performed using two equivalent software applications: (1.) GEPASI version 3.30[82] (**Paper I**); and, (2.) COPASI version 4.8 (build 35)[83] (**Papers III** and **IV**). A deterministic routine algorithm called *LSODA (Livermore Solver for Ordinary*

Differential Equations) was used to compute the numerical solution of a set of ODEs. LSODA is a very robust adaptive step-size solver that calculates the stiffness of the continuity equations and dynamically switches the method of integration according to this measure.[84-87] To construct the computed output curves, all elementary chemical reaction steps, initial reactant concentrations and individual rate coefficients were first entered and the programs allowed solving the system of ODE's as a function of time. Unknown intrinsic rate coefficients specified for *propagation* and *chain-transfer* steps were optimized *via* a parameter estimation routine task that COPASI has built-in following the Hooke & Jeeves algorithm coupled to an objective function that minimizes the distance between experimental and computed data.[88, 89]

3.3.8 Film-formation and UV-curing

For the photoinduced crosslinking of the different (co)polymers, thiol–ene mixtures were spread on glass substrates that were previously cleaned and rinsed with acetone. Liquid films were applied sequentially up to two layers by letting the solvent evaporate between applications and then melted in the oven preheated to 85°C for 2–3 min until transparent films were observed. The coated slides were immediately placed in the conveyor belt while still in the molten-state (by use of a 0.4 cm thick glass plate to help the sample retain the molten temperature) and passed four times under the UV-lamp with a line speed of 6.52 $m \cdot min^{-1}$ to give an overall exposure dose of 0.14 $J \cdot cm^{-2}$. The samples were then left at room temperature to cool. Smooth, non-tacky films of 30–40 μm thickness resulted.

Pre-cure thiol–ene samples based on limonene were formulated by mixing mole amounts of thiol and ene functional groups in the stoichiometric mole ratio range (ene:thiol): 1:1, 1:1.10, 1:1.25, and 1:1.45 from direct and/or cross-combination of resins 1 and 2 with the multifunctional thiols **6** and **8** as exemplified in Scheme 11 (see section 4.2.3). Each sample was supplemented with ~2.0 wt.% of DMPA and thoroughly mixed under moderate heating for complete dissolution of the photoinitiator. The mild heating did not cause any detectable reaction as determined by ^{1}H NMR (results not shown). The liquid neat monomer mixtures were gently applied onto dried microscopy glass slides and placed in the vacuum oven pre-set at 50°C for about 3-hours to remove any air bubbles trapped inside. Individual samples were cured under a low pressure mercury UV-lamp at an intensity of 25 $mW \cdot cm^{-2}$ for 1-hour. To ensure complete post-polymerization, the resulting crosslinked films having 475±67 μm thickness were dried in vacuum at 50°C overnight and then stored in the dark for 2-weeks at room temperature before any measurements could be performed. The cured films were fully transparent and adhered strongly to the glass substrates.

3.3.9 Dynamic Scanning Calorimetry (DSC)

The thermal properties of the crosslinked films were analyzed by DSC. The experiments were conducted on a DSC 820 equipped with a sample robot and a cryocooler (Mettler Toledo). The DSC runs were carried out in closed sample pans sealed in air, using the following temperature program (globalide/caprolactone copolymers and ensuing crosslinked films): heating from 25 to 120°C (50°C·min^{-1}), cooling from 100°C to –65°C (50°C·min^{-1}), then heating up to 120°C (5°C·min^{-1}). Isothermal segments of 5 min were performed at the conclusion of each dynamic segment. The melt enthalpy was determined from the integration of the T_m peak of the second heat. For limonene-based thiol–ene films the following temperature program was executed: first heating from 25°C to 200°C, isothermal for 5 min at 200°C, cooling from 200°C to –40°C, isothermal for 5 min at –40°C and then second heating from –40°C to 200°C. Cooling/heating cycles were performed at a constant rate of 5°C·min^{-1}. The glass-transition temperature (T_g) was determined from the second heating scan and taken at the mid-point (second derivative) of the transition curve.

3.3.10 Dynamic Mechanical Thermal Analysis (DMTA)

To examine the final rheological properties of the thiol–ene networks, DMTA was performed on a TA Instruments Q800 dynamic mechanical analyzer, equipped with a film fixture for tensile mode testing and a gas cooling accessory. Dried film-specimens of rectangular geometry were processed from the original UV-cured samples and then tightened in the clamps of the sample holder. Temperature was lowered to –30°C or –70°C and isothermally held for a period of 5-min before the temperature was increased to 140°C at a ramping rate of 3 or 5°C·min^{-1} (globalide- *versus* limonene-based films). The tests were performed in controlled strain mode with a frequency of 1.0 Hz, a constant oscillating amplitude of 0.12 μm (or 15.0 μm), and forcetrack of 125%. Storage (E') and loss (E'') moduli and loss factor, tan δ ($=E''/E'$), were recorded as a function of temperature. The glass-transition temperature (T_g) was determined as the peak maximum of the tan δ *versus* temperature curve.

3.3.11 Sol-content determination

All crosslinked thiol–ene film materials were cut into small rectangular sections with approximate dimensions of 1.0 cm × 2.0 cm, dried in the vacuum oven at 50°C for 1-hour, weighed and then soaked in 5.0 ml of THF under gentle stirring conditions. The films were subsequently washed (2×) with THF solvent and placed again in the vacuum oven until the residual solvent was fully evaporated. Sol-fractions for the film specimens were determined from mass losses relative to initial dry mass according to the following equation:

$$\text{Sol content } (\%) = \left(1 - \frac{W_f}{W_s}\right) \times 100 \quad (7)$$

where W_s is the initial dry weight of the film samples and W_f is the dry weight of the same film specimens after sol-extraction. The analyses were performed in triplicate from two independent UV-cured films and the results averaged.

4 Results and Discussion

4.1 Thiol–Ene Addition of 1,2-disubstituted Alkenes:

4.1.1 *Z/E*-isomerization mechanism and kinetics

Studies on the effect of thiols on the isomerization of fatty acids demonstrate that the reversible addition of thiyl radicals to 1,2-disubstituted alkenes is an important reaction.[39, 48, 90] It is however still unclear which main reaction routes governs the overall reaction system and how the initial ene structure (*cis*- or *trans*-) affects the final coupled product at high conversions. It is vital in polymerization reactions that a high yield of the desired product is achieved at high conversions in order to obtain high molecular weight polymers, *i.e.*, the influence of side reactions should be minimized. In this part of the study the influence of the reversible *cis*/*trans*-isomerization mechanism and kinetics on the efficiency in end-product formation is evaluated by reacting in bulk equally balanced thiol–ene mixtures of methyl oleate (MO) *versus* methyl elaidate (ME) based on TMP-trimercapto propionate ester under photochemical conditions. The purpose is to investigate if this reaction presents enough potential to yield the final coupled C–S product in high conversions and in a timely fashion relevant for the development of cross-linkable polymeric materials that could be used in coating applications.

4.1.1.1 Thiol–ene reaction dynamics

To assess the production rate of primary free-radicals obtained from the photolysis of Irgacure 184 in MO, a series of irradiation experiments were performed at different timed intervals and the resulting solution analysed by UV/Vis-spectrophotometry (Figure 4.1). Irgacure 184 is a Norrish type I photoinitiator (α-cleavage) frequently used in the polymerization of thin-films and coatings given its high efficiency. Under UV-light it decomposes from its lowest triplet state into benzoyl and cyclohexanol radicals which, to a lesser or larger extent, have the ability to abstract hydrogens from thiol groups and produce reactive thiyl radicals.[91-96] An estimate from the initial slope shown in the graph indicates a rate of photolysis of ~1.2×10^{-6} $M^{-1}\cdot s^{-1}$ up to 110 seconds of reaction with a first-order decomposition rate constant, k_d, of ~1.4×10^{-3} s^{-1}. The rate coefficient for the decomposition of photoinitiator was then used in subsequent model simulations of the overall reaction system (Table 2).

RT–FTIR spectroscopy has demonstrated to be a versatile tool for monitoring the course of photoinduced polymerization reactions.[34, 90, 97-100] Figure 4.2 depicts the 3D-spectra evolution of methyl elaidate (ME) during the thiol–ene reaction between methyl oleate (MO) and the trithiol monomer. At the beginning, the reaction system consists of stoichiometric functional group amounts of thiol and ene supplemented with a small percentage of photoinitiator. Immediately upon exposure to UV-light a sharp development of *trans*-unsaturations directly from the *cis*-alkene is observed reaching a maximum at ~40 seconds which then slowly fades out as the intermediary alkyl radical adduct ($A^{\bullet}$) reacts with the thiol monomer to give the coupled thiol–ene product. The observed behaviour goes well along with the conceived *isomerization/propagation–chain-transfer* mechanism.[28, 39, 48]

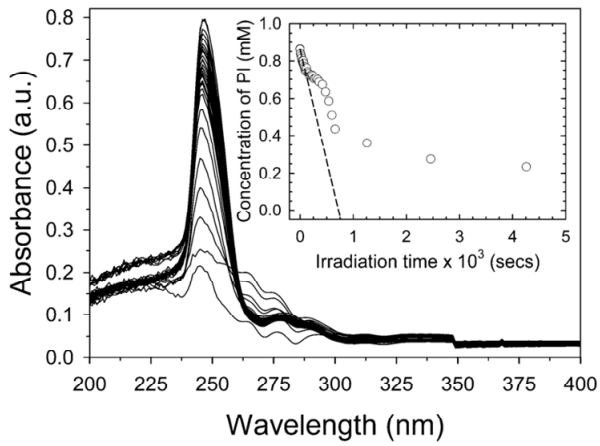

Figure 4.1 Spectral evolution of the main UV/Vis-absorption peak at 247 nm and photoinitiator concentration for a diluted solution of Irgacure 184 in MO. Dashed line indicates the linear decay of PI extrapolated from the first 110 seconds of reaction.

To better evaluate the combined action of the *cis/trans*-isomerization step with the product formation route in the equilibrium, complementary FT–Raman measurements were conducted discontinuously throughout the photoinduced reaction (Figure 4.3). Very early in the reaction the *cis*-peaks appearing at 3010 cm^{-1} (C═C–H, symmetric stretching) and 1652 cm^{-1} (C═C, symmetric stretching, non-conjugated) immediately decreased their intensities followed by a shift towards the formation of a *trans*-ene peak occurring at ~1670 cm^{-1} (isolated C═C *trans*-stretching) which reduced in intensity as the reaction proceeded. Simultaneously, depletion of the thiol peak at ~2576 cm^{-1} was observed over time which further supports the results obtained from RT–FTIR.

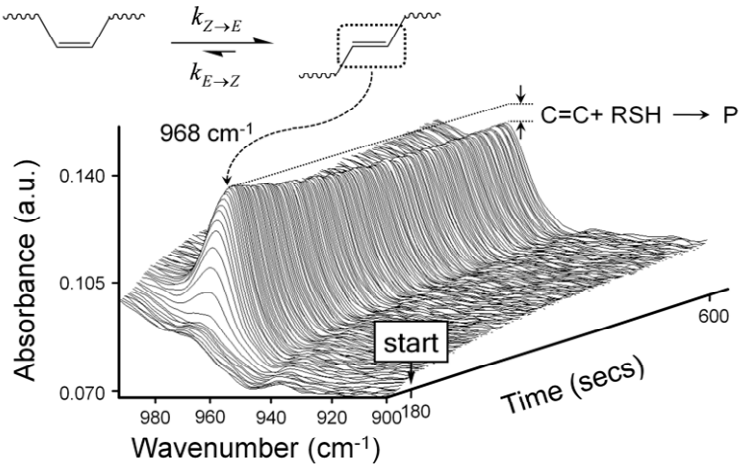

Figure 4.2 Stacked waterfall plot for the RT–FTIR spectra recorded continuously over time showing the 3D-evolution of the *trans*-isomer band from the reaction of an equimolar trithiol/MO mixture in the presence of air and supplemented with 2.0 wt.% Irgacure 184.

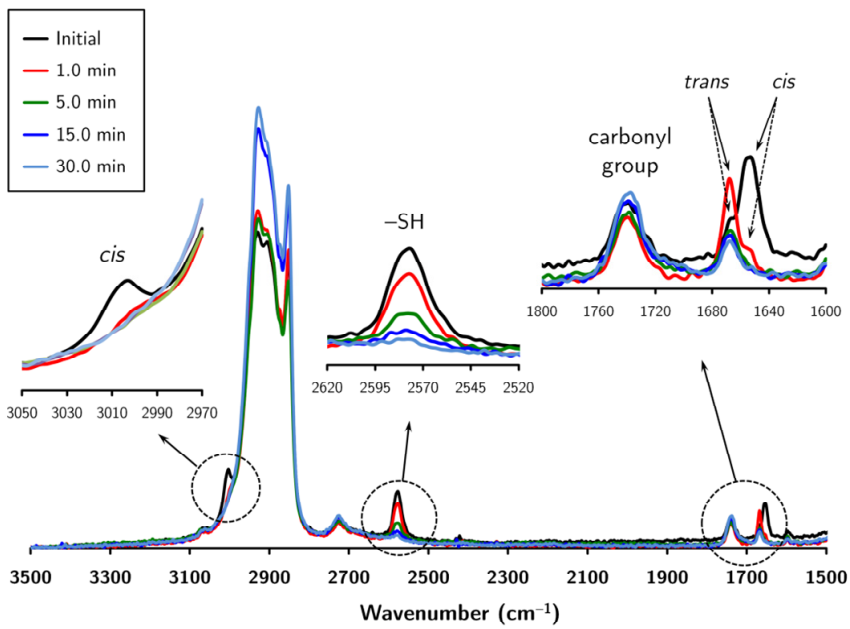

Figure 4.3 Changes observed in the FT–Raman spectra over selected times for the photoreaction of a stoichiometric thiol–ene mixture containing MO.

4.1.1.2 Product formation

To further confirm the existence of the final thiol–ene addition product and quantify the loss of total unsaturations over time, NMR spectroscopy was employed (Figure 4.4). After 30 min of reaction about 80% of double-bonds initially present in the reaction mixture were converted into thioether linkages as shown by ^{1}H NMR. This proves the high efficiency and robustness of the thiol–ene reaction undertaken even when using these *cis*-enes given the high conversions achieved. The signals for the allylic (*CH*$_2$–*CH*, c) and vinylic (*CH*═*CH*, d) protons centered at 2.00 and 5.34 ppm almost completely disappeared, respectively. Also, initial methylene protons (*k*) and (*l*) next to the thiol group significantly decreased their intensity and were shifted slightly as a new signal appeared at the vicinity which strongly suggests the formation of a covalent C–S bond. No important side-reactions were detected such as homopropagation of the 1,2-disubstituted ene nor termination reactions such as the homocoupling of carbon-centered radicals, disulphide formation and the heterocoupling with thiyl radicals thus indicating the viability of this reaction for network forming purposes. Complementary ^{13}C NMR spectra further support these results (results not shown) together with analogous studies reported in the literature.[101, 102] A study published in 2001 based on the photo-addition of 2-mercaptoethanol onto oleic acid is also supportive of the NMR results obtained in this work.[103]

4.1.1.3 Kinetic modeling

In order to verify the reaction scheme proposed in Scheme 3 and give a better view of the dynamic behaviour of the system, a numerical simulation of the kinetics was performed (Table 2). An exhaustive analytical treatment of the reaction kinetics has been reported previously for solutions of MO with β-mercaptoethanol in *tert*-butyl alcohol under photochemical or γ-radiolysis conditions using the steady-state approximation.[39, 48] One particular benefit of numerical kinetic modeling with GEPASI (or COPASI) is that the same kind of mechanistic information can be obtained (graphically) without the need of employing sophisticated mathematical techniques to solve analytically the system of differential equations under unsteady-state conditions. This simple tool offers a convenient and easy methodology to directly test the validity of the detailed mechanism by comparing the simulated kinetic profiles with those obtained from experimentation, disregarding any influence of diffusional effects. Simulation of both reaction systems (MO *versus* ME) confirms the reaction mechanism as demonstrated by the excellent trend-shape agreement with the experimental profiles, despite the observed deviations (Figure 4.5). The differences could be ascribed to an expected increase in the medium viscosity with reaction time slowing down the diffusion of reactants in the system, the existence of parallel competing reactions unaccounted in the model[101], in addition to the evident inaccuracy of the rate coefficients given that measurements were performed at 60°C and not at

room-temperature as stated by the literature values. Despite the visible differences, these are not extremely pronounced to question the mechanism. However, the purpose was not to obtain accurate values for the rate constants but to use the kinetic model proposed as tool for interpreting the experimental results.

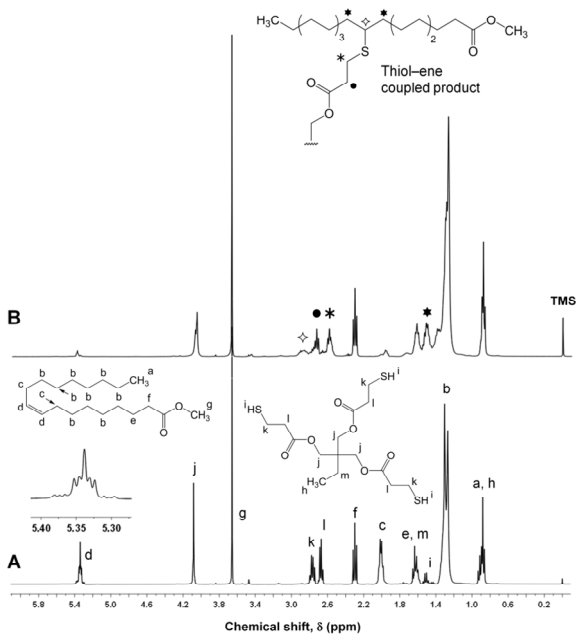

Figure 4.4 ^{1}H NMR spectra of a thiol–ene mixture starting from pure *cis*-isomer (MO). (A) before reaction; (B) after 30 min of reaction at 60°C.

Table 2. Model definition used to generate the numerical simulations in GEPASI.

Reaction Step	Chemical Equation [a]	Rate Constants	References
(1)	$PI \xrightarrow{k_d} 2\,I^{\bullet}$	$k_d \approx 1.4\times10^{-3}\ s^{-1}$	this work
(2)	$I^{\bullet} + RSH \xrightarrow{k_{RSH1}} IH + RS^{\bullet}$	$k_{RSH1} = 1.0\times10^{7}\ M^{-1}s^{-1}$	[39]
(3a)	$RS^{\bullet} + Z \underset{k_f^Z}{\overset{k_a^Z}{\rightleftharpoons}} A^{\bullet}$	$k_a^Z = 1.6\times10^{5}\ M^{-1}s^{-1}$ $k_f^Z = 2.0\times10^{7}\ s^{-1}$	[48] [39]
(3b)	$A^{\bullet} \underset{k_a^E}{\overset{k_f^E}{\rightleftharpoons}} E + RS^{\bullet}$	$k_a^E = 2.9\times10^{5}\ M^{-1}s^{-1}$ $k_f^E = 1.6\times10^{8}\ s^{-1}$	[48] [39, 48]
(4)	$A^{\bullet} + RSH \xrightarrow{k_{RSH2}} P + RS^{\bullet}$	$k_{RSH2} = 1.0\times10^{7}\ M^{-1}s^{-1}$	[39, 48]
(5)	$2\,RS^{\bullet} \xrightarrow{k_t} RSSR$	$k_t = 3.0\times10^{9}\ M^{-1}s^{-1}$	[48]

[a] Initial concentrations: $[PI]_0 = 4.48\times10^{-2}$ M and $[RSH]_0 = [Z]_0 = [E]_0 = 2.21$ M.

According to the analysis, initial configuration of the 1,2-disubstituted double-bonds significantly affects the progress and outcome of the reaction. Aliphatic *trans*-enes are consumed directly into product while showing insignificant reversible conversion into the *cis*-isomer (plot (a)), whereas *cis*-enes are dominantly converted to the corresponding *trans*-form in the beginning of the reaction and then consumed into product as described by the progressive decay of *trans*-unsaturations (plots (c–d)). In this case, before the maximum *trans*-peak is reached the governing route is the conversion of *cis*- into *trans*- unsaturations with only a minor fraction of *cis*-isomer being re-formed from the *trans*-monomer given the reversible condition of the equilibrium, although this was not observed experimentally. It has been shown that preference in formation of *trans*-unsaturations is essentially ascribed to a stabilization of the *E*-transition state which occupies a lower enthalpy level with respect to the *Z*-transition state.[48] By starting with the *trans*-isomer, the higher energy barrier encountered turns difficult conversion into *cis*-unsaturations and the product formation route is strongly favoured.

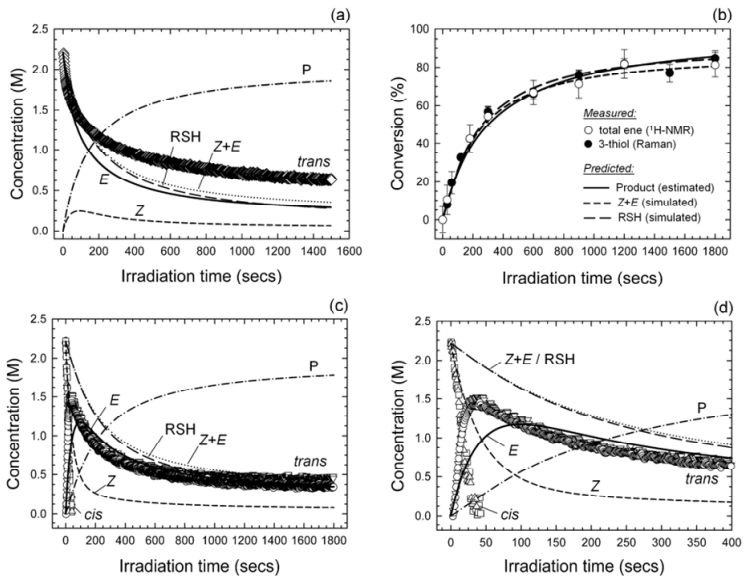

Figure 4.5 Experimental results (symbols) *vs.* simulated data (lines) for the photoreaction of a stoichiometric thiol–ene mixture[†]. (a) concentration–time profiles for a mixture starting with pure *trans*-ene isomer (ME); (b) evolution of conversion (based on absolute moles) for a mixture starting from pure *cis*-alkene (MO); (c) *cis*/*trans*-isomerization of MO with concurrent product formation; (d) *zoom-in* of graph (c) showing the first 400 seconds of reaction. Simulated data for product (P), *cis*-isomer (*Z*), *trans*-isomer (*E*) and thiol (RSH) are given on the inset in each graph. Predicted product line shown in graph (b) was obtained from equation (8).

[†] Initial bulk concentrations for the thiol–ene monomers are given with respect to group functionalities and not to individual chemical compounds.

Within the experimental errors, loss of total unsaturations (*cis*+*trans*) is to large extent matched by the disappearance of thiol groups and reach reasonably high conversions (~80%) after 30 min of reaction as determined experimentally from graph (b). To a first approximation, the thiol–ene coupling reaction into product (P) could be empirically modelled as an 'apparent' second-order kinetics (eqn. (8)), although the deterministic *propagation/chain-transfer* mechanism does not allow this.[39, 48]

$$r_{\text{C-S}}^{\text{app}} = \frac{d[\text{P}]_t}{dt} = k_{\text{obs}}[\text{RSH}]_t[\text{C=C}]_t \qquad (8)$$

Particularly for this case, an 'observed' second-order rate constant, k_{obs}, for the S–C bond-forming reaction indicated a value of ~1.5×10^{-3} $\text{M}^{-1}\cdot\text{s}^{-1}$ obtained from the slope of the linearized (integrated) plot of eqn (8). The results also point out that *cis/trans*-isomerization is extremely rapid when compared with the *chain-transfer* reaction which leads to product. This re-confirms that the rate-determining step controlling the overall reaction is the hydrogen-abstraction from the thiol by the intermediary adduct radical ($\text{A}^{\bullet}$) given that it is the slowest step. All these results are fully consistent with previous findings well documented in the literature.[28, 39, 48, 49]

The work detailed in this first part illustrates the usefulness of the thiol–ene reaction involving naturally occurring 1,2-dialkyl substituted alkenes in the synthesis of sulphide-modified vegetable oils in bulk reaction conditions. The kinetic and mechanistic information collected provides a fundamental basis for the design of real photocurable systems involving multifunctional thiol–ene monomers intended for new materials and coating applications. One possible example, and if miscibility in bulk permits, consists of incorporating multifunctional thiols as crosslinking agents in drying oils or alkyd resin formulations as a means of increasing the curing rate in outdoor surface coatings without need to utilize environmentally unfriendly metal catalysts as air-drying accelerators or their substitutes.[57] This would enable the creation of a semi-synthetic coating system but still too a large extent composed of unmodified renewable alkene structures.

4.1.2 Globalide/ε-caprolactone-based thermosets

In this second part a different approach is utilized to investigate if the thiol–ene coupling reaction involving 1,2-disubstituted alkenes is still feasible when a mobility restriction factor is introduced into the system, as consequence of crosslinking, given the sluggish reactivity of these enes.[104-107] The purpose is to establish a relationship between initial ene-density, UV-cure thiol–ene kinetics and resulting conversion, and how the final crosslinked network structure affects the thermal and viscoelatic properties of the photocured polymers.

As role model pre-polymers for these studies a series of linear aliphatic polyesters derived from the macrocyclic lactone *globalide* (GI) were employed. Globalide (11/12-pentadecen-15-olide) is a synthetic unsaturated analogue of the naturally occurring fragrance *ambrettolide* (Am), widely used by the perfume industry due to its strong musky odour and ability to lose scent slowly.[72] These unsaturated polyesters have been successfully synthesized by lipase catalysed polymerization (Figure 4.6) using ε-caprolactone (ε-CL) as intercalating monomer to provide random alkene copolymers with different degrees in ene-functionality along the backbone.[72, 108] The amount of globalide was adjusted between 10–50 mol.%, depending on how much caprolactone was introduced by the enzyme (Table 3). The 1,2-disubstituted enes of poly(globalide) (PGI) and related polyesters such as poly(ambrettolide) (PAm), has successfully allowed the thermal crosslinking in the molten-state with dicumyl peroxide (DCP) affording fully transparent network structures that contrasted significantly with the semi-crystalline morphology of the initial polymers.[72] The same approach was used by means of employing copolyesters derived from GI (or Am) in combination with 1,5-dioxepan-2-one (DXO), ε-caprolactone (ε-CL) or 4-methyl caprolactone (4MeCL) affording essentially the same results as with PGI and PAm alone.[108] In a recent study based solely on PGI was demonstrated the effectiveness of the thiol–ene reaction as a new straightforward methodology for the side-chain functionalization of these polymeric enes with butyl-3-mercaptopropionate, mercapto-1-hexanol and *N*-acetylcysteamine that could be aimed at a myriad of purposes.[102] It would however be of more interest if the alkene polymers could be reacted directly without any intermediate modifications. Here is reported the utility of the thiol–ene coupling reaction as an efficient chemistry for the direct crosslinking of these unsaturated groups to high conversions and at reasonable reaction rates that could be of utility for practical applications.

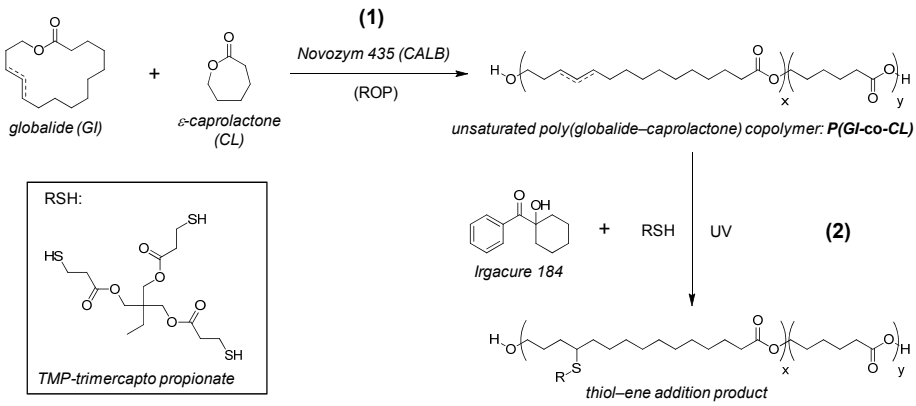

Figure 4.6 Enzymatic ring-opening copolymerization of globalide/ε-caprolactone monomers (1) followed by thiol–ene UV-curing of the poly(globalide–caprolactone) copolymers with a tri-functional thiol in the presence of photoinitiator (2). Copolymer synthesis and characterization are reported elsewhere.[72, 108]

Table 3. Properties of the synthesized polymers. General enzymatic polymerization process and characterization of the (co)polymers can be found elsewhere.[72, 108]

Polymer	Molar composition (G:C) [a]	M_n [b] (g·mol^{-1})×10^3	DI (Đ) [b]	DP [b]	1,2-disubstituted ene functionality [c]
P(G:C) 100:1	100:0	15.0	2.8	65	65
P(G:C) 50:50	47:53	20.0	3.3	118	55
P(G:C) 40:60	40:60	21.0	3.0	125	50
P(G:C) 30:70	32:68	23.0	2.4	152	49
P(G:C) 20:80	22:78	18.0	2.8	125	28
P(G:C) 10:90	10:90	16.0	2.4	125	13

[a] Determined by ^{1}H NMR. [b] Determined by SEC in THF at 40°C using PS standards.[108] [c] Number of ene functionalities per copolymer chain.

4.1.2.1 Thiol–ene curing kinetics and conversion

To investigate the direct influence of functional ene-density on the thiol–ene curing kinetics the various polymers differing in amount of unsaturations along the aliphatic chain were exposed to UV-light and the progress of the reaction monitored *via* RT–FTIR spectroscopy. It was postulated that an increased dilution of double-bonds would make the system exhibit low reactivity early in the reaction due to thiol inaccessibility caused by a wider average spacing between unsaturated groups along the chain and then as the level of crosslinking increased higher conversions would be reached because of proximity effects. Conversely, a system based on higher density of unsaturations would cure faster initially but then reach a higher plateau with less conversion as a consequence of severe diffusion limitations, mobility restriction and seclusion of functional groups caused by the locked network structure (gel-point) (Scheme 6). The assumption is fairly consistent with results obtained from previous studies using DCP as curing agent.[108] In addition, it is well known from traditional multifunctional thiol–ene systems that the incipient gelation (x_c) can be easily predicted using the classical Flory-Stockmayer theory of gelation[109, 110], given by equation (9), and so if $f_{ene} \gg f_{thiol}$ as one would anticipate for linear polyfunctional ene polymers, then the onset of gelation would occur at fairly low thiol–ene conversions.[16, 111] In fact, according to the expression, using PGI as the highest ene-density polymer, a critical conversion at gel point of ~0.09 is attained which represents only 8.84% of the gel-point obtained (x_c=0.5) if standard tri-functional thiol–ene comonomers were reacted at the same functional group stoichiometry ($r = [\mathrm{RSH}]_0/[ene]_0 = 1$).

$$x_c = \frac{1}{\sqrt{r\,(f_{thiol}-1)(f_{ene}-1)}} \tag{9}$$

Surprisingly, by using these polymeric main-chain alkenes *via* the thiol–ene reaction, no dramatic differences were observed experimentally as all kinetic profiles showed essentially the same range in decay values while attaining near-quantitative conversions. The multiple curves over time are illustrated in Figure 4.8 using the example given in Figure 4.7 as demonstrative spectra. Obtaining similar curves for all copolymers, including the pure PGI, infers that the overall polymerization rate (expressed as $M \cdot s^{-1}$) increases with ene-functionality as expected since the density of ene is directly proportional to the globalide content incorporated. The existence of comparable final conversions to all reaction systems irrespective of comonomer feed ratios indicates that the step-wise growth mechanism leading to delayed gel-point, in association with high chain mobility owed to low T_g values (Table 5), allows the reactive groups to continue accessible throughout the cure until very high conversions are attained. A dynamic balance between kinetics and mobility established within the network seems therefore to exist. This distinctive feature has beneficial implications in the network formation process enabling the adjustment of the resulting mechanical properties without significant interference of structural restraints, *i.e.*, changes in cure behaviour. Moreover, it was found that these 1,2-disubstituted enes can be crosslinked to high conversions at reasonable reaction rates. Conversion up to ~87% can be seen already at 5.7 min reaching a maximum of ~95% near the end of the polymerization (Figure 4.8). Also, from Table 4, relatively high thiol–ene film conversions (76–92%) with only minute amounts of sol-content extracted (≤11%), indicates the formation of final C–S linkages in high yields for all the networks. This was further supported from exploratory NMR tests of leached sol-fractions which showed mostly thiol–ene coupling with no evidence of important side-reactions such as homopolymerization of the ene monomer (results not shown). Indeed, it is well known that 1,2-disubstituted enes exhibit very poor ability for homopolymerization since they are electron-rich.[28, 112] All these results agree well with the conclusions achieved in the previous section on monounsaturated oils thus allowing an extensive array of natural alkenes of this kind to be exploited in new crosslinkable systems.

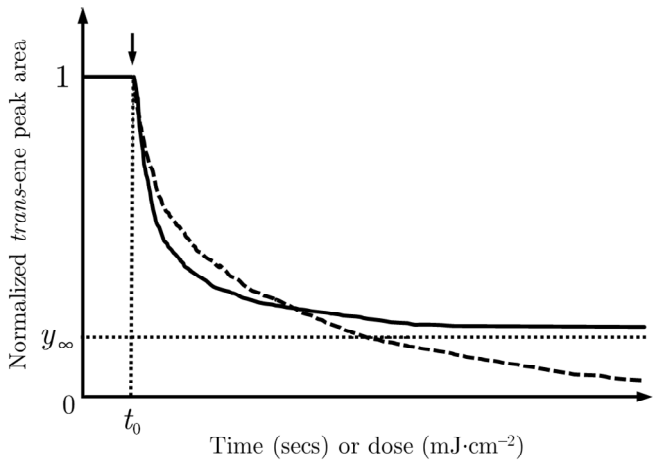

Scheme 6. Hypothesized effect of double-bond dilution on photocure behaviour. Low content ene-density copolymers (dashed line). High content ene-density copolymers (solid line). Arrow denotes the start of the UV-induced thiol–ene polymerization.

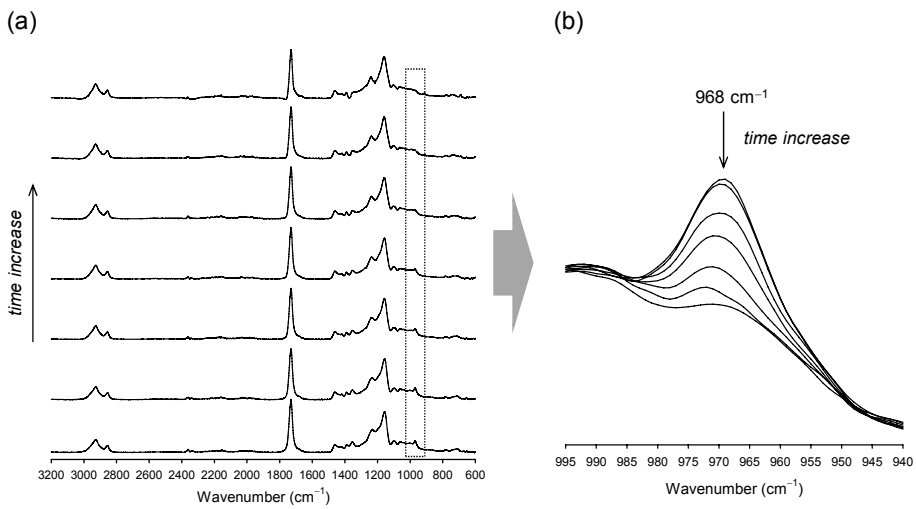

Figure 4.7 Changes observed in the IR-spectra at selected reaction times of the photoinduced thiol–ene crosslinking involving the copolymer P(G:C) 32:68 as monitored by RT–FTIR (representative spectra). (a) overall spectra taken at time = 0, 60, 98, 116, 172, 278 and 1800 seconds, (b) region of interest showing the time-consumption of *trans*-double bonds.

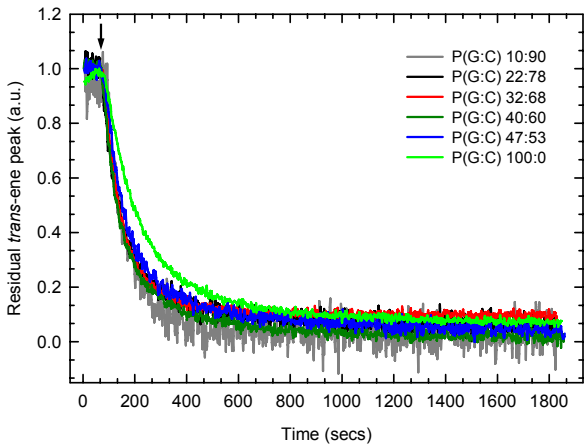

Figure 4.8 Kinetic RT–FTIR profiles showing the temporal decay of residual *trans*-isomer for all P(GI-*co*-CL) copolymers upon photoinduced thiol–ene reaction with the trithiol crosslinker. Original *trans*-peak area curves were corrected using the analytical procedure appended in **Paper II**. Arrow indicates the start of the photoinduced polymerization after a waiting period of 1 min.

4.1.2.2 Characterization of thermosets

Polymers are often crosslinked to improve the thermo-mechanical properties. All P(GI-*co*-CL) polyesters were photo-crosslinked in the melt with equal mole amounts of the tri-functional thiol with respect to the amount of ene functionality by irradiating with the UV-fusion lamp. In order to evaluate the final properties of the resulting tridimensional networks, the films were characterized with respect to the curing performance (FT–Raman spectroscopy), residual sol-fraction (leaching tests) and thermal and viscoelastic behaviour (DSC and DMTA measurements).

FT–Raman results displayed in Table 4 indicate that the extent of conversion in most of the thiol–ene films is higher than 80% and superior than thermally cured copolymers.[74] This indicates that incorporation of caprolactone does not seem to have a significant impact on enhancing the overall conversion of the 1,2-disubstituted ene functionality in the thiol–ene coupling reaction as was initial theorized.

The copolymers were also evaluated with respect to the ability to homopolymerize *via* free-radical chain growth in total absence of thiol monomer. The results shown in Table 4 indicate that most of the copolyesters display very low degrees of homopolymerization except for the f-H (G:C) 30:70 and f-H (G:C) 20:80 where slightly higher conversions were attained. This could be attributed to the development of an optimal balance between chain mobility and density in

functional groups within the system when compared to f-H(G:C) 10:90 where conversion decreases again. Moreover, conventional chain-growth homopolymerizations are well-known to constrain chain mobility at much lower conversions than polymerizations growing in a step-wise manner as is the case of the thiol–ene reaction. For the thiol–ene system the extent of homopolymerized ene occurring in parallel with the thiol–ene reaction was negligible as the second route proceeds much faster than competing chain-growth.

Table 4. Conversion degrees and leaching tests results (thiol–ene films).

Polymer Composition	**Ene–Ene Conversion (mol.%) [a]**	**Thiol–Ene Conversion (mol.% ± SD) [b]**	**Sol Content (wt.% ± SD) [c]**
P(G:C) 100:0	14.2	76.7 ± 2.3	1.0 ± 0.6
P(G:C) 50:50	3.3	85.3 ± 5.4	2.7 ± 0.7
P(G:C) 40:60	12.6	91.5 ± 1.8	3.6 ± 0.2
P(G:C) 30:70	52.4	83.5 ± 4.1	4.1 ± 0.04
P(G:C) 20:80	31.9	86.8 ± 4.2	5.9 ± 0.5
P(G:C) 10:90	12.2	82.1 ± 4.2	10.6 ± 1.3

[a] Measured by FT–Raman for the homopolymerized films (cured without trithiol in the initial mixtures); [b] Determined by FT–Raman: numbers are expressed as the average ± SD of individual conversion values of thiol and ene functional groups; and, [c] Measured gravimetrically.

Leaching tests were performed on the different films to assess the efficiency of the thiol–ene reaction in the formation of networks based on linear P(GI-*co*-CL) polyesters. The results presented in Table 4 reveal a clear relationship between initial ene functionality, crosslink density and soluble fractions occluded within the networks. Although all the films reached reasonably high thiol–ene conversions, the unbound sol-fraction decreases proportionally with increasing globalide content as the result of increasingly higher crosslink densities of the final networks. It is worth noting, however, that the soluble fraction is rather low in all cases showing equivalent gel-content to thermally cured films.[74]

Table 5. Thermal properties as determined from DSC melting curves (second heating).

	T_g (°C)			T_m (°C)			Crystalline Melt Exotherm (J·g^{-1})		
		Homo–Ene			Homo–Ene			Homo–Ene	
Composition	Polymer	Films	TE–Films	Polymer	Films	TE–Films	Polymer	Films	TE–Films
G:C 100:0	—	—	—	46.2	44.3	—	73.7	56	—
G:C 50:50	–49	—	–32	31.9	33.0	—	39.9	47	—
G:C 40:60	—	—	–46	29.5	26.8	—	50.7	44	—
G:C 30:70	—	—	–42	34.7	30.8	—	63.0	56	—
G:C 20:80	—	—	–46	38.6	34.5	–2	60.9	57	6
G:C 10:90	—	—	—	49.8	42.0	28	55.6	55	29

With respect to the thermal properties measured by DSC (Table 5) it can be observed for the copolyesters with a mole content in G:C of 100:00 and 10:90 that the melting temperature (T_m) is the highest, ~50°C, but decreases to about 30°C once equimolar amounts in G:C of 50:50 are incorporated in the copolymers. The T_g could not be detected for most of the P(GI-*co*-CL) copolymers, a consequence of either high crystallinity or it value is below the detection limit offered by the DCS instrument (–60°C). The same lack of T_g values follows for the homopolymerized films since the degree of curing obtained was very low. However, the different levels of caprolactone incorporated in the copolymers resulted in thiol–ene films exhibiting T_g's between –32°C (f-TE(G:C) 100:0) to about –45°C (f-TE(G:C) 30:70). As the relative amount of caprolactone increases the crystallinity of the thiol–ene networks also increases which results in a reduction of the T_g values. Once the mole content of caprolactone reaches 80:20 relative to that of globalide no glass-transition is observed due to the high crystallinity. The homopolymerized films exhibit a reduction in the crystallinity upon UV-cure moving from pure polyglobalide to a ratio of G:C of 40:60; but since the conversions were also very low a large degree of crystallinity still remains. The thiol–ene films with a mole content in G:C of 100:0 to 30:70 lose all the crystallinity, but once the crosslink density drops and the ene fraction decreases (with 70 and 80% caprolactone content), crystallinity appears. The last column entries of Table 5 show the amount of crystallinity in the networks and further confirm these points.

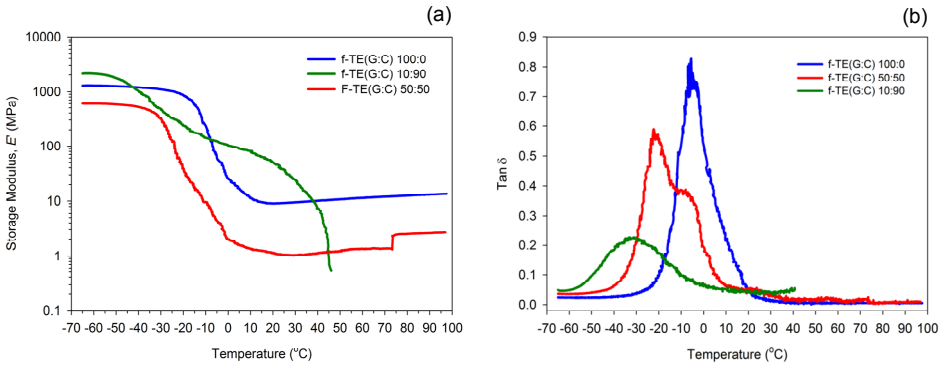

Figure 4.9 Dynamic mechanical thermal analysis plots of storage modulus (left) and loss tangent, tan δ, (right) as a function of temperature for thiol–ene networks photocured from (co)polymers bearing different comonomer ratios.

DMTA results shown in plots (a) and (b) of Figure 4.9, provide a complementary analysis to the previous DSC results and allows evaluating the thermal and viscoelastic properties of the final crosslinked networks. In DMTA, a sinusoidal mechanical stress is applied to the sample and the resulting sinusoidal strain is measured by the instrument. DMTA can be used to obtain the storage modulus (E'), glass-transition temperature (T_g) and determine the level of structural homogeneity. The crosslink density is normally determined by the storage modulus at the rubbery plateau: the higher the level of this plateau relative to the other curves, the higher the amount of crosslinks per unit volume of material. The storage (elastic) modulus gives a measure of the amount of energy stored by the material during one oscillating cycle, whereas the loss (viscous) modulus measures the amount of energy dissipated (as heat) during the same oscillating cycle. The ratio, of the loss and storage moduli, E''/E', affords the loss tangent (tan δ), a damping factor, which relates the energy dissipation relative to the energy stored within the material when the sample specimen is subjected to periodic deformation. The degree of homogeneity is usually quantified by the shape of the tan δ curve *versus* temperature determined by the full-width-at-half-maximum peak height ('fwhm'), which also specifies the nominal range in T_g. A narrow and symmetrical (unimodal) curve characterizes a very homogeneous material with equal distribution of crosslinks throughout the whole network whereas a broad and/or asymmetrical (bimodal) curve describes a material with uneven distribution of crosslinks, disordered topology and presence of residual crystallinity. The intensity of maximal tan δ value at the T_g is related with the degree of mobility of the chain segments between crosslinks at this particular temperature. Higher peak intensities reflect greater energy loss and, therefore, more viscous behavior; whereas lower intensities characterize more elastic behavior (*i.e.*, more energy is stored within the material).

Thermo-mechanical properties of the final networks represented by the thiol–ene films: f-TE(G:C) 100:0, f-TE(G:C) 50:50, and f-TE(G:C) 10:90 were investigated in order to determine the effect of intercalated caprolactone on the storage modulus, T_g and crosslink homogeneity. The analyses were performed between –70°C and 140°C although the results are reported only up to 100°C. As shown in Figure 4.9-a the storage modulus (E') versus temperature show very similar traces for the crosslinked thiol–ene films f-TE(G:C) 100:0 and 50:50, indicating that the corresponding networks exhibit similar crosslinking patterns; although the modulus at the rubbery plateau region is higher for the f-TE(G:C) 100:0 due to an increased crosslink density. This effect is translated into an increment in T_g from approximately –20°C to about 0°C and more uniform network structure as shown in Figure 4.9-b. The presence of crystallinity is furthermore observed above T_g for the least crosslinked system. A narrower tan δ peak is also seen with increased crosslinked density showing the influence of a step-wise crosslinking mechanism. The height of the tan δ peak increases with crosslink density. The cause of this trend is not fully clear since not only the crosslink density is changed but also variations in polarity, chain rigidity, and presence of crystallinity occur at the same time.

The synergistic interplay between crosslink density, network uniformity, extent of thiol–ene conversion *versus* homopolymerization degree, mode of assembly (chain-growth *versus* step-growth), topology, level of mobility and rigidity of the chains, and secondary force interactions between chain all determine the thermal and viscoelastic properties of the final thermosets.

4.2 Terpene-Based Renewable Thermosets:

4.2.1 Thiol–ene coupling kinetics of *D*-limonene: model studies, mechanism and selectivity

In this section a systematic kinetic study is performed to evaluate the reactivities of the exocyclic (*exo*) and endocyclic (*endo*) unsaturations occurring in *D*-limonene towards free-radically induced thiol–ene photo-additions involving two mono- and tri-functional thiol monomers (as model compounds) bearing a propionate ester moiety. A simplified mechanistic kinetic model of the coupling reaction is first developed and tested *via* dynamic numerical simulations in an attempt to explain the observed double bond selectivity measured from experimental conversion data. The purpose is to establish a correlation between alkene structure and reactivity and identify the fundamental phenomena behind the differences in double bond reactivity towards this particular class of thiol. The model is then extended to include secondary coupling reactions and the effect of the initial reaction conditions such as starting thiol–ene stoichiometry is evaluated to determine the potential applicability of *D*-limonene in the design of multifunctional macromonomer resins. A detailed analytical treatment of the reaction kinetics (mechanistic and empirical), as well as assumptions adopted, can be found in **Appendix** and **Papers III** and **IV**, respectively. Equation numbers referred in sub-section 4.2.1.1 are exclusively from kinetic expressions derived in the **Appendix** section.

4.2.1.1 Relative reactivity: kinetic analysis and modeling

To evaluate the discriminative power of both double bonds regarding thiol–ene additions, limonene (**1**) was first reacted at room-temperature in $CDCl_3$ solution separately with each of the two thiol compounds (**2** or **6**), mixed on a half-mole alkene group stoichiometry in respect to the thiol, in the presence of a small amount of DMPA (Scheme 7). Observed concentrations obtained experimentally from ^{1}H NMR measurements of each double bond conversion indicate that the consumption rate of limonene (or thiol functional groups) can be approximated to an empirical second-order power-law kinetics, eqn (13), giving an estimated value of $k_{obs} = 4.98\times10^{-4}$ $M^{-1}\cdot s^{-1}$ (Figure 4.10-a). In fact, $[RSH]_t < [Lim]_t$ attributed to the unavoidable occurrence of secondary coupling reactions leading to formation of compound **5**; however, for simplification purposes it can be assumed that $[RSH]_t \approx [Lim]_t$ since at this particular stoichiometry the impact of di-addition reactions can be considered insignificant (see next sub-section for further details). Two individual empirical factors, denoted by $m_{1,2}$, characterizing the reactivity of each double bond, could be easily determined by plotting $\Delta[ene]_t$ *versus* $\Delta[Lim]_t$ according to plot (b) displayed in Figure 4.10. More correctly, $\Delta[ene]_t$ should have been plotted against $\Delta[ENE_T]_t$ since this was the quantity

that was effectively measured from total conversion of double bonds (*exo*+*endo*). Nevertheless, if secondary coupling reactions are neglected or the influence of di-addition product (**5**) formation is considered negligible when compared to formation of mono-addition products (**3** and **4**), then $[ENE_T]_t$ approaches $[Lim]_t$ and $\Delta[ENE_T]_t \approx \Delta[Lim]_t$. Applying eqn (19), one finds the individual values of the two overall second-order rate parameters, $k_1 = 4.32\times10^{-4}$ $M^{-1}\cdot s^{-1}$ and $k_2 = 6.62\times10^{-5}$ $M^{-1}\cdot s^{-1}$, for the *exo*- and *endo*- coupling routes (cycles **I** and **II** in Scheme 8), respectively. As a result, the discrete concentration profiles (Figure 4.10-c) could be reconstructed with extremely high fidelity by means of eqn (14) describing the consumption of limonene (or RSH groups), and eqn (24) describing the depletion of alkene functional groups. The notable regular level of overlap between experimental data obtained from mono- and tri-functional thiol–ene systems verifies the expected independence of thiol monomer functionality on conversion rate. A double bond selectivity, $S_{exp} = 6.54$ was thus obtained by applying empirical eqns (16), (21) or (22).

Contrarily to the measured selectivity, S_{exp}, which is independent of the conditions of initiation and valid throughout the entire course of the reaction; the numeric values of the individual empirical parameters ($m_{1,2}$), consumption rates ($r_{1,2}$, and $r_{Lim\ or\ RSH}$) and overall rate coefficients (k_{obs} and $k_{1,2}$) are all function of the reaction conditions specified for this particular thiol–ene system.

To confirm unequivocally the validity of the sequential reaction mechanism proposed in Table 6 and support the value obtained for the measured selectivity, numerical kinetic simulations were computed in COPASI in an attempt to extract the 'apparent' values of the individual rate coefficients intrinsic to the *propagation* (*addition–elimination*) and *chain-transfer* (*hydrogen-abstraction*) steps describing the two coupling cycles (Scheme 8). The values used as inputs into the model are listed in the first right-hand side column, whereas the output values returned by the software, by best-fitting recursively the mechanistic model to the experimental data points, are listed in the second right-hand column. Within tolerance errors, the simulated output concentration profiles presented in Figure 4.10-d are in excellent agreement with the discrete data which validates the mechanism. The estimated kinetic coefficients were then used in the analysis of the detailed mechanism by assuming the steady-state approximation in order to elucidate the fundamental factors governing the reactivities of the two distinct unsaturations.

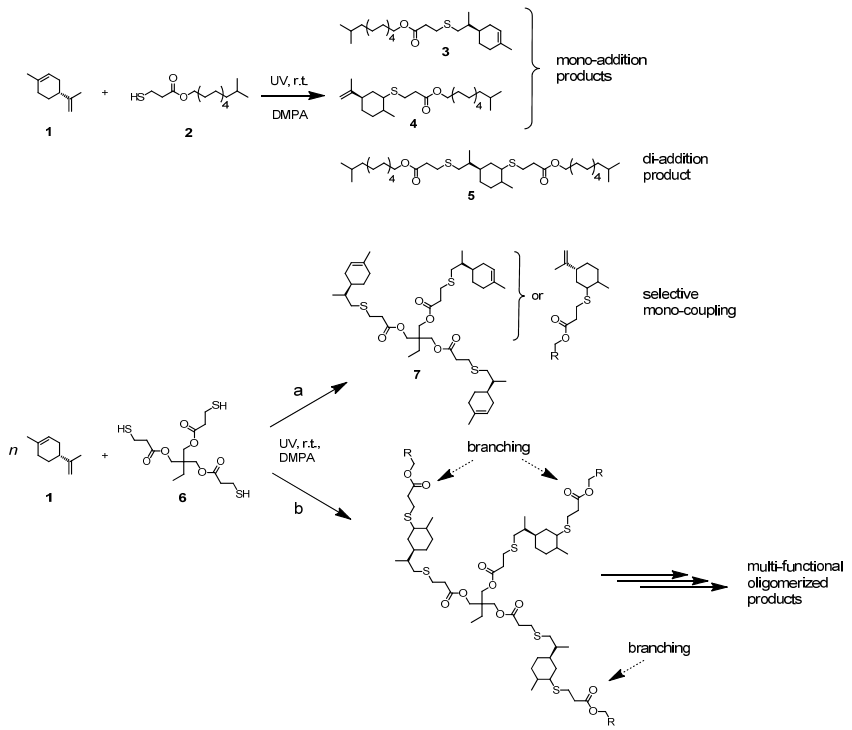

Scheme 7. Thiol–ene coupling between *D*-limonene (**1**) and mono- (**2**) or tri-functional (**6**) propionate ester thiols accounting both for primary (mono-additions) and secondary (di-addition) reactions. Pathways (a) and (b) denote preferential formation routes depending on initial co-reactant stoichiometry.

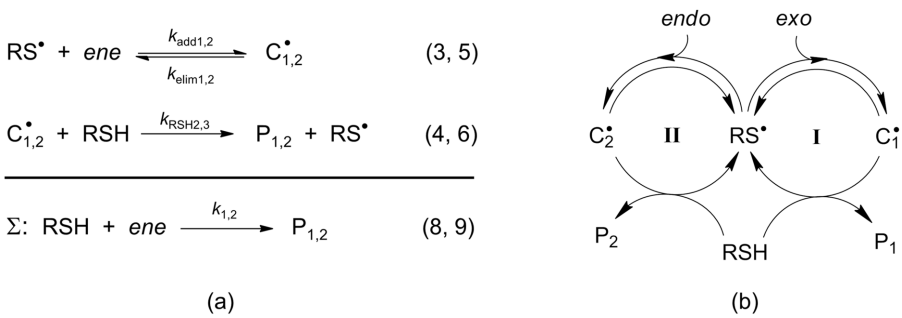

Scheme 8. Two-route linear step-growth mechanism sharing a common radical intermediate (RS$^\bullet$). (a) elementary propagation/chain-transfer steps; and, (b) corresponding cyclic representation describing the thiol–ene reaction involving the two unsaturated structures of limonene (*exo* and *endo*). The algebraic sum sign (Σ) denotes overall (observed) coupling reactions described by the underlying mechanism. The terminology '*ene*' represents either '*exo*' or '*endo*' unsaturations in limonene.

Table 6. Kinetic model definition used to generate the numerical simulations in COPASI.

Reaction Step	Chemical Equation	Rate Constants	
		Literature Values [a]	Estimated Values [b]
(1)	$PI \xrightarrow{k_d} I^{\bullet}$	—	$k_d = 1.0\times10^{-4}\ s^{-1}$
(2)	$I^{\bullet} + RSH \xrightarrow{k_{RSH1}} IH + RS^{\bullet}$	$k_{RSH1} = 1.0\times10^{7}\ M^{-1}s^{-1}$	—
(3)	$RS^{\bullet} + exo \underset{k_{elim1}}{\overset{k_{add1}}{\rightleftharpoons}} C_1^{\bullet}$	$k_{add1} = 1.6\times10^{5}\ M^{-1}s^{-1}$ $k_{elim1} = 2.0\times10^{7}\ s^{-1}$	$k_{add1} = 2.0\times10^{6}\ M^{-1}s^{-1}$ $k_{elim1} = 8.5\times10^{7}\ s^{-1}$
(4)	$C_1^{\bullet} + RSH \xrightarrow{k_{RSH2}} P_1 + RS^{\bullet}$	$k_{RSH2} = 1.0\times10^{6}\ M^{-1}s^{-1}$	$k_{RSH2} = 5.4\times10^{5}\ M^{-1}s^{-1}$
(5)	$RS^{\bullet} + endo \underset{k_{elim2}}{\overset{k_{add2}}{\rightleftharpoons}} C_2^{\bullet}$	$k_{add2} = 2.9\times10^{5}\ M^{-1}s^{-1}$ $k_{elim2} = 1.6\times10^{8}\ s^{-1}$	$k_{add2} = 1.4\times10^{6}\ M^{-1}s^{-1}$ $k_{elim2} = 6.6\times10^{8}\ s^{-1}$
(6)	$C_2^{\bullet} + RSH \xrightarrow{k_{RSH3}} P_2 + RS^{\bullet}$	$k_{RSH3} = 1.0\times10^{6}\ M^{-1}s^{-1}$	$k_{RSH3} = 6.0\times10^{5}\ M^{-1}s^{-1}$
(7)	$2\ RS^{\bullet} \xrightarrow{k_t} RSSR$	$k_t = 3.0\times10^{9}\ M^{-1}s^{-1}$	—

[a] Partially taken from literature[39, 48]. [b] Computed from the parameter estimation task that COPASI has built-in. Model definition accounts only for primary coupling reactions taking place selectivity at each double bond. Details on the estimation of the value of k_d can be found in appended **Paper III**.

Table 7.
Analysis of kinetic results obtained from model computations in COPASI.

Cycle	Reversibility	Kinetic Ratio	Eq. Constant (M^{-1})
	($k_{elim1,2}/k_{add1,2}\times[ene]_t$)	($k_{add1,2}/k_{RSH2,3}$)	($K_{eq1,2} = k_{add1,2}/k_{elim1,2}$)
I	18 ($[exo]_0$)	3.7	2.35×10^{-2}
	128 ($[exo]_\infty$)	—	—
II	201 ($[endo]_0$)	2.3	2.12×10^{-3}
	233 ($[endo]_\infty$)	—	—

Coefficient Ratios			
k_{add1}/k_{add2}	k_{elim2}/k_{elim1}	$K = K_{eq1}/K_{eq2}$	k_{RSH2}/k_{RSH3}
1.43	7.76	11.2	0.91

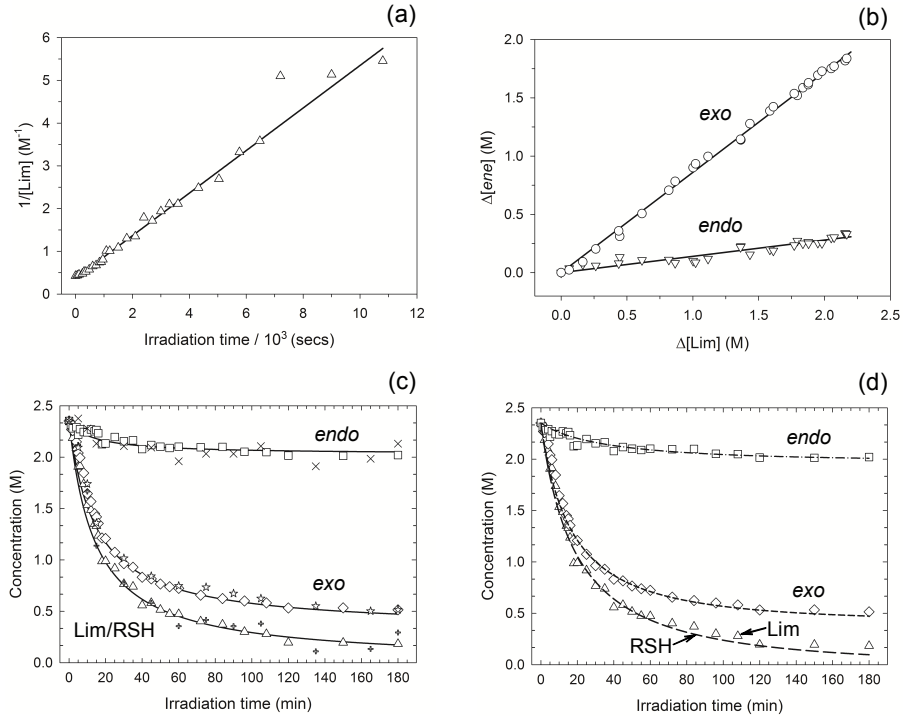

Figure 4.10 Observed and simulated reaction kinetics plots used to estimate the empirical parameters, 'apparent' rate coefficients and selectivity. (a) determination of k_{obs} from linear regression of the reciprocal data points describing the consumption of limonene (R^2 = 0.98); (b) linear regression fits to the measured variables: m_1 = 0.87 (R^2 = 0.98), m_2 = 0.13 (R^2 = 0.90), with $\Delta[ene] = [ene]_0 - [ene]_t$; (c) comparison between fitted curves and overlapped concentration profiles from experimental kinetic evaluations with monofunctional (open signs and star) and tri-functional (closed markers) thiols; and, (d) comparison between experimental data (symbols) and simulated model predictions (lines). Thiols and limonene were mixed on a 1:0.5 thiol–ene mole stoichiometry with respect to chemical functional groups and diluted with ~50 wt.% of $CDCl_3$ solvent. DMPA (1.0 wt.% total) was used as photoinitiator and the samples irradiated with a UV-light intensity of 4.2 mW·cm^{-2} at room-temperature under constant magnetic stirring (10^3 rpm).

The kinetic results compiled in Table 7 derived from the mechanism offer insights about the main possible causes responsible for the differences in reactivity observed for the two double bonds. For instance, the high extent of reversibility of the second propagation step over the first, $k_{elim2}/k_{add2}\cdot[endo]_t \gg k_{elim1}/k_{add1}\cdot[exo]_t$, associated with large differences in the addition and fragmentation ratios with respect to the two propagation steps appreciably outweighs the second thiyl-ene propagation route (step 5). Moreover, the 'apparent' equilibrium constants for

addition/elimination reactions show that $K_{eq1} \approx 11.2 \cdot K_{eq2}$ in full support of the preceding analysis. Since the two intermediate carbon-centered radicals appear to display equivalent radical stabilization in the chain-transfer steps, $k_{RSH2} \approx k_{RSH3}$, most probably ascribed to very similar geometric tertiary structures, in addition to a value of ~1.4 for the insertion coefficients ratio, k_{add1}/k_{add2}, which rules out any major contribution of steric hindrance and/or electron-density effects in the thiyl-ene addition steps, then differences observed in the selectivity seem to be dictated by preferential β-cleavage of the $C_2^\bullet$ radical over $C_1^\bullet$. As the $[C_1^\bullet]_t > [C_2^\bullet]_t$ throughout the reaction, then the rate-limiting step controlling the overall reaction is identified as the third chain-transfer reaction (step 6) given that it is the slowest step. Finally, by using eqn (6) defining the selectivity based on the mechanism, one obtains $d[exo]_t/d[endo]_t \approx 10.1$ with $[RSH]_0 = 2.4$ M; and, using eqn (7) when $k_{RSH2,3} \cdot [RSH]_t \to 0$ (in s^{-1}) one obtains $d[exo]_t/d[endo]_t \approx 10.22$. The rather close numeric values and magnitude returned by these two equations, not only reveal that **cycle I** shows a faster coupling effectiveness over **cycle II** but also the contribution of the chain-transfer routes to the relative double bond reactivity is negligible; this being explained predominantly by the propagation steps. Furthermore, the two figures represent slightly less than the double of the observed selectivity, which proves the suitability of the analytical approach in describing the global kinetics. An additional support of this statement comes from eqn (11) which affords the values: $k_1 = 3.7\times10^{-4}$ $M^{-1}\cdot s^{-1}$ and $k_2 = 3.65\times10^{-5}$ $M^{-1}\cdot s^{-1}$. The two values agree extremely well with those resulting from experimentation. In the same manner, by applying eqn (28a) yields the values: 1.3×10^4 $M^{-2}\cdot s^{-1}$ for **cycle I**, and 1.3×10^3 $M^{-2}\cdot s^{-1}$ for **cycle II** (left member of equation), which also lie very close to the corresponding values obtained from observed kinetics; *i.e.*, 1.5×10^4 $M^{-2}\cdot s^{-1}$ for **cycle I**, and 2.3×10^3 $M^{-2}\cdot s^{-1}$ for **cycle II** (right member of equation).

Altogether, these kinetic results can be simply interpreted in terms of relative energies of the two tertiary carbon-centered radicals as illustrated by the partial reaction profile in Figure 4.11. Assuming essentially equal pre-exponential (frequency) factors for the Arrhenius dependences in the elementary thiyl–ene insertion/elimination steps, it is easily verified the two following relationships:

$$\ln\left(\frac{k_{add1}}{k_{add2}}\right) = \frac{E_{a2} - E_{a1}}{RT} \qquad (10\text{-}1); \qquad \ln\left(\frac{k_{elim2}}{k_{elim1}}\right) = \frac{E_1 - E_2}{RT} \qquad (10\text{-}2)$$

After the thiyl–ene addition transition state, the intermediate radical $C_2^\bullet$ occupies a higher energy level relative to $C_1^\bullet$ of ~5.1 $kJ\cdot mol^{-1}$ ('apparent' value) at 298.15 K (25°C) which minimizes the energy barrier required for elimination and, therefore, formation of the corresponding reactive species *via* β-fragmentation is strongly favoured. These results agree well with those obtained previously from

reversible *cis*/*trans*-isomerization of 1,2-disubstituted olefins although the alkene structures occurring in limonene do not undergo isomerization.

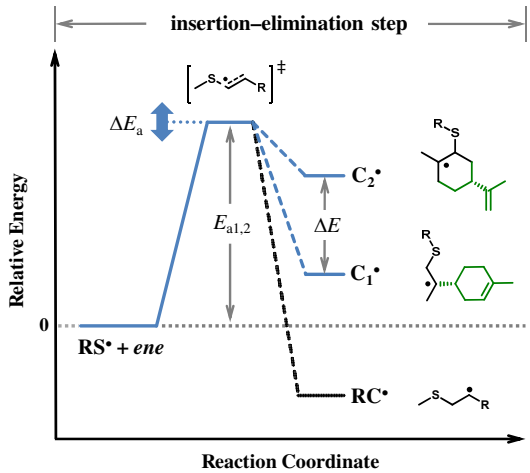

Figure 4.11 Theoretical partial reaction energy diagram and corresponding intermediary product structures for the elementary addition-elimination reactions of the two propagation steps. The RC$^\bullet$ structure appearing bellow the dotted reference line denotes any stabilized carbon-centered radical representative of highly reactive olefins.[29]

Overall, it can be concluded that although steric effects may occur upon addition of the thiyl radical onto the two alkene structures combined with unknown differences in electron-density, the main fundamental phenomenon explaining the very distinct double bond reactivities seems to be a difference in relative energy (ΔE) of the two insertion radical products which favours back-fragmentation over addition; with elimination of the second carbon radical then occurring at faster rate than the first carbon-centered radical.

4.2.1.2 Effect of stoichiometry

Presented here is an extension to the previous basic two-route linear cyclic mechanism depicted in Scheme 8. The new mechanism describes the selective thiol–ene coupling reactions in *D*-limonene under bulk reaction conditions. The main goal is to examine the effect of the initial co-reactant composition on the overall coupling dynamics and final outcome of the reaction in order to understand which operational parameters can be altered experimentally towards the design of multifunctional limonene-based resins useful for the synthesis of cross-linkable thiol–ene networks.

The new kinetic model illustrated in Scheme 9 accounts both for the primary and secondary coupling reactions leading to formation of mono-addition (**3** and **4**) and di-addition (**5**) thiol–ene products; here denoted by $\mathbf{P_1}$, $\mathbf{P_2}$ and $\mathbf{D}$, in the same numbering order. The upper part outlines a series of elementary propagation/chain-transfer reactions involving reactants, products and intermediate species; whereas the bottom part represents the net set of four observed coupling reactions defined by the system of elementary chemical steps. Initiation and termination reactions occur according to the corresponding chemical equations depicted in Table 6. The extended mechanism was run in COPASI by adopting the values of the 'apparent' rate coefficients estimated in Table 6 accounting for the initiation and propagation/chain-transfer steps. A value of $k_t = 3.0\times10^8$ $M^{-1}\cdot s^{-1}$ was introduced for the thiyl-radical self-termination reaction, which is placed one order of magnitude bellow the termination rate constant considered in the preceding section, since the liquid medium viscosity increases by changing from solution to bulk reaction conditions.[36, 113] Alteration of the reaction conditions was necessary in order to follow the reaction *via* size-exclusion chromatography (SEC). To reduce system complexity, it was assumed that selective primary thiol–ene coupling does not affect significantly the reactivity of the unreacted double bonds in secondary coupling reactions; *i.e.*, $k_{add1,2} = k_{add4,3}$, $k_{elim1,2} = k_{elim4,3}$, and $k_{RSH2,3} = k_{RSH5,4}$. The numerical model simulations covered a representative segment of co-monomers feed ratio ranging from 1:20 to 20:1 with respect to thiol–ene functional groups and were performed up to a final running time of 180-min. Empirical kinetic data resulting from reaction experiments performed under starting molar ratios of 1:2 (*i.e.*, 1:0.5) and 1:1, were compared with corresponding simulated kinetic curves to qualitatively assess the level of fidelity and verify the mechanism.

The kinetic behaviour of the reaction system is controlled by the concerted action of initial co-reactant stoichiometry, double bond selectivity (which is invariant with time if ideally the viscosity remains constant); and, variation in reactants composition throughout the reaction which affects the reaction rates. FT–Raman spectral acquisitions displayed in Figure 4.12 combined with the two experimental DMF–SEC elugrams with kinetic plots (trends only) shown in Figure 4.13 provide a coherent qualitative description of the impact of the initial thiol–ene stoichiometry on the evolution dynamics of co-reactants and coupled products. In either of the two distinct compositions, production of di-addition product (**5**) is always observed as result of secondary coupling reactions issued from each mono-addition product and monothiol, thus, showing an effective activation of steps (10)–(13) from the mechanism (Scheme 9). Yet, each stoichiometry yields different thiol–ene addition sequences and consumption profiles of thiol and ene functional groups. Under a starting molar ratio of 1:0.5, formation of mono-addition products, **3** + **4** = **P**, is preferred over the production of **5** (MW, 713.21 $g\cdot mol^{-1}$); whereas under an initial stoichiometry of 1:1 the formation of **5** is favoured at the expense of **3** and **4** (MW, 424.72 $g\cdot mol^{-1}$) which are predominantly formed in the beginning of the reaction. Since the two mono-additions

share exactly the same molecular weight they could not be distinguished by SEC. Consumption of the two individual alkene structures was followed by total consumption of thiol functional groups as provided by FT–Raman spectroscopy; although the evolution patterns of both enes and consumption rates change markedly with stoichiometry. In both cases, preferential thiol–ene coupling at the *exo*-vinylidene bond was verified, simultaneously followed by a progressive increase in consumption of the internal trisubstituted 1-methyl-cyclohexene unsaturation. This observation is fully consistent with the measured differences in double bond reactivity reported in the previous section.

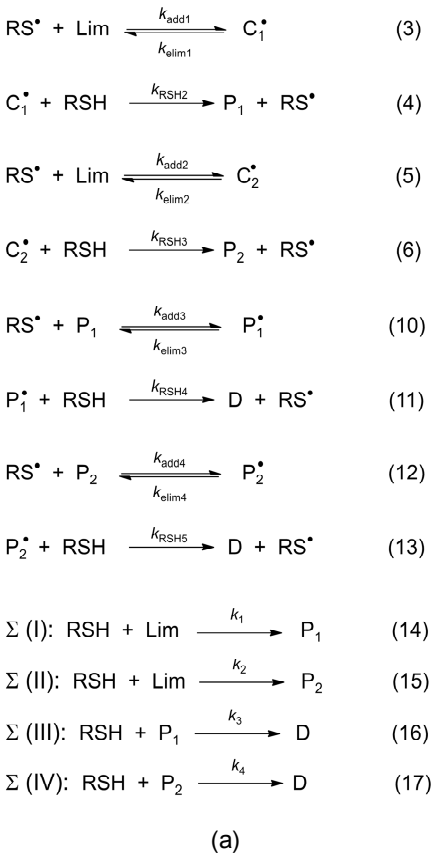

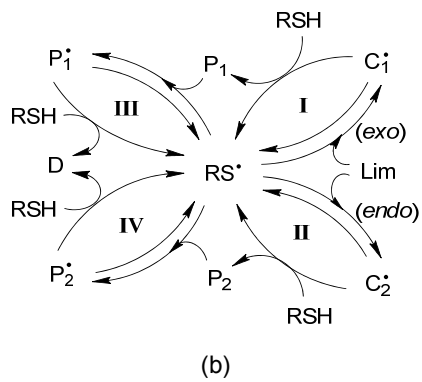

Scheme 9. Four-route linear step-growth mechanism sharing a common radical intermediate ($RS^{\bullet}$). (a) elementary propagation/chain-transfer steps accounting for primary and secondary coupling reactions; and, (b) corresponding cyclic representation. The sum sign (Σ) denotes net coupling reactions explained by the underlying mechanism.

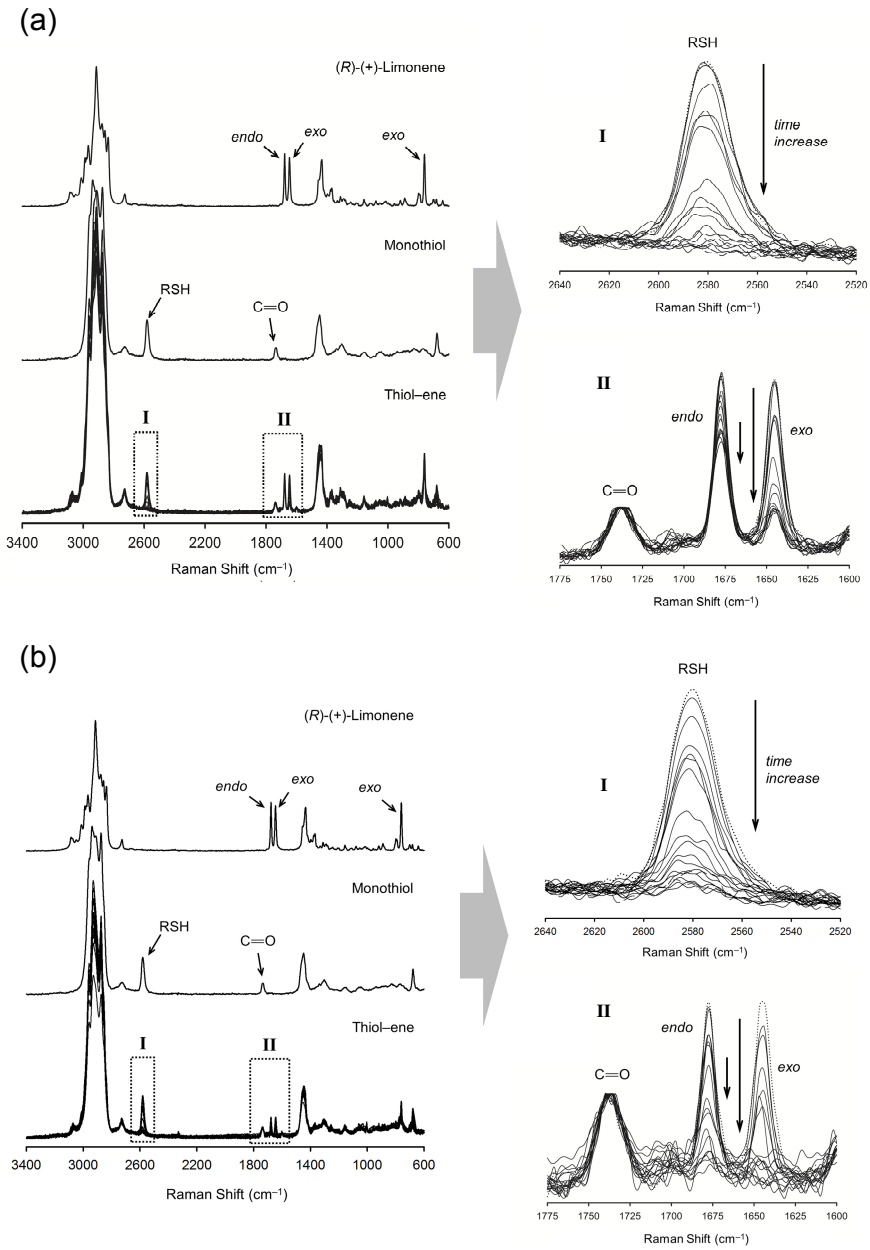

Figure 4.12 Normalized FT-Raman spectra collections showing the time-evolution of thiol and alkene functional groups as a function of initial thiol–ene stoichiometry: (a) ratio of 1:0.5, (b) ratio of 1:1. Dotted lines refer to the initial mixture. Long arrows denote fast consumption of functional groups whereas the small arrows indicate slow disappearance of endocyclic double bonds.

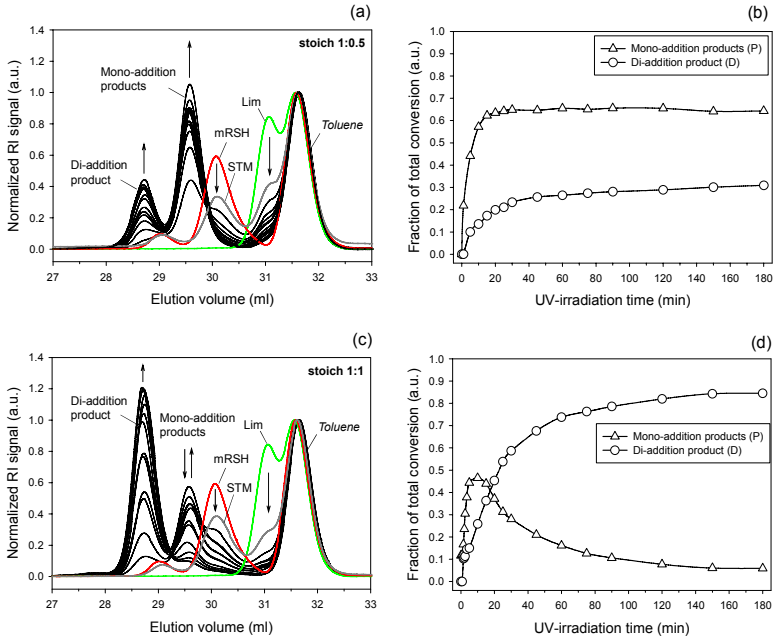

Figure 4.13 DMF–SEC elugrams (left) and corresponding estimated kinetic profiles (right) showing the time-evolution of mono-addition (**P**) and di-addition (**D**) products resulting from selective thiol–ene coupling under photochemical reaction conditions for the two stoichiometries. Starting thiol–ene mixture (STM; grey line); Limonene (Lim, **1**; green line); and, monothiol (mRSH, **2**; red line). Flow rate marker (toluene) was set at 31.5 ml. Arrows denote directions in increase or decrease of the given coupled products.

The new mechanistic model was again tested by plotting the computed output curves against the experimental kinetic profiles for comparison (Figure 4.14). In both stoichiometries evaluated, the continuous lines describing the time-evolution of reactants concentrations are in good trend agreement with the corresponding data points despite the obvious deviations. Evolution of total mono-additions (**3** + **4**) and di-addition (**5**) concentrations shown in Figure 4.13 are also well described by simulation which helps confirming the validity of the extended mechanism. The results also reveal that a development of **5** is always obtained for a stoichiometry of 1:0.5 which necessarily translates into a divergence from the typical second-order rate kinetics approximation observed in the previous section. Yet, the extent of this deviation seems to be minimal. The results compiled in Figure 4.15-a/c reflecting the evolution of the reaction system as a function of stoichiometry demonstrate well that when the two monomers are reacted at equimolecular concentrations, formation of di-addition product (**5**) reaches only 12.5% (or ~15%) of ~84% (or 100%) converted limonene at 180-min

of reaction. This residual value strongly suggests that under this particular stoichiometry the influence of formation of **5** can be considered negligible when compared to formation of mono-additions **3** and **4** as main reaction products and, therefore, deviation from the empirical second-order kinetics should be not too significant. Deviation from the empirical second-order kinetics should become gradually more pronounced towards higher conversion times and not in the initial period of the reaction as is the main focus of this analysis.

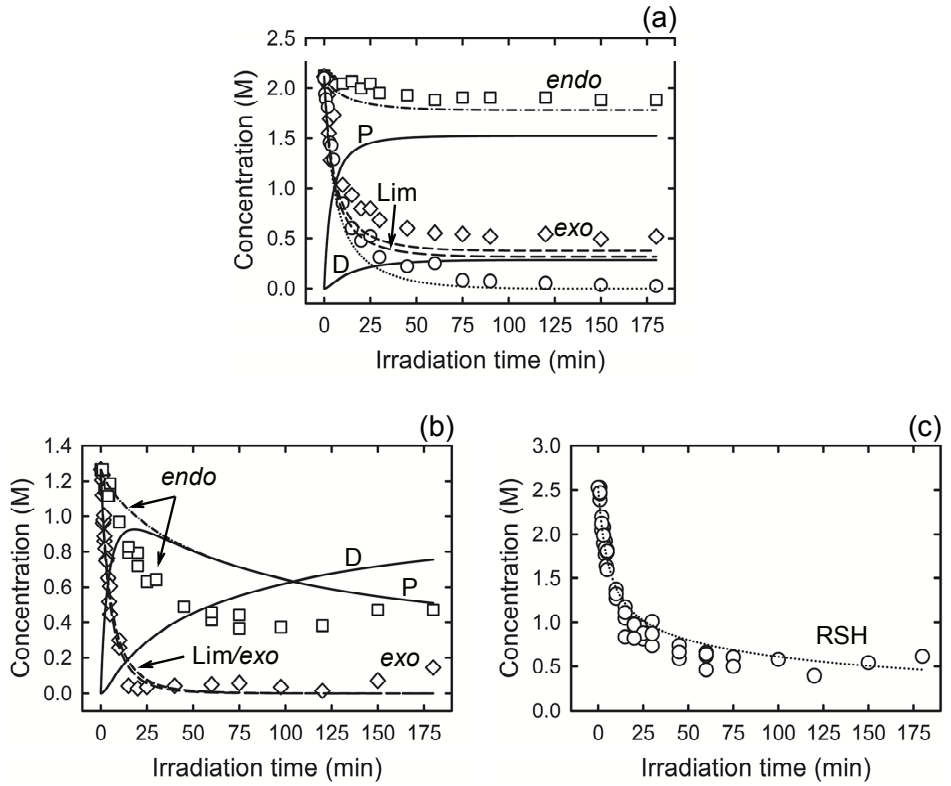

Figure 4.14 Comparison between experimental data (symbols) and simulated model predictions (lines) for the photoinduced reaction of limonene and monothiol. Initial thiol–ene stoichiometry: (a) 1:2 (*i.e.*, 1:0.5), and (b)/(c) 1:1. Legend: *thiol* (RSH; ○, dotted line), *limonene* (Lim, long-dashed line), *endocyclic* 1,1,2-trisubstituted unsaturation (*endo*; □, dashed-dotted line); and, *exocyclic* 1,1-disubstituted unsaturation (*exo*; ◇, medium-dashed line). Mono- (P) and di-addition (D) products are depicted by continuous solid lines. Temporal evolution of overall alkene functional groups (*i.e.*, enes present both in limonene and di-addition products) were calculated as: $[exo]_t = [\mathrm{Lim}]_t + [\mathrm{P_2}]_t$ and $[endo]_t = [\mathrm{Lim}]_t + [\mathrm{P_1}]_t$ from computed limonene and individual mono-additions. $\mathrm{P} = \mathrm{P_1} + \mathrm{P_2}$.

Figure 4.15 provides a complete overview of the influence of initial thiol–ene stoichiometry on the overall reaction kinetics of the system discounting any temporal effects and, therefore, can be regarded as a rational guidance tool for designing thiol–ene reaction systems based on limonene. Plots (a) and (b) demonstrate the excellent ability of numerical simulations to reproduce the kinetic results obtained from experimentation, indicating that this modeling approach represents an important complementary technique to assist experimental determinations. Plots (c) and (d) represent different manifestations of the same kinetic behaviour and basically reflect the extent of conversion of the system variables (except radical intermediates) for the propagation/chain-transfer reactions as a function of stoichiometry. Towards high thiol–ene stoichiometries, formation of di-addition product (**5**) is clearly stimulated at the expense of mono-addition products (**3** + **4**); whereas, moving in direction of lower stoichiometries (*i.e.*, increasingly higher relative excess of limonene) the reaction system favours thiol–ene coupling selectively at the *exo*-vinylidene bond *via* formation of mono-addition compound **3** whilst production of compound **5** is progressively suppressed. The latter situation may very well turn beneficial synthetically toward the design of multifunctional 'limonene'-terminated macromonomers without significant participation of secondary coupling reactions which necessarily leads to formation of 'hyperbranched-like' oligomeric structures as represented by pathway (b) in Scheme 7. Another striking feature related with Figure 4.15 is that any set of experimental data points collected at a given stoichiometry can be viewed just as a prolongation of experimental data collected at lower stoichiometries. This feature is well patent in plots (a) and (b) as the solid lines deviate only slightly from their dotted counterparts. Therefore, the chart represented in plot (c) is applicable to any workable stoichiometry without any major loss in accuracy.

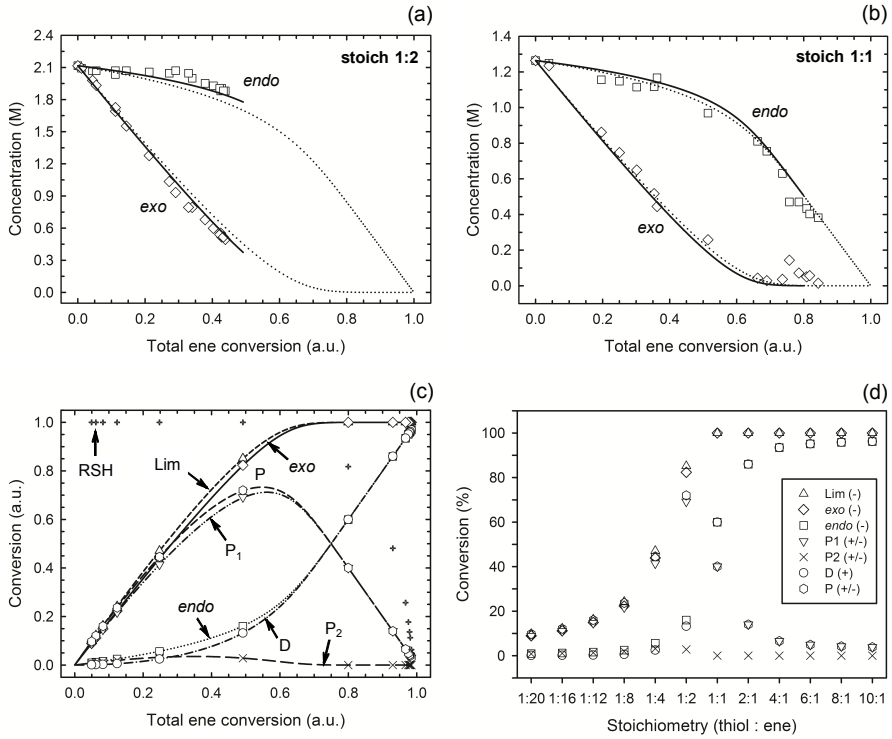

Figure 4.15 Concentration–conversion plots (a)–(b) and evolution of conversion as a function of total ene conversion or thiol–ene stoichiometry (c)–(d). Experimental (symbols) *vs.* simulated (lines) data for a composition mole ratio of (a) 1:2 (*i.e.*, 1:0.5), and (b) 1:1 with respect to thiol–ene functionalities. (c) general simulation chart covering a stoichiometry range of 1:20 ≤ thiol:ene ≤ 10:1. Full-range plot-lines represent a maximal thiol–ene stoichiometry of 20:1. (d) effect of stoichiometry on the final conversion of variables. Individual symbols as data points in plots (c) and (d) denote final computed concentrations changed to conversions (at t_f = 180 min) of each variable at a given initial thiol–ene stoichiometry. $[DMPA]_0$ = 0.07 M (~2.0 wt.% of total reactants) in all simulations. Symbols (+) and (–) in plot (d) denote positive or negative conversions of a given variable, respectively.

To obtain ample experimental evidence of the influence of initial co-reactant stoichiometry on the final outcome of the reaction involving multifunctional thiol–ene systems, the trithiol (**6**) was reacted in organic EtOAc solution with limonene (**1**) under isothermal conditions for an extended period of 6-hours and the photo-reaction products analysed by DMF–SEC after proper evaporation of the solvent. The two elugrams plotted graphically in Figure 4.16 give a consistent and clear confirmation that the numerical predictions derived from the extended mechanism are well reproduced experimentally as demonstrated by the two very distinct patterns in molecular weight distribution of final thioether coupled products. Elugram (a) clearly shows the production of multifunctional 'hyper-

branched-like' oligomers resulting from di-addition reactions occurring in parallel formation of mono-addition products; whereas, in elugram (b) the reaction system visibly favours formation of mono-addition products from selective thiol–ene coupling over di-addition reactions. The two residual high molecular weight bands occurring at low elution volumes in elugram (b) indicate that even with the tentative manipulations in the starting co-reactant stoichiometry is not possible to obtain compound **7** in its pure form without minor contribution of secondary di-addition reactions. Overall, these results confirm the adjustable (but not controllable) nature of free-radical thiol–ene additions involving multi-substituted olefins in combination with the '*non-click*' chemistry character inherent to these particular alkene structures.

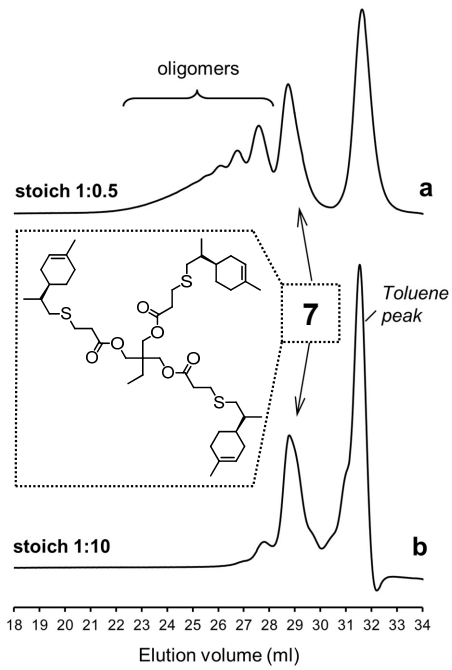

Figure 4.16. Qualitative DMF-SEC elugrams for the multifunctional system based on the photoinitiated reaction of (*R*)-(+)-limonene (**1**) with TMP-trimercapto propionate (**6**) using two different thiol-to-ene stoichiometries. In elugram (b) the small band shoulders located at ~29.5, 30.5 and 31.0 ml represent vestigial amounts of partially coupled products, unreacted trithiol and limonene, respectively. Thiol:Ene = *x*:*y* (functional group stoichiometry).

4.2.2 Synthesis and characterization of multifunctional resins

Limonene and the two multifunctional thiols evaluated are not originally miscible at room temperature which prohibits any direct photoinduced thiol–ene synthesis of macromolecular materials in bulk based on these compounds. To circumvent this incompatibility issue the thiols were first reacted with limonene in ethyl acetate solution (50 wt.%) under a starting co-reactant stoichiometry of 1:0.5 to afford multifunctional macromonomer resins which could then be used in a second synthesis step to produce thiol–ene thermoset films under UV-irradiation.

The first synthesis step is illustrated in Scheme 10. Although a relative excess of terpene in the reaction system preferentially yields compounds **7** or **9** in high amounts, this synthesis route was not preferred as the low relative vapour-pressure of limonene, 3.39×10^{-2} (EtOAc/b.p., 77.1°C)[114, 115], hampers its removal *via* evaporation. Additionally, from a material synthesis perspective it is not entirely required to have the two macromonomers (**7** or **9**) synthesized in pure form since the chemical skeletal structure of limonene works as a crosslinker unit between sulphur groups once thioether linkages are formed. After solvent evaporation, the resins were obtained as clear, faintly yellow, viscous liquids exhibiting a fresh citreous odour note.

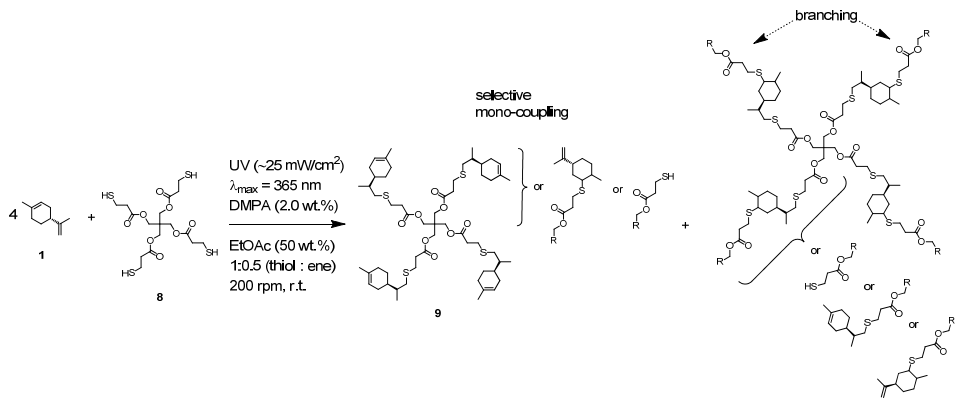

Scheme 10. Idealized synthesis of resin 2 issued from limonene (**1**) and tetrathiol (**8**). Also valid for the synthesis of resin 1 issued from compounds **1** and **6**. Non-ideal synthesis of resins comprises a mixture of all possible coupling combinations (complete or partial).

Photo-initiated conversions of individual thiol–ene functional groups into resins 1 and 2 after 6-hours of reaction were 81.8±1.6% for the *exo*-unsaturation, 18.2±1.4% for the endocyclic ene and, 100% (overall) for the thiol group as determined by ^{1}H NMR (enes) and FT–Raman (thiol) (Figures 4.17 and 4.18, respectively). A significant decrease of the doublet signal (*b*) at 4.5 ppm assigned to the terminal protons of the *exo*-vinylidene bond was accompanied by a small reduction of signal (*a*) at 5.4 ppm attributed to the single proton of the 1,1,2-trisubstituted 1-methyl-cyclohexene functional group. Decrease of these two signals was also followed by a significant loss of triplet signal (*f*) at 1.75 ppm characteristic of the methyl protons adjacent to the terminal ene and practically no decrease in the triplet signal (*g*) located at 1.65 ppm; thus, indicating favoured coupling at the exocyclic double-bond position. Moreover, proton signals (*e*) and (*d*) located between the ester and thiol groups (~1.5 ppm) and centered at 2.66 and 2.78 ppm respectively, were slightly shifted followed by formation of two new neighbouring signals: a faint singlet (solid star) at ~2.92 ppm and a strong

quadruplet (white diamond) at 2.25–2.5 ppm assigned to the CH proton at position 2 and CH_2 at position 10, respectively. Two novel signals at 0.98–1.20 ppm (white star) and 0.88–0.98 ppm (two doublets, solid diamond) ensuing from the coupling reactions were also detected corresponding to the methyl groups located at positions 7 and 9, respectively. The numbering terminology of each nucleus used for the assignment of proton-NMR signals was adopted from a previous reference.[76] Characterization by FT–Raman spectroscopy represented qualitatively in Figure 4.18 shows a significant reduction of the exocyclic ene band over that of the endocyclic ene with practically no vestigial amounts of thiol detected within the system. This supports the ^{1}H NMR results described and complies well with the previous model studies (experimental and simulated). Indeed, the double bond conversion ratio obtained experimentally yielded a value of ~4.5 in favour of the exocyclic ene which is remarkably well explained by its homologous ratio obtained from simulation, ~4.8, after a running time of 6-hours.

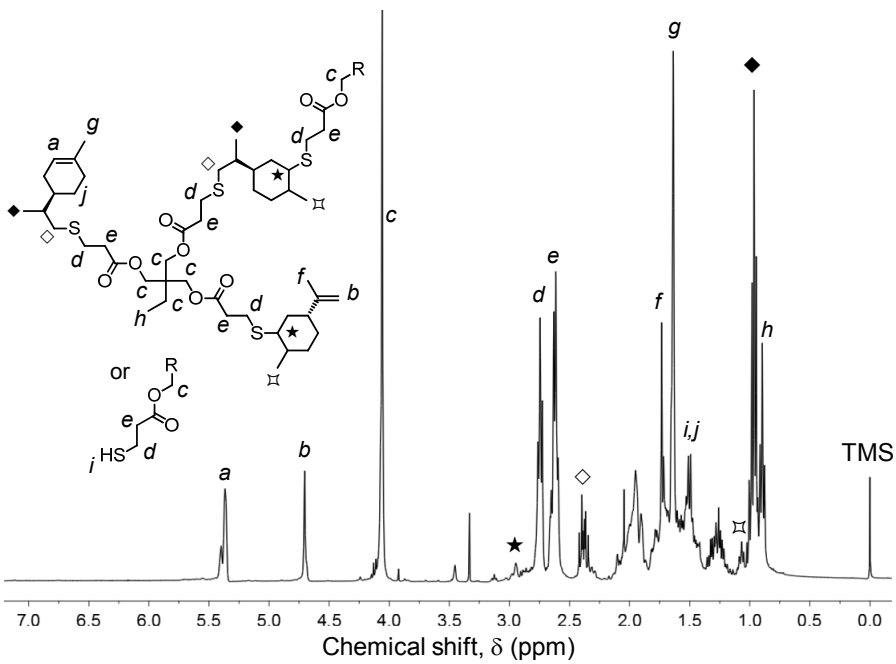

Figure 4.17 ^{1}H NMR (400 MHz, $CDCl_3$) spectrum of resin 1 (representative structure) with principal signal assignments resulting from photoinduced thiol–ene reaction between compounds **1** and **6** mixed at 1:0.5 functional group stoichiometry. Reaction was conducted for a period of 6-hours at room-temperature in EtOAc solution. Integration value of ethyl ester protons signal (*c*) was used as reference peak for the calculation of double bond conversion.

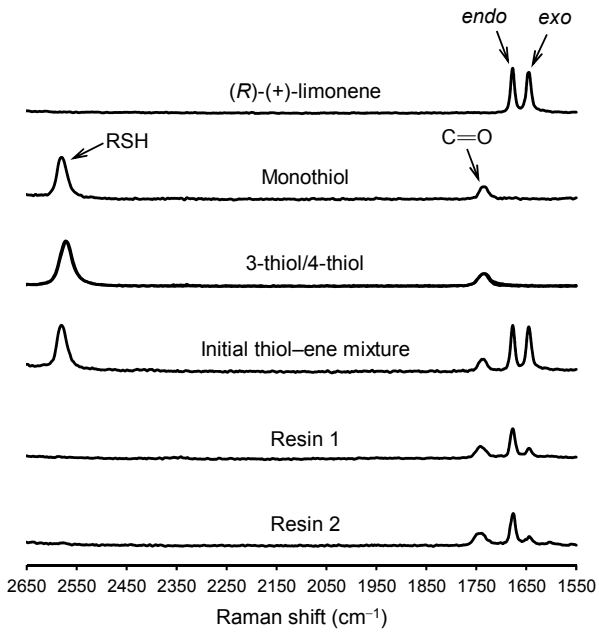

Figure 4.18 Normalized FT–Raman spectra (partial) showing the important bands regarding the synthesis of resins 1 and 2 issued from multifunctional thiols **6** and **8**, respectively. Initial thiol–ene reference sample was comprised of limonene and monothiol mixed in bulk at a stoichiometry of 1:0.5. All spectra (except limonene) are normalized against the carbonyl ester peak (~1735 cm^{-1}).

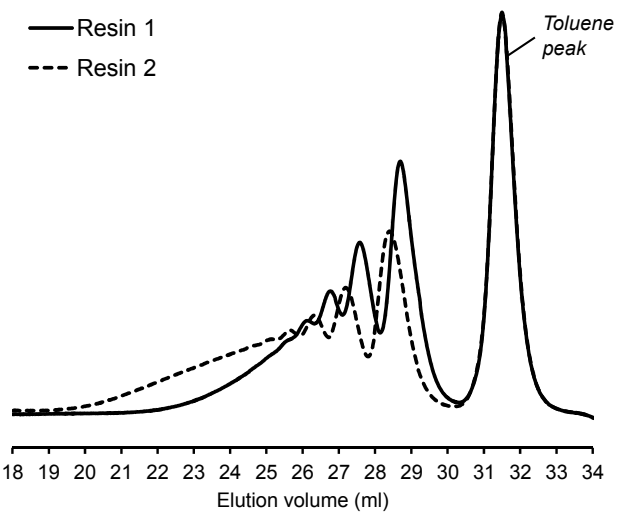

Figure 4.19 Superposition of normalized DMF–SEC traces of the two synthesized resins.

DMF–SEC analyses of the two resins derived from limonene shown in Figure 4.19 confirm an effective presence of multifunctional high molecular weight oligomers as result of a combination of primary and secondary coupling reactions. *Dispersity Index* (Đ)[116] was 2.1 for resin 1, 2.7 for resin 2 and, 1.1 for the two individual macromonomers **7** and **9** (first bands appearing immediately after the flow rate marker). Dispersities of the first three individual bands corresponding to the oligomers took unit values although moving gradually towards low elution volumes an increasing loss of resolution (separation capacity) is observed. The relative proportion of individual compounds **7** (MW_{theo}/MW_{SEC} = 0.76) and **9** (MW_{theo}/MW_{SEC} = 0.81) plus partially coupled macromonomers in each of the corresponding resins was 31.4±4.4%; *i.e.*, ~25% of **7** or **9** and ~6.3% of partial additions in both peaks if a molecular weight ratio, MW_{theo}/MW_{SEC}, of 0.8 is assumed. This indicates that roughly 68.6% of the overall mixtures were constituted by primary (mono-addition) and secondary (di-addition) coupling products (complete and partial oligomers). In the 25% of individual macromonomers **7** or **9**, about 21% are coupled at the *exo*-unsaturation and only ~4.6% coupled at the *endo*-unsaturation. In the same manner, of the 68.6% corresponding to 'hyper-branched-like' oligomers, about 56.5% of these are coupled at the *exo*-unsaturation whereas only ~12.6% corresponds to coupling at the *endo*-unsaturation. Since the simulation ratio of mono-*to*-di-addition products after 6-hours is $[P]_f/[D]_f \approx 5.5$, and the double bond conversion ratios obtained from ^{1}H NMR measurements and simulation remarkably agree with each other, than is expectable that both resins will contain similar distribution of mono- and di-addition products. The fact that resin 2 yielded a slightly higher dispersity index over resin 1 associated to a much broader molecular weight distribution curve is very likely to be attributed to influence of an extra mercapto propionate ester arm which increases the probability for high order coupling combinations in the pre-synthesis step. This effect was obviously translated into development of much higher viscosity for resin 2 when compared to resin 1 observed during and after synthesis. All these results demonstrate the efficacy of the thiol–ene reaction in the preparation of poly-functional macromonomer resins based on limonene.

4.2.3 Photo-crosslinking and network characterization

Limonene represents an excellent diene monomer to prepare thiol–ene thermosets. Not only we observed that the two alkene structures retain enough reactivity necessary for the thiol–ene addition process but the presence of a slightly rigid cycloaliphatic ring may also turn advantageous at conferring extra strength properties to the final materials. Thiol–ene networks usually lack this feature when compared to their acrylate counterparts as consequence of the formation of a more flexible S–C thioether bond (1.8 Å) *versus* the C–C bond (1.2–1.5 Å).[33, 117-119]

One particular requirement involving conventional thiol–ene thermoset materials is the need for full stoichiometric control. In this case, equimolar mixtures of multifunctional thiol and ene components taking the form $x\mathrm{R}_1\text{–}(\mathrm{SH})_m$ and $y\mathrm{R}_2\text{–}(\text{`}ene\text{'})_n$ require that $xm = yn$, where x and y are the number of molecules of each monomer and m and n denote the number of thiol and ene functionalities per molecule, respectively. Off-stoichiometric thiol–ene networks (OSTE's) can be prepared by manipulating these parameters, ensuring that $xm \neq yn$, as recently demonstrated in microfluidic device applications.[120] This strategy allows for the fine-tuning of the viscoelastic properties and glass-transition temperatures of the final networks according to the needs as well as other uses such as post-functionalization. Here this concept is revisited by allowing small gradual amounts of thiol relative to the ene (xm/yn = 1.10, 1.25, and 1.45) to be introduced in the system to inspect its relative impact on the physicomechanical properties of the ensuing limonene-based thiol–ene thermosets.

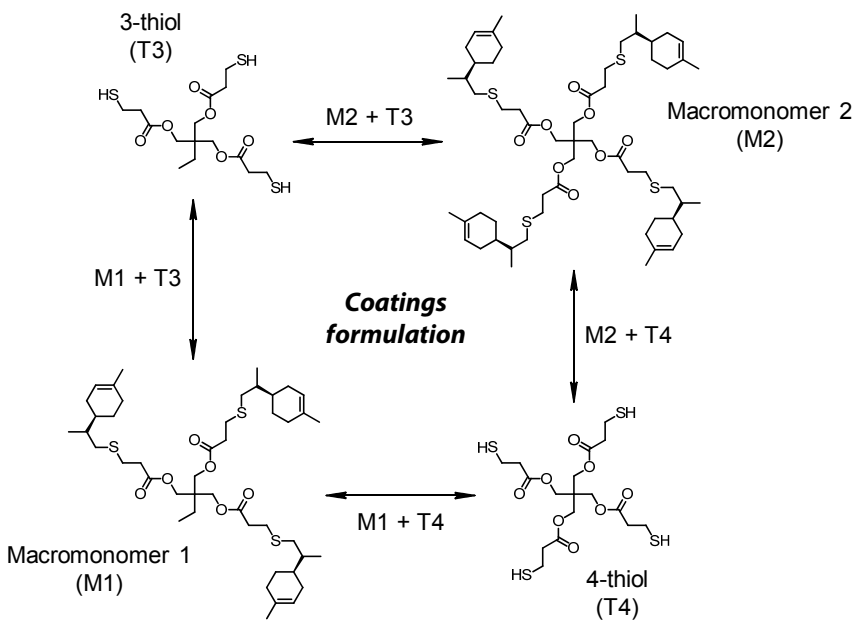

Scheme 11. Multifunctional thiol–ene combinations and nomenclature adopted in the preparation of thermoset film coatings based on limonene.

4.2.3.1. Thiol–ene photopolymerization

A series of crosslinked thiol–ene networks were synthesized through photopolymerization of the two multifunctional macromonomer resins with the two polyfunctional thiol monomers. Different cross-over combinations of the monomers,

with and without an excess of thiol functional groups at different levels, were prepared leading to a total of 16 different compositions. The nomenclature adopted is represented in Scheme 11 and/or Table 8. All photocured thiol–ene films were obtained as clear (amorphous) homogeneous and flexible materials without any discernible thiol odour. However, films with low functionality (M1+T3) resulted to be much stickier to the glass surface than films with higher functionality (M2+T4). This difference may be ascribed to different crosslink densities achieved for the two materials. In general, the higher the crosslink density, the higher the stress build-up during cure[121] which results in higher contraction energies developed at the film-substrate interface and peeling is facilitated.

To gain a first assessment of the curing degree and density of crosslinks within the networks achieved after photopolymerization, sol-content determinations were performed by immersing the films in an appropriate organic solvent. As known from before, the higher the crosslink density of the cured film the lower the fraction of unbound material occluded into the network; and, therefore, the lower the sol-content. Leaching tests results are shown in Figure 4.20. Films with incremental mole amounts of thiol functional groups resulted in higher fractions of soluble material trapped inside because once the network is chemically locked (gel-point) the remaining unreacted portion becomes occluded into the network. Upon swelling the network releases most of this soluble fraction and a reduction in mass is detected gravimetrically. This was particularly evident from networks resulting from the two intermediate cross-combinations of high and low functionality components (M1+4T and M2+T3). Conversely, both low (M1+T3) and high (M2+T4) functionality formulations afforded materials with relatively high and very low (or none) sol-content, respectively. An increase in functionality of the reacting system leads to higher number of chemical crosslinks per unit volume of material and, therefore, the chances to extract any fraction of unreacted material occluded are lower: it is observed that networks having the highest functionality reach full crosslinking upon UV-cure (Figure 4.21) regardless of the amount of thiol used and practically no leaching of the unbound fraction was detected. In contrast, materials having the lowest functionality have much higher tendency to leach out upon swelling in a very good solvent such as THF even if full thiol–ene cure is achieved with respect to the limiting enes. It is remarkable the differences in extraction capacity observed between systems with and without presence of one extra propionate ester arm (on average)! These results re-confirm the impact of the system co-functionality in the crosslinking density achieved after cure. One should note, however, that even in the worst case situation the fraction of unbound material is always lower than 25%. This indicates, in one instance, the importance of having good control over the composition mole ratio in the preparation of pure stoichiometric (one-*to*-one) thiol–ene networks; and, in another instance, the properties of the final thermosets can be further adjusted by adding small incremental amounts of thiol acting as a plasticizer. The plasticizing role of the thiol will be discussed in more detail in the following subsection.

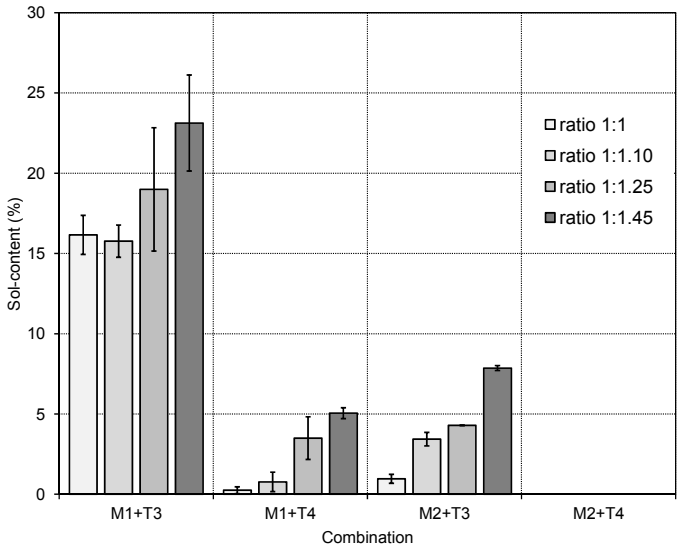

Figure 4.20 Sol-fraction of the thiol–ene films as determined gravimetrically. Inset ratios refer to mole amounts of ene-to-thiol functional groups.

FT–Raman measurements were performed for the different formulations before and after cure. The results given in Figure 4.21 illustrate well the extent of cure for the combination M1+T3 which are also representative of the other thiol–ene systems evaluated. Practically full conversion of alkene functional groups were obtained for all cases accompanied by an equal conversion of thiol groups. Residual thiol peaks correspond to unreacted fractions, consequence of an excess of thiol functional groups introduced within the system. It is also likely that as the tri-dimensional network develops minute amounts of thiol groups become gradually restrained inside the liquid-gel transition phase due to the step-wise nature of the polymerization; but it is only near or at the gel-point that a larger fraction of unreacted thiol gets occluded throughout the crosslinked material because it is when a macromolecular cluster is produced that is sufficiently large to span across the whole sample size resulting in an infinite network. Evidently, this process has an impact on the evolving rheological properties during build-up of the network.[109] Moving towards higher thiol–ene stoichiometries, increasingly more amounts of unreacted thiol become occluded onto the network resulting in higher peak heights as observed. The extent and density of the chemical crosslinks in conjunction with functionality and thiol–ene stoichiometry of the reacting system ultimately dictates the final thermal and mechanical properties of the fully cured thermosets.

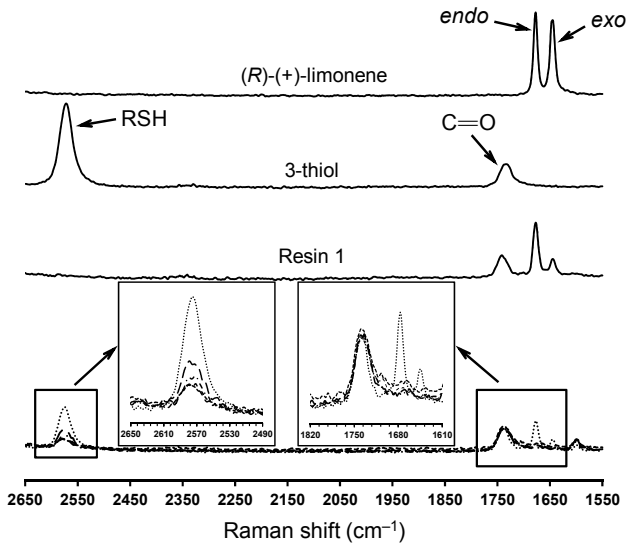

Figure 4.21 Spectral FT–Raman changes observed in thiol and alkene functional groups after UV-cure of the thiol–ene mixture composed of M1+T3. Dotted line refers to the initial thiol–ene mixture (before cure) with 45% relative excess of thiol functional groups. After cure: long-dashed line (ratio 1:1.45), dash-dotted line (ratio 1:1.25), short-dashed line (ratio 1:1.10); and, mid-dashed line (ratio 1:1). All spectra (except limonene) are normalized against the carbonyl ester peak (~1735 cm^{-1}).

4.2.3.2. Thermo-mechanical properties

To determine more accurately the influence of these operational parameters, DSC (*Differential Scanning Calorimetry*) and DMTA *(Dynamical Mechanical Thermal Analysis*) measurements were again conducted on the final thermoset films accounting for thiol–ene stoichiometries of 1:1 and 1:1.45. The results presented both in Figure 4.22 and Table 8 give a global unifying perspective of this effect.

The thermal properties were first investigated by DSC. It can be observed that the T_g increases changing from low to high functionality materials due to an increase in crosslink density. The full range in different T_g was 18.4°C for pure stoichiometric films and 19.5°C for off-stoichiometric materials, suggesting that an extra unreacted thiol trapped within the networks works as a plasticizer softening the materials irrespective of network density. This is effectively confirmed by a decrease in T_g with excess of thiol which modifies the physical properties of the thermosets. To have a better account of this effect DMTA measurements were performed because changes in modulus are usually much more pronounced than, for example, changes of heat capacity, c_p, in a DSC cycle.

Plots (a) and (b) of Figure 4.22 compare the evolution of the storage (elastic) modulus (E') as a function of temperature. In both plots the storage modulus values depart from 2.6±0.4 GPa (at –70°C), which is considered typical of crosslinked polymers bellow T_g. As heating continues the modulus decreases gradually followed by a sudden glass-transition phase and then stabilizing at the rubbery plateau region. As know from before, the relative level of this final plateau is directly correlated to the crosslink density of the networks with higher modulus values corresponding to higher crosslink densities. The curves in plot (a) exhibit a narrow rubbery plateau when compared to film coatings cured with higher amount of thiol (plot (b)). This was anticipated since an excess of free thiol intercalated throughout the networks reduces the crosslink density. In both cases the crosslink densities follow the order: M2+T4 > M2+T3 ≈ M1+T4 > M1+T3, which is well correlated with the previous sol-content results. The corresponding tan δ curves are displayed in plots (c) and (d). The shoulders at lower temperatures verified for the intermediary films M1+T4 (1:1) and M2+T3 (1:1) resulting in asymmetrical (bimodal) transition curves and larger widths at half-maximum peak heights are probably accredited to relaxation of chain segments for distinct crosslinked regions which indicates the presence of a non-uniform network structure. Intensities of the tan δ peaks also vary from each sample at the respective T_g values. Plot (d) shows a reduction in peak heights moving from very low functionality to very high functionality materials tightly associated to variations in crosslink density and T_g. A rise in T_g with increasing crosslink density results in lower energy loss (more energy is stored in the material) during the thermal transition and, therefore, more elastic behaviour (small heights) is observed; whereas, higher tan δ values indicate greater energy (heat) dissipation and increasing viscous behaviour (large heights) as consequence of lower amount of crosslinks and reduced T_g. Therefore, a more dominating plasticizing (viscous) effect is observed in less densely crosslinked materials. A similar trend is observed in materials M1+T3 (1:1) and M2+T4 (1:1) represented in plot (c) but not for the intermediate networks for the reason pointed. Equivalent tan δ curves of the two intermediate functionality materials (M1+T4 (1:1.45) and M2+T3 (1:1.45)) with respect to height and T_g values were observed indicating that these networks exhibit relatively similar thermo-mechanical properties. In the former case the plasticizing effect can be excluded attributed to an excess of thiol and the viscoelastic properties are determined exclusively by the crosslink density and regularity of the network. The widths at half-maximum peak height give an account of the degree of homogeneity of the final networks with broader widths reflecting a material more heterogeneous in structure than networks exhibiting narrow widths. Interestingly, almost all materials with higher thiol content afforded narrower widths when compared to their stoichiometric counterparts. Possibly, this may be consequence of the extra amount of thiol involved enabling a more ordered and regular build-up of the network.

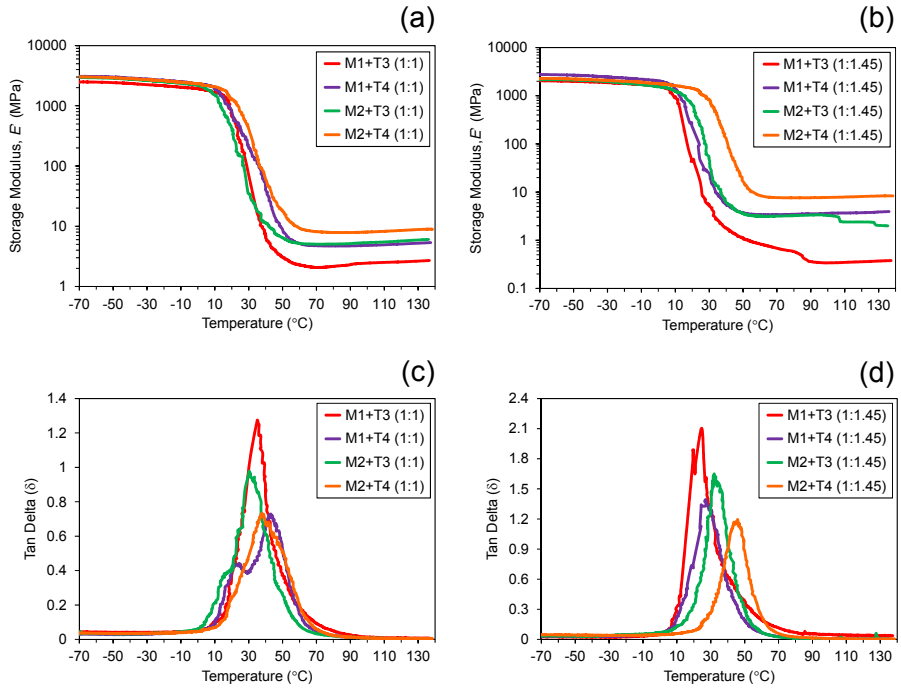

Figure 4.22 Influence of the type of thiol–ene formulation (combination and stoichiometry) on the thermo-viscoelastic properties of the final cured film coatings. Plots of (a) and (b) storage modulus *vs.* temperature; and, plots of (c) and (d) tan δ (=E''/E') *vs.* temperature.

Table 8. Thermo-mechanical properties of the final cured thiol–ene films.

Formulation/ Sample	Stoichiometry	T_g (°C)[a]	T_g (°C)[b]	E'_{Rubb} (MPa)	Height (MPa) of Tan (δ) peak	Tan (δ) fwhm (°C)
M1 + T3	1:1	-6.0	35.0	2.7	1.27	17.05
	1:1.45	-8.0	24.6	0.4	2.10	17.04
M1 + T4	1:1	-2.0	43.1	5.3	0.73	33.83
	1:1.45	-5.0	27.1	3.9	1.39	19.12
M2 + T3	1:1	5.0	30.3	5.9	0.98	19.71
	1:1.45	-2.0	32.0	3.3	1.65	14.44
M2 + T4	1:1	12.4	37.8	8.9	0.73	28.43
	1:1.45	11.5	45.8	8.3	1.19	16.78

[a] determined from DSC measurements, [b] determined from DMTA.

It should be noted that the overall temperature difference between the different compositions is at the most in the range of 20°C (Table 8). Using limonene as a cycloaliphatic monomer in comparison to conventional aliphatic systems demonstrates a more pronounced effect. The presence of the alicyclic ring in the final network increases the rigidity and significantly enhances the T_g in comparison to, for example, allyl ether based thiol–ene systems.[122] This evidence further motivates the use of terpenes as renewable monomers in this type of organic systems as an ingenious route to obtain higher T_g materials. This feature combined with off-stoichiometric manipulations in the thiol–ene composition and/or functionality, as well as the possibility to employ an assortment of thiol cross-linkers (*e.g.*, thiol glycolates, triazine-based mercaptans and/or mercapto propionates) opens the door to tailor the thermo-mechanical properties of such organic thermoset systems without resorting to more complex hybrid organic-inorganic thiol–ene networks.[126]

5 Conclusions

The stoichiometric reaction of an internal *cis*-alkene monomer (MO) with TMPMP was found to consist of a sequential *insertion-isomerization-elimination* process promoted by photogenerated thiyl radicals, which lead to a fast formation of the corresponding *trans*-isomer. The reversible *cis*/*trans*-isomerization equilibrium dominated the early instants of the reaction and was subsequently followed by thiol addition yielding the final thiol–ene C–S product without significant influence of side-reactions. When a *trans*-alkene (ME) was used instead, thiol addition took place at a much higher rate showing insignificant conversion into the *cis*-isomer. This is attributed to existence of an enthalpy barrier which favours product formation over transformation to a *cis*-conformation. Since isomerization occurred more rapidly than thiol addition, it was found that the rate-limiting step, in the two cases, was the chain-transfer hydrogen-abstraction from the labile thiol group promoted by the intermediate alkyl carbon-centered radical ($A^{\bullet}$). This indicates that although *trans*-structures have kinetic preference in the formation of end coupled product, aliphatic main-chain *cis*-alkenes can still be employed as starting monomers since isomerization supersedes the rate-limiting hydrogen-transfer step and the slowest step controls the overall reaction.

Random linear globalide/ε-caprolactone based copolyesters, P(GI-*co*-CL), differing in degree of mono-unsaturations along the main-chain were photopolymerized in the melt with the same trithiol crosslinker giving fully amorphous and insoluble elastomeric thiol–ene materials with different thermal and viscoelastic properties dependent on functionality. The addition of ε-caprolactone to globalide represents an efficient method to increase chain mobility, while enabling high thiol–ene conversions (>80%) and maintaining the cure kinetics irrespective of functionality; although, this results in thermosets with residual crystallinity and more uneven distribution of crosslinks. It was found that high ene-density copolymers resulted in networks with higher glass-transition temperatures and narrower distribution of crosslinks than films with lower ene composition.

A systematic kinetic study indicated that although the external isobutylene bond of *D*-limonene reacts about 6.5 times faster with thiols bearing a propionate ester moiety than the trisubstituted 1-methy-cyclohexene unsaturation, this internal ene retains enough reactivity necessary for the creation of thiol–ene networks. It is strongly suggested that the different reactivities of the two unsaturations are attributed to steric impediments coupled with unequal electron-densities of the enes; but, more importantly, to a difference in relative energies of the ensuing carbon-centered radicals immediately formed after thiyl-ene radical insertion which, in this case, governs the individual rates of propagation. The contribution of this phenomenon combined with the presence of a rate-limiting

step characterizes the slow rates of reaction commonly observed in thiol–ene systems involving multi-substituted olefins when compared to more reactive enes (*e.g.*, allyl ethers), which are less prone to reversibility in the propagation step.

Numerical time-course simulations revealed to be an appropriate method to:

- Test the validity of the thiol–ene mechanisms suggested for each reaction system by comparison with overall kinetic data obtained experimentally.
- Estimate 'apparent' rate coefficients accounting for propagation and chain-transfer elementary steps in the absence of reliable information about their absolute values. When combined with analytical modeling of the mechanism conceived for limonene under steady-state conditions, these values allowed to confirm the double bond selectivity estimated from empirical determinations (observed kinetics).
- Predict the impact of the initial reaction conditions on the kinetic behavior of the system(s) and final outcome of the reaction by changing the starting thiol–ene stoichiometry.

The differences in intrinsic double bond reactivity of limonene allow for the preparation of intermediary *ene*-terminated resins as multifunctional macromolecular precursors for the photo-induced synthesis of thiol–ene thermosets. Manipulations in the initial thiol–ene stoichiometry indicate that coupling at the *exo*-vinylidene bond of limonene can be addressed regioselectively by increasing the concentration of terpene relative to that of the thiol. Although this route brings a clear advantage toward the synthesis of well-defined multifunctional limonene-based macromonomers in organic solution the characteristic low vapour-pressure of limonene hinders its simple removal (or recycling) *via* evaporation after synthesis. Alternatively, by carrying out the reaction under a starting stoichiometry of 1:0.5, this enables production of high molecular weight resins in the form of 'hyperbranched oligomeric-like' structures as a consequence of secondary di-addition reactions explained by the extended mechanism. UV-curing of these resins combined with equal mole compositions of multifunctional alkyl ester 3-mercaptopropionates afforded highly sticky amorphous elastomeric materials with different thermo-mechanical properties. These can be further modulated by varying the amount of unreacted thiol occluded within the networks working as a plasticizer. Introduction of a renewable bulky structure such as the cycloaliphatic ring of limonene as intermediary crosslinking unit between thioether linkages offers a convenient way to improve the T_g and stiffness of these typical networks without need of calling for hybrid organic-inorganic design approaches.

The two thiol–ene systems evaluated here serve as model example for the sustainable incorporation of naturally occurring 1,2-disubstituted alkenes and monoterpenes into semi-synthetic thiol–ene networks in a timely fashion without major influence of side-reactions while reaching high conversions and exhibiting a range of thermo-mechanical properties.

6 Future Work

Although the work detailed in this thesis has brought into evidence the possibility of incorporating these two classes of alkene structures into thiol–ene networks using a chemically green and straightforward synthesis route, it would be of great interest to examine other types of alkene monomers in combination with thiol–ene chemistry. For example, *itaconic acid* can be obtained in vast quantities as by-product of the glucose fermentation industry[123] and seems to be a very promising renewable building-block for polymer synthesis. However, it has been reported for this unsaturated di-carboxylic acid that structural rearrangement to citraconic and mesaconic acids takes place in aqueous solution under elevated thermal conditions (Scheme 12). The dynamic equilibrium established for the unsaturated moiety at high temperatures may thus have an effect on the rate of thiol–ene coupling upon thermal or UV-curing conditions and, therefore, would be of prime interest to study the influence of this rearrangement in the thiol–ene mechanism, kinetics and reactivity to assess its potential for the creation of linear polymers and the thereof thiol–ene thermosets.

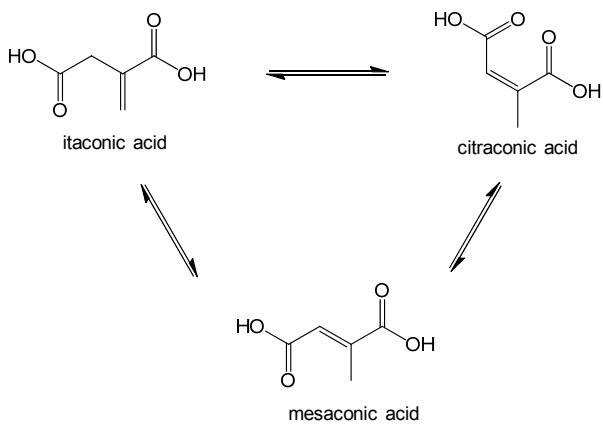

Scheme 12. Thermal isomerization-rearrangement equilibrium established between itaconic acid and its two isoforms citraconic and mesaconic acids.[124]

We have seen that limonene represents a rather important natural monoterpenic monomer for free-radical thiol–ene additions. Not only its pleasant fragrant odour may help neutralise the repellent scent characteristic of thiol–ene based formulations, but the two occurring double bonds are readily reactive with thiol compounds. Additionally, the cycloaliphatic ring structure conveys a certain

degree of rigidity to the final thermosets when compared to more regular aliphatic structures. In this context, it would be relevant to test the effect of this alicyclic structure within the networks in comparison to the simple aromatic structure of benzene (*e.g.*, 1,4-divinylbenzene) and evaluate the relative degree of variation. Moreover, the possibility to combine limonene with vast array of different multifunctional thiol structures represents a convenient future strategy worth exploring to improve the T_g of these final thermosets while enabling them to be tailored for a range of applications of potential commercial significance. Finally, in addition to being abundant and inexpensive, *D*-limonene can also be obtained practically in stereochemically pure form from orange peel oil, and it has been demonstrated that the thiol–ene addition process generates preferentially coupled products consisting of a mixture of four distinct diastereomers of a total of eight that are possible.[76, 77] The introduction of multi-chirality *via* thiol–ene coupling enables the ensuing crosslinked materials to be used in asymmetric catalysis, chiral purification, non-linear optics and even as conducting materials, which further expands the range of possible applications of these organic thermosets outside the field of coating technology.[125]

7 Acknowledgements

My doctoral research has been a scientific journey which has taken me through many fields of chemical science, including: polymer chemistry, radical chemistry, enzymatic biocatalysis, photochemistry, reaction kinetics, physical chemistry, green chemistry, analytical and instrumental chemistry, organic synthesis, and photopolymerization; and the present work would not have been materialized without the guidance and assistance from many people.

First of all I would like to express my deepest gratitude to my main supervisor Professor Mats Johansson and co-supervisor Professor Mats Jonsson for accepting me as a PhD-student at the Division of Coating Technology of KTH, for giving me the necessary time to learn, the freedom to make mistakes and the oriented supervision not to repeat them again as well as the autonomy to test my own sometimes 'fruitless' theories and ideas. Your advisory efforts and patience in dealing with my questions have been nothing short than extraordinary. Thank you both for trusting and believing in my potentialities, for the excellent scientific guidance, support, encouragement and dignifying example over these five incredible years which has left a profound mark inside me. I have learnt so much from you! I grew both as a person and as scientist having the honour of having you as my mentors. – Hope I was a good disciple!

I am also very grateful to the Swedish Research Council (VR) for providing financial support of this project.

Professor Anders Hult, Professor Eva Malmström, Professor Mats Johansson, Associate Professor Michael Malkoch, Associate Professor Anna Carlmark Malkoch and Dr. Linda Fogelström are gratefully acknowledged for promoting an outstanding and highly stimulating research environment within the coatings group where students are encouraged to develop their own initiative, creativity and self-confidence as scientists and discuss their projects as whole without barriers or limitations. A dedicated word of acknowledgement goes to Professor Eva Malmström for recruiting me to KTH under the 'BioMaDe' project, although nearly close to its end, and for introducing me to the extraordinary world of Polymer Science. A deepest Thank You for this Eva! All members of the 'BioPol' group, including Prof. Mats Martinelle, Prof. Karl Hult, Prof. Eva Malmström, Prof. Mats Johansson, Dr. Stacy M. Trey, Dr. Linda Fogelström, PhD-student Peter Hendil-Forssell, PhD-student Stefan Semlitsch, PhD-student Susana Torron Timhagen and Maja Finnveden are gratefully acknowledged for the motivating and brainstorming meetings where biochemistry meets polymer science. Inger Lord is thanked for all the help with the administrative tasks and practical issues in the division. I would also like to thank Sonny Jönsson for the helpful discussions and excellent knowledge regarding photochemistry and photopolymerizations. I also very much appreciate the help from Professor Minna Hakkarainen

for proofreading my thesis.

I thank all members of the Department of Fibre and Polymer Technology, in special to my 'Ytgruppen' friends, colleagues and office-roommates (former and present) for creating such a nice and pleasant workplace atmosphere; for all the parties, conference trips together, the funny 'gris' soccer kicks after lunch, 'fika' breaks, long beer rounds every Friday afternoon, the fun, the talks, and for all the great joyful and funny moments spent in and outside the laboratory. Thank you: Camilla Nilsson, Hanna Lönnberg, Daniel Nyström, Emma Östmark, Per Antoni ('Pelle'), Katarina Johansson ('Kattis'), Lina Erixon, Axel Nordberg, Magnus Jonsson, Helena Bergenudd, Stacy M. Trey, Linda Fogelström, Pontus Lundberg, Petra Nordqvist, Maribel Montañez, Robert Westlund, Niklas Nordgren, Yvonne Hed, Marie V. Walter, Sara Olsson, Sara Khosravi, Ting Yang, Susanne Hansson, Alireza Salehi, Markus Willgert, Carl Bruce, Emelie Norström, Christian Porsch, Emma Larsson, Hui Long, Kim Öberg, Linn Carlsson, Kristina Olofsson, Martin Wåhlander, Surinthra Mongkhontreerat ('Janne'), Eric J. Johansson Salazar-Sandoval, Assya Boujemaoui, Carmen Cobo Sanchez, Oliver Andrén, Susana Torron Timhagen, Viktor Granskog, Daniel Hult, Jonas Bengtsson, Vilhelm Olsson and Samuel Pendergraph. You are the best! Every single one of you has become a significant part of my life and it has been a true privilege for me to be with you throughout these five wonderful years.

A sincere thank you to Dr. Stacy M. Trey, for always being so optimistic and supporting, for all your friendship, fruitful discussions and collaboration which resulted in significant contributions to **Paper II**, and for all the help and assistance you gave me in the beginning when I just arrived into the group.

Marcus Jawerth and Jeanne-Marie Mathevet are gratefully acknowledged for the extra help with some time-consuming experiments in which results are integrant part of this thesis.

Dr. Alireza Salehi is gratefully acknowledged for sharing with me the responsibility on the FT-IR/Raman instrument and for being a great friend. Thank you for everything!

Huge thanks to my exceptional family, especially my parents, Eduardo and Mariana, who have always supported my desire to pursue a higher degree education, and have coped well with losing their son to Sweden.

Last but not least, I am particularly grateful to my beloved wife, Leila, for all your love, never-ending support and kindness and for always staying by me in every aspect of my life.

Stockholm, 29th of August, 2013
Mauro Claudino

8 References

1. *PlasticsEurope - Association of Plastics Manufacturers, Plastics - the facts 2012: An analysis of European plastics production, demand and waste data for 2011*, 2012.
2. M. A. R. Meier, J. O. Metzger and U. S. Schubert, *Chemical Society Reviews*, 2007, **36**, 1788-1802.
3. P. Anastas and N. Eghbali, *Chemical Society Reviews*, 2010, **39**, 301-312.
4. C. H. Hare, ed., *Protective Coatings: Fundamentals of Chemistry and Composition*, Technology Publishing Company, 1998.
5. M. P. Stevens, *Polymer Chemistry*, Oxford University Press, New York, 1999.
6. D. Hosler, S. L. Burkett and M. J. Tarkanian, *Science*, 1999, **284**, 1988-1991.
7. A. J. Stone, *Ancient Mesoamerica*, 2002, **13**, 21-39.
8. T. Posner, *Ber. Dtsch. Chem. Ges.*, 1905, **38**, 646-657.
9. J. V. Braun and R. Murjahn, *Chem Ber*, 1926, **59**, 1202-1209.
10. M. S. Kharasch, A. T. Read and F. R. Mayo, *Chem. and Ind.*, 1938, 752.
11. K. Griesbaum, *Angewandte Chemie, International Edition in English*, 1970, **9**, 273-287.
12. A. F. Jacobine, *Thiol-ene photopolymers*, Elsevier, London, 1993.
13. C. Chatgilialoglu, M. P. Bertrand and C. Ferreri, *S-Centered Radicals*, 1999, 311-354.
14. C. E. Hoyle, A. B. Lowe and C. N. Bowman, *Chem Soc Rev*, 2010, **39**, 1355-1387.
15. A. J. D. Magenau, J. W. Chan, C. E. Hoyle and R. F. Storey, *Polym. Chem.*, 2010, **1**, 831-833.
16. C. E. Hoyle, T. Y. Lee and T. Roper, *Journal of Polymer Science Part A: Polymer Chemistry*, 2004, **42**, 5301-5338.
17. U. Biermann, W. Butte, R. Koch, P. A. Fokou, O. Tueruenc, M. A. R. Meier and J. O. Metzger, *Chemistry - A European Journal*, 2012, **18**, 8201-8207, S8201/8201-S8201/8227.
18. C. E. Hoyle and C. N. Bowman, *Angew Chem Int Ed Engl*, 2010, **49**, 1540-1573.
19. A. Gress, A. Voelkel and H. Schlaad, *Macromolecules*, 2007, **40**, 7928-7933.

20. A. Gress and H. Schlaad, *Polym. Prepr. (Am. Chem. Soc., Div. Polym. Chem.)*, 2008, **49**, 230-231.

21. K. L. Killops, L. M. Campos and C. J. Hawker, *J. Am. Chem. Soc.*, 2008, **130**, 5062-5064.

22. M. J. Kade, D. J. Burke and C. J. Hawker, *J. Polym. Sci., Part A Polym. Chem.*, 2010, **48**, 743-750.

23. O. Tueruenc and M. A. R. Meier, *European Journal of Lipid Science and Technology*, 2013, **115**, 41-54.

24. J. Fossey, D. Leffort and J. Sorba, *Free Radicals in Organic Chemistry*, John Wiley & Sons, 1995.

25. C. Chatgilialoglu, *Helv. Chim. Acta*, 2006, **89**, 2387-2398.

26. M. A. Cole, K. C. Jankousky and C. N. Bowman, *Polymer Chemistry*, 2013, **4**, 1167-1175.

27. A. F. Parsons, *An Introduction to Free Radical Chemistry*, Blackwell Science, 2000.

28. T. M. Roper, C. A. Guymon, E. S. Jönsson and C. E. Hoyle, *Journal of Polymer Science Part A: Polymer Chemistry*, 2004, **42**, 6283-6298.

29. B. H. Northrop and R. N. Coffey, *J. Am. Chem. Soc.*, 2012, **134**, 13804-13817.

30. T. F. Scott, C. J. Kloxin, R. B. Draughon and C. N. Bowman, *Macromolecules*, 2008, **41**, 2987-2989.

31. N. B. Cramer, T. Davies, A. K. O'Brien and C. N. Bowman, *Macromolecules*, 2003, **36**, 4631-4636.

32. N. B. Cramer, S. K. Reddy, A. K. O'Brien and C. N. Bowman, *Macromolecules*, 2003, **36**, 7964-7969.

33. L. Lecamp, F. Houllier, B. Youssef and C. Bunel, *Polymer*, 2001, **42**, 2727-2736.

34. N. B. Cramer and C. N. Bowman, *Journal of Polymer Science Part A: Polymer Chemistry*, 2001, **39**, 3311-3319.

35. O. Okay and C. N. Bowman, *Macromolecular Theory and Simulations*, 2005, **14**, 267-277.

36. S. K. Reddy, N. B. Cramer and C. N. Bowman, *Macromolecules*, 2006, **39**, 3673-3680.

37. S. K. Reddy, N. B. Cramer and C. N. Bowman, *Macromolecules*, 2006, **39**, 3681-3687.

38. S. K. Reddy, O. Okay and C. N. Bowman, *Macromolecules*, 2006, **39**, 8832-8843.

39. C. Chatgilialoglu, A. Altieri and H. Fischer, *Journal of the American Chemical Society*, 2002, **124**, 12816-12823.

40. M. Desroches, S. Caillol, R. Auvergne and B. Boutevin, *European Journal of Lipid Science and Technology*, 2012, **114**, 84-91.

41. M. Stemmelen, F. Pessel, V. Lapinte, S. Caillol, J. P. Habas and J. J. Robin, *Journal of Polymer Science, Part A: Polymer Chemistry*, 2011, **49**, 2434-2444.

42. B. M. Abdullah and J. Salimon, *Journal of Applied Sciences*, 2010, **10**, 1545-1553.

43. P.-P. Jiang, M. Chen, Y.-M. Dong, Y. Lu, X. Ye and W.-J. Zhang, *Journal of the American Oil Chemists' Society*, 2010, **87**, 83-91.

44. P. Zhang and J. Zhang, *Green Chemistry*, 2013, **15**, 641-645.

45. D. W. Janes, K. Shanmuganathan, D. Y. Chou and C. J. Ellison, *ACS Macro Lett.*, 2012, **1**, 1138-1142.

46. A. Rybak and M. A. R. Meier, *Green Chemistry*, 2007, **9**, 1356-1361.

47. Z. S. Petrovic, W. Zhang and I. Javni, *Biomacromolecules*, 2005, **6**, 713-719.

48. C. Chatgilialoglu, A. Samadi, M. Guerra and H. Fischer, *Chemphyschem*, 2005, **6**, 286-291.

49. C. Walling and W. Helmreich, *J. Am. Chem. Soc.*, 1959, **81**, 1144-1148.

50. C. Chatgilialoglu, L. Zambonin, A. Altieri, C. Ferreri, Q. G. Mulazzani and L. Landi, *Free Radical Biology & Medicine*, 2002, **33**, 1681-1692.

51. D. S. Sgoutas and F. A. Kummerow, *Lipids*, 1969, **4**, 283-287.

52. T. M. Roper, T. Y. Lee, C. A. Guymon and C. E. Hoyle, *Macromolecules*, 2005, **38**, 10109-10116.

53. C. Ferreri and C. Chatgilialoglu, *Chembiochem*, 2005, **6**, 1722-1734.

54. C. Chatgilialoglu, M. Ballestri, C. Ferreri and D. Vecchi, *Journal of Organic Chemistry*, 1995, **60**, 3826-3831.

55. C. Chatgilialoglu and C. Ferreri, *Accounts of Chemical Research*, 2005, **38**, 441-448.

56. C. Ferreri, M. Panagiotaki and C. Chatgilialoglu, *Molecular Biotechnology*, 2007, **37**, 19-25.

57. F. Miccichè, PhD Thesis, Eindhoven University of Technology, 2005. http://repository.tue.nl/595390.

58. S. J. F. Erich, PhD Thesis, Eindhoven University of Technology, 2006. http://repository.tue.nl/608982.

59. G. Odian, *Principles of Polymerization*, John Wiley & Sons, Inc., Hoboken, N.J., 2004.

60. K. D. Belfield and J. V. Crivello, *Photoinitiated Polymerization*, American Chemical Society (ACS) Distributed by Oxford University Press, 2003.

61. A. K. O'Brien, N. B. Cramer and C. N. Bowman, *J. Polym. Sci., Part A Polym. Chem.*, 2006, **44**, 2007-2014.

62. N. B. Cramer, S. K. Reddy, M. Cole, C. Hoyle and C. N. Bowman, *J. Polym. Sci., Part A Polym. Chem.*, 2004, **42**, 5817-5826.

63. N. A. Rosenthal and G. Oster, *J. Am. Chem. Soc.*, 1961, **83**, 4445-4448.

64. J. Shin, S. Nazarenko and C. E. Hoyle, *Macromolecules*, 2008, **41**, 6741-6746.

65. P. T. Anastas and E. S. Beach, *Green Chemistry Letters and Reviews*, 2007, **1**, 9-24.

66. V. Dichiarante, D. Ravelli and A. Albini, *Green Chemistry Letters and Reviews*, 2010, **3**, 105-113.

67. I. Rico-Lattes, E. Perez, S. Franceschi-Messant and A. Lattes, *Comptes Rendus Chimie*, 2011, **14**, 700-715.

68. M. A. R. Meier, J. O. Metzger and U. S. Schubert, *Chem Soc Rev*, 2007, **36**, 1788.

69. L. Montero de Espinosa and M. A. R. Meier, *European Polymer Journal*, 2011, **47**, 837-852.

70. M. N. Belgacem, A. Gandini and Editors, *Monomers, Polymers and Composites from Renewable Resources*, 2008.

71. M. Black and J. W. Rawlins, *European Polymer Journal*, 2009, **45**, 1433-1441.

72. I. van der Meulen, M. de Geus, H. Antheunis, R. Deumens, E. A. J. Joosten, C. E. Koning and A. Heise, *Biomacromolecules*, 2008, **9**, 3404-3410.

73. Z. Ates, P. D. Thornton and A. Heise, *Polymer Chemistry*, 2011, **2**, 309-312.

74. I. van der Meulen, Y. Li, R. Deumens, E. A. J. Joosten, C. E. Koning and A. Heise, *Biomacromolecules*, 2011, **12**, 837-843.

75. O. Tueruenc, L. Montero de Espinosa, M. Firdaus and M. A. R. Meier, *Polymer Preprints (ACS, Division of Polymer Chemistry)*, 2010, **51**, 724-725.

76. M. Firdaus, L. Montero de Espinosa and M. A. R. Meier, *Macromolecules*, 2011, **44**, 7253-7262.

77. M. Firdaus and M. A. R. Meier, *Green Chem.*, 2013, **15**, 370-380.

78. C. Vilela, L. Cruciani, A. J. D. Silvestre and A. Gandini, *RSC Advances*, 2012, **2**, 2966-2974.

79. P. A. Wilbon, F. Chu and C. Tang, *Macromolecular Rapid Communications*, 2013, **34**, 8-37.

80. J. Zhao and H. Schlaad, *Advances in Polymer Science*, 2013, **253**, 151-190.

81. K. Yao and C. Tang, *Macromolecules*, 2013, **46**, 1689-1712.

82. http://www.gepasi.org/.

83. http://www.copasi.org/tiki-view_articles.php.

84. P. Mendes, *Computer applications in the biosciences : CABIOS*, 1993, **9**, 563-571.

85. P. Mendes, *Trends in Biochemical Sciences*, 1997, **22**, 361-363.

86. P. Mendes, *GEPASI, ver. 3.30*, The University of Walles, Aberystwyth, UK., 2002.

87. L. A. H. Petzold, *LSODA (Livermore Solver of Ordinary Differential Equations)*, Livermore, CA, 1997.

88. S. Hoops, S. Sahle, R. Gauges, C. Lee, J. Pahle, N. Simus, M. Singhal, L. Xu, P. Mendes and U. Kummer, *Bioinformatics*, 2006, **22**, 3067-3074.

89. P. Mendes, S. Hoops, S. Sahle, R. Gauges, J. Dada and U. Kummer, *Methods Mol. Biol.*, 2009, **500**, 17-59.

90. J. Samuelsson, M. Jonsson, T. Brinck and M. Johansson, *Journal of Polymer Science Part A: Polymer Chemistry*, 2004, **42**, 6346-6352.

91. J. Lalevee, X. Allonas, S. Jradi and J.-P. Fouassier, *Macromolecules*, 2006, **39**, 1872-1879.

92. T. Caceres, M. V. Encinas and E. A. Lissi, *Journal of Photochemistry*, 1984, **27**, 109-114.

93. N. S. Allen, P. N. Green and W. A. Green, *Eur. Polym. J.*, 1986, **22**, 49-56.

94. H. F. Gruber, *Prog. Polym. Sci.*, 1992, **17**, 953-1044.

95. J. Segurola, N. S. Allen, M. Edge, A. McMahon and S. Wilson, *Polymer Degradation and Stability*, 1999, **64**, 39-48.

96. J. Segurola, N. Allen, M. Edge and I. Roberts, *Polymer Degradation and Stability*, 1999, **65**, 153-160.

97. N. B. Cramer, S. K. Reddy, M. Cole, C. Hoyle and C. N. Bowman, *Journal of Polymer Science Part A: Polymer Chemistry*, 2004, **42**, 5817-5826.

98. T. M. Roper, T. Kwee, T. Y. Lee, C. A. Guymon and C. E. Hoyle, *Polymer*, 2004, **45**, 2921-2929.

99. T. M. Roper, C. A. Guymon, E. S. Joensson and C. E. Hoyle, *J. Polym. Sci., Part A Polym. Chem.*, 2004, **42**, 6283-6298.

100. J. Shin, H. Matsushima, C. M. Comer, C. N. Bowman and C. E. Hoyle, *Chemistry of Materials*, 2010, **22**, 2616-2625.

101. G. B. Bantchev, J. A. Kenar, G. Biresaw and M. G. Han, *Journal of Agricultural and Food Chemistry*, 2009, **57**, 1282-1290.

102. Z. Ates, P. D. Thornton and A. Heise, *Polymer Chemistry*, 2011, **2**, 309-312.

103. M. Desroches, S. Caillol, V. Lapinte, R. m. Auvergne and B. Boutevin, *Macromolecules*, 2011, **44**, 2489-2500.

104. C. Decker and T. Nguyen Thi Viet, *Macromol. Chem. Phys.*, 1999, **200**, 358-367.

105. C. Decker and T. N. T. Viet, *Macromol. Chem. Phys.*, 1999, **200**, 1965-1974.

106. C. Decker and T. N. T. Viet, *Journal of Applied Polymer Science*, 2000, **77**, 1902-1912.

107. C. Decker and T. N. T. Viet, *Polymer*, 2000, **41**, 3905-3912.

108. I. van der Meulen, Y. Li, R. Deumens, E. A. Joosten, C. E. Koning and A. Heise, *Biomacromolecules*, 2011, **12**, 837-843.

109. B.-S. Chiou, R. J. English and S. A. Khan, *Macromolecules*, 1996, **29**, 5368-5374.

110. B.-S. Chiou and S. A. Khan, *Macromolecules*, 1997, **30**, 7322-7328.

111. A. F. Jacobine, D. M. Glaser, P. J. Grabek, D. Mancini, M. Masterson, S. T. Nakos, M. A. Rakas and J. G. Woods, *Journal of Applied Polymer Science*, 1992, **45**, 471-483.

112. M. Johansson and A. Hult, *Journal of Polymer Science, Part A: Polymer Chemistry*, 1991, **29**, 1639-1644.

113. J. Fossey, D. Lefort and J. Sorba, eds., *Free Radicals in Organic Chemistry*, John Wiley & Sons Ltd, 1995.

114. F. M. Kerton and Editor, *Alternative solvents for green chemistry*, 2009.

115. R. A. Clara, A. C. Gomez Marigliano and H. N. Solimo, *Journal of Chemical & Engineering Data*, 2009, **54**, 1087-1090.

116. R. F. T. Stepto, *Polymer International*, 2010, **59**, 23-24.

117. C. Nilsson, E. Malmström, M. Johansson and S. M. Trey, *Journal of Polymer Science, Part A: Polymer Chemistry*, 2009, **47**, 5815-5826.

118. C. Nilsson, E. Malmström, M. Johansson and S. M. Trey, *Journal of Polymer Science, Part A: Polymer Chemistry*, 2009, **47**, 589-601.

119. C. Nilsson, PhD Thesis, KTH Royal Institute of Technology, 2008. http://kth.diva-portal.org/smash/record.jsf?searchId=1&pid=diva2:127775.

120. C. F. Carlborg, PhD Thesis, KTH Royal Institute of Technology, 2011. http://kth.diva-portal.org/smash/record.jsf?searchId=6&pid=diva2:437739.

121. J. Lange, PhD Thesis, KTH Royal Institute of Technology, 1995.

122. I. Carlsson, A. Harden, S. Lundmark, A. Manea, N. Rehnberg and L. Svensson, *ACS Symposium Series*, 2003, **847**, 65-75.

123. L. J. Molhoek, M. Skudlarek, S. Duyvestijn, H. Hogenkamp and C. Gehrels, Isomerization of Itaconic Acid During Direct Polycondensation, Roldduc Abey, The Netherlands, 2010.

124. M. Sakai, *Bulletin of the Chemical Society of Japan*, 1976, **49**, 219-223.

125. M. Firdaus, PhD Thesis, KIT Karlsruhe Institute of Technology, 2013. http://digbib.ubka.uni-karlsruhe.de/volltexte/1000034639.

126. B. J. Sparks, T. J. Kushera, M. J. Jungman, A. D. Richardson, D. A. Savin, S. Hait, J. Lichtenhan, M. F. Striegel and D. L. Patton, *Journal of Materials Chemistry*, 2012, **22**, 3817-3824.

Appendix

1. Mechanistic analysis

This section is devoted to the mathematical interpretation of the sequential reaction mechanism detailed in Table 6, in particular to what concerns the two propagation–chain-transfer routes (catalytic cycles **I** and **II**) which underlie and explain the two overall thiol–ene coupling reactions observed experimentally (Scheme 8). For simplification purposes it will be assumed that the consumption rates of reactive functional groups by initiation and radical termination rates are negligible relative to the individual rates of propagation and chain-transfer steps; *i.e.*, $R_i + R_t \ll r_{p1,2} + r_{CT1,2}$.

The aim is to derive a simplified analytic expression *via* a step-by-step sequential approach that relates both chain-transfer rate coefficients, $k_{RSH2,3}$, and the individual equilibrium coefficients, $K_{eq1,2} = k_{add1,2}/k_{elim1,2}$, in an effort to determine double bond selectivity by adopting the steady-state approximation. The '*actual*' rates of the forward and reverse reactions are assumed to obey the '*law of mass-action*' which stipulates that the rate at which a reaction takes place is directly proportional to the product of the concentrations of the reacting entities, raised to a power equal to the stoichiometric coefficient (also called molecularity), and must only be applied to the 'elementary' step reactions.

Starting by performing a general rate balance with respect to the intermediate β-thioether carbon-radical species, $[C^{\bullet}_{1,2}]_t$, gives:

$$\frac{d[C^{\bullet}_{1,2}]_t}{dt} = k_{add1,2}[RS^{\bullet}]_t[ene]_t - \left(k_{elim1,2} + k_{RSH2,3}[RSH]_t\right)[C^{\bullet}_{1,2}]_t \quad (1)$$

Under continuous UV-light irradiation the stationary-state condition (*i.e.*, when $R_i = R_t$, $r_{p1,2} = r_{CT1,2}$ and $d[ene]_t/d[RSH]_t = 1$) is reached in a relatively short time interval, where the following relations:

$$\frac{d[C^{\bullet}_{1,2}]_t}{dt} = 0 \text{ , or } [C^{\bullet}_{1,2}]_t = \text{constant} \quad (2a)$$

$$\frac{d[RS^{\bullet}]_t}{dt} = 0 \text{ , or } [RS^{\bullet}]_t = \left(\frac{R_i}{2k_t}\right)^{1/2} = \text{constant} \quad (2b)$$

hold over most of the course of the reaction. Therefore, in the steady-state regime, the concentrations of thiol and ene functional groups are equivalent throughout the reaction (*i.e.*, $[ene]_t/[RSH]_t = 1$). Applying the equality of eqn (2a) to eqn (1) and then solving with respect to $[C^{\bullet}_{1,2}]_t$, results in the following steady-state relationship:

$$[C^{\bullet}_{1,2}]_{ss} = \frac{k_{add1,2}[RS^{\bullet}]_t[ene]_t}{k_{elim1,2} + k_{RSH2,3}[RSH]_t} \quad (3)$$

The denominator of eqn (3) characterizes how the consumption of the two intermediary carbon-centered radicals is competitively distributed along the two coupling cycles *via* the corresponding propagation and chain-transfer steps. Therefore, the magnitude of the first-order kinetic parameters with respect to β-fragmentation ($k_{elim1,2}$, in s^{-1}) and hydrogen-abstraction ($k_{RSH2,3}[RSH]_t$, in s^{-1}) indicate which elementary step contributes mostly for the overall propagation–chain-transfer kinetics and define the relative reactivity of the two unsaturations. Considering the two possible limiting cases applied to eqn (3); *i.e.*, when:

1. $k_{elim1,2} \gg k_{RSH2,3}[RSH]_t \Rightarrow \dfrac{[C^{\bullet}_{1,2}]_t}{[RS^{\bullet}]_t} \approx K_{eq1,2}[ene]_t$

and the relative amount of intermediate radical species is essentially proportional to the concentration of ene which decreases as the reaction proceeds since $[ene]_t$ also decreases with reaction time. Contrarily, when elimination of the intermediate carbon radicals by β-cleavage is considered negligible compared to the corresponding chain-transfer parameters:

2. $k_{\mathrm{elim1,2}} \ll k_{\mathrm{RSH2,3}}[\mathrm{RSH}]_t \;\Rightarrow\; \dfrac{[\mathrm{C}^{\bullet}_{1,2}]_t}{[\mathrm{RS}^{\bullet}]_t} \approx \dfrac{k_{\mathrm{add1,2}}}{k_{\mathrm{RSH2,3}}}$

and the relative amount of intermediate radical species is essentially controlled by the propagation-*to*-chain-transfer ratio, $k_{\mathrm{add1,2}}/k_{\mathrm{RSH2,3}}$ (referred here to as the *kinetic ratio*).

Under steady-state conditions both propagation and chain-transfer elementary steps occur at the same rates, which are also equal to the rates of the corresponding overall reactions, since the rate of thiyl radical production by initiation is exactly counterbalanced by its bimolecular self-termination rate. Therefore, the rate of consumption of each alkene functional group remains essentially identical to the production rate of its corresponding mono-addition product:

$$-\frac{d[ene]_t}{dt} = \frac{d[\mathrm{P}_{1,2}]_t}{dt} = k_{\mathrm{RSH2,3}}[\mathrm{C}^{\bullet}_{1,2}]_t[\mathrm{RSH}]_t \qquad (4)$$

Dividing the two individual chain-transfer rates, one obtains the desired double bond selectivity based on the mechanism, S_{m}:

$$\frac{d[exo]_t}{d[endo]_t} = \frac{k_{\mathrm{RSH2}}[\mathrm{C}^{\bullet}_1]_t}{k_{\mathrm{RSH3}}[\mathrm{C}^{\bullet}_2]_t} = S_{\mathrm{m}} \qquad (5)$$

Introducing eqn (3) into eqn (5) in place of each carbon-centered radical concentration and then knowing that $[exo]_0/[endo]_0 = 1$, as provided by $[exo]_0 + [endo]_0 = 2\times[\mathrm{Lim}]_0$, yields the final desired ratio:

$$\frac{d[exo]_t}{d[endo]_t} = \frac{k_{\mathrm{add1}}k_{\mathrm{RSH2}}\left(k_{\mathrm{elim2}} + k_{\mathrm{RSH3}}[\mathrm{RSH}]_t\right)}{k_{\mathrm{add2}}k_{\mathrm{RSH3}}\left(k_{\mathrm{elim1}} + k_{\mathrm{RSH2}}[\mathrm{RSH}]_t\right)} \qquad (6)$$

However, if one accounts in eqn (6) for the two previous extreme situations, the following boundary condition for the relative reactivity derived from the mechanism is obtained, for $k_{\mathrm{elim1,2}} \to 0$ (lower limit) or $k_{\mathrm{RSH2,3}}[\mathrm{RSH}]_t \to 0$ (upper limit):

$$\frac{k_{\mathrm{add1}}}{k_{\mathrm{add2}}} < \frac{d[exo]_t}{d[endo]_t} < \frac{K_{\mathrm{eq1}}k_{\mathrm{RSH2}}}{K_{\mathrm{eq2}}k_{\mathrm{RSH3}}} \qquad (7)$$

Equations (6) and (7) help identify the rate-determining step and indicate which elementary reaction (insertion, back-elimination or hydrogen-abstraction) contributes mostly for the relative double bond reactivity when evaluating distinct thiol–ene systems comprising different kinds of reactive enes ('non-homopolymerizable').

2. Overall kinetics from mechanism

In order to establish a relation between each cycle of elementary propagation/chain-transfer steps and the corresponding observed net coupling reactions, a general expression for the overall rate parameters, $k_{1,2}$, is derived from the kinetic equations describing the two coupling cycles, eqn (11).

The individual rates of propagation and chain-transfer are given by eqns (8) and (9), respectively:

$$r_{\mathrm{p1,2}} = -\frac{d[ene]_t}{dt} = k_{\mathrm{add1,2}}[\mathrm{RS}^{\bullet}]_t[ene]_t - k_{\mathrm{elim1,2}}[\mathrm{C}^{\bullet}_{1,2}]_t \qquad (8)$$

$$r_{\mathrm{CT1,2}} = -\frac{d[\mathrm{RSH}]_t}{dt} = \frac{d[\mathrm{P}_{1,2}]_t}{dt} = k_{\mathrm{RSH2,3}}[\mathrm{C}^{\bullet}_{1,2}]_t[\mathrm{RSH}]_t \qquad (9)$$

Substituting eqn (3) onto eqn (8) or eqn (9) gives the overall steady-state rate expression based on the mechanism:

$$r_{1,2} = \frac{k_{\mathrm{add1,2}}k_{\mathrm{RSH2,3}}}{k_{\mathrm{elim1,2}} + k_{\mathrm{RSH2,3}}[\mathrm{RSH}]_t}[\mathrm{RS}^{\bullet}]_t[ene]_t[\mathrm{RSH}]_t \qquad (10)$$

with the global kinetic parameter, $k_{1,2}$, defined as:

$$k_{1,2} = \frac{k_{\mathrm{add1,2}}k_{\mathrm{RSH2,3}}}{k_{\mathrm{elim1,2}} + k_{\mathrm{RSH2,3}}[\mathrm{RSH}]_t}[\mathrm{RS}^{\bullet}]_t \qquad (11)$$

Eqn (11) states that is not possible to determine the absolute values of the individual rate coefficients intrinsic to the propagation/chain-transfer mechanism based solely on observed kinetic results. In order to accomplish that, it is neces-

sary to break-down the mechanism experimentally and isolate the elementary reactions of the two individual addition/elimination and hydrogen-abstraction steps. However, depending on which type of ene is involved in the reaction, one can make reasonable simplifications in the expression. Again, if one accounts just for the two limiting cases above mentioned; then, considering that $k_{\mathrm{elim1,2}} \gg k_{\mathrm{RSH2,3}}[\mathrm{RSH}]_t$, one finds:

$$k_{1,2} \approx K_{\mathrm{eq1,2}} k_{\mathrm{RSH2,3}} [\mathrm{RS}^{\bullet}]_t \tag{12a}$$

and, considering that $k_{\mathrm{elim1,2}} \ll k_{\mathrm{RSH2,3}}[\mathrm{RSH}]_t$, then:

$$k_{1,2} \approx \frac{k_{\mathrm{add1,2}}}{[\mathrm{RSH}]_t} [\mathrm{RS}^{\bullet}]_t \tag{12b}$$

3. Observed kinetic dependences

In this section will be derived two homologous empirical rate expressions, given by eqn (18), that define the observed consumption of *exo* or *endo* double bonds by free-radical thiol–ene coupling under a starting co-reactant stoichiometry of 1:0.5 with respect to thiol–ene functional groups. Other kinetic dependences will also be described.

Invoking ideal stoichiometry (*i.e.*, thiol : ene of 1:0.5) and assuming only primary coupling at the two unsaturations leading just to formation of mono-addition products, then the following second-order mixed (AB-type) rate law is obtained for the consumption of limonene as a species:

$$r_{\mathrm{Lim}} = -\frac{d[\mathrm{Lim}]_t}{dt} = k_{\mathrm{obs}} [\mathrm{Lim}]_t [\mathrm{RSH}]_t \tag{13}$$

with, k_{obs}, regarded as a global operational bimolecular rate parameter. Due to the mutual consumption of limonene at each unsaturation and thiol functional groups (*i.e.*, $[\mathrm{Lim}]_t = [\mathrm{RSH}]_t$), eqn (13) is also valid for the consumption of reactive thiol groups (RSH). The analytical solution of eqn (13), obtained by integration of r_{Lim} with $[\mathrm{Lim}]_0 = [\mathrm{RSH}]_0$, yields the linear inverted model describing the time-depletion of limonene:

$$[\mathrm{Lim}]_t = \frac{[\mathrm{Lim}]_0}{1 + [\mathrm{Lim}]_0 k_{\mathrm{obs}} t} \tag{14}$$

and linearization of eqn (14) by means of eqn (15)

$$\frac{1}{[\mathrm{Lim}]_t} = k_{\mathrm{obs}} t + \frac{1}{[\mathrm{Lim}]_0} \tag{15}$$

allows the value of k_{obs} to be determined experimentally *via* linear regression by plotting the data reciprocally as: $1/[\mathrm{Lim}]_t$ *versus* time. Since the two distinct unsaturations in *D*-limonene exhibit intrinsically different reactivities towards thiol–ene addition, $m_{1,2}$ (with m_1 'for *exo*' $> m_2$ 'for *endo*'), then the *relative reactivity* of the two double bonds can be expressed in terms of a global *selectivity* parameter, S_{exp}, defined by the quotient of the two overall alkene consumption rates, $r_{1,2} = -d[ene]_t/dt$, in such a way that:

$$S_{\mathrm{exp}} = \frac{r_1}{r_2} = \frac{d[exo]_t}{d[endo]_t} = \frac{m_1}{m_2} = \text{constant} \tag{16}$$

The total rate of disappearance of co-reactants *via* selective thiol–ene coupling, r_{C}, is equal to the accumulation rate of one-to-one addition products, r_{P}, in accordance to the following relation:

$$r_{\mathrm{C}} = -r_{\mathrm{Lim}} = -(r_1 + r_2) = -r_{\mathrm{RSH}} = r_{\mathrm{P}} = r_{\mathrm{P1}} + r_{\mathrm{P2}} \tag{17}$$

with, $\mathrm{P}_{1,2}$ (P_1 and P_2) corresponding to the two mono-addition reaction products resulting from thiol–ene coupling at the *exo* and *endo* double bonds, respectively. Combining eqn (13) with eqns (16) and (17) derived from the observed kinetics, results the following experimental rate expression for the consumption of each alkene functional group ('*ene*' = *exo* or *endo*):

$$r_{1,2} = -\frac{d[ene]_t}{dt} = k_{1,2} [\mathrm{Lim}]_t^2 \tag{18}$$

with,

$$k_{1,2} = m_{1,2} k_{\mathrm{obs}} \tag{19}$$

$$m_1 = \frac{S_{exp}}{S_{exp}+1} = \frac{r_1}{r_C} \tag{20a}$$

$$m_2 = \frac{1}{S_{exp}+1} = \frac{r_2}{r_C} \tag{20b}$$

The two overall reaction parameters, $k_{1,2}$ (k_1 and k_2), represent sub-operational rate coefficients for the observed external (*exo*) and internal (*endo*) thiol–ene coupling routes, respectively. In the same manner, the empirical parameters, m_1 and m_2, denote individual fractions of k_{obs} assigned to each thiol–ene coupling route (*i.e.*, $m_1 + m_2 = 1$). Hence,

$$S_{exp} = \frac{k_1}{k_2} \tag{21}$$

Solving eqns (20a/b) with respect to the experimental selectivity, S_{exp}, yields the expression:

$$S_{exp} = -\frac{m_1}{m_1 - 1} = \frac{1}{m_2} - 1 \tag{22}$$

which states that the relative double bond reactivity for diolefinic substrates, such as limonene, can be obtained by knowing just m_1 or m_2 independently.

A close inspection to the first-order linear differential equation (18) indicates no exclusive explicit dependence on the dependent variable $[ene]_t$. However, substituting in the second member of eqn (18) by eqn (14) and then solving the resulting ordinary differential equation (ODE) subjected to the initial condition: $[\mathrm{Lim}]_t = [\mathrm{Lim}]_0$ at $t = 0$; one obtains the following analytical solution after integration:

$$[ene]_t = [ene]_0 - m_{1,2}[\mathrm{Lim}]_0 + \frac{m_{1,2}[\mathrm{Lim}]_0}{1 + [\mathrm{Lim}]_0 k_{obs} t} \tag{23}$$

Simplification of eqn (23) provides the general equation describing the consumption profiles of each alkene functional group:

$$[ene]_t = [ene]_0 - m_{1,2}\Delta[\mathrm{Lim}] \tag{24}$$

with $\Delta[\mathrm{Lim}] = [\mathrm{Lim}]_0 - [\mathrm{Lim}]_t$. Rearranging eqn (24) by making

$$\frac{[ene]_0 - [ene]_t}{[\mathrm{Lim}]_0 - [\mathrm{Lim}]_t} = \frac{\Delta[ene]}{\Delta[\mathrm{Lim}]} = m_{1,2} \tag{25a}$$

enables extraction of the values of $m_{1,2}$ by plotting the discontinuous data points measured experimentally in the form: $\Delta[ene]$ *versus* $\Delta[\mathrm{Lim}]$; and then fitting a straight line to the data *via* linear regression. Consequently, the continuous lines afford:

$$\lim_{\Delta \to 0} \frac{\Delta[ene]}{\Delta[\mathrm{Lim}]} = \frac{d[ene]_t}{d[\mathrm{Lim}]_t} = m_{1,2} \tag{25b}$$

The evolution of each alkene functional group concentration can also be described by the general eqn (26) resulting from the initial composition stoichiometry and disregarding any secondary coupling reactions:

$$[exo]_t + [endo]_t = [\mathrm{Lim}]_0 + [\mathrm{Lim}]_t \tag{26}$$

Combining eqns (11) and (19) resulting from the mechanism and observed kinetics, respectively; results:

$$\frac{k_{add1,2} k_{RSH2,3}}{k_{elim1,2} + k_{RSH2,3}[\mathrm{RSH}]_t} \left(\frac{R_i}{2k_t} \right)^{1/2} = m_{1,2} k_{obs} \tag{27}$$

Therefore, for multi-substituted olefins showing highly reversible kinetic behaviour, as accounted in eqn (12a),

$$K_{eq1,2} k_{RSH2,3} \approx m_{1,2} k_{obs} \left(\frac{2k_t}{R_i} \right)^{1/2} \tag{28a}$$

and is not possible also to decouple the coefficients term located in the left hand side of eqn (28a) into its individual rate constants. However, for olefins exhibiting no or very low extents of reversibility in the propagation step, one can obtain a rough estimation of the maximum attainable value of $k_{add1,2}$, as described by the approximation implicit in eqn (28b):

$$k_{add1,2} \approx m_{1,2} k_{obs} [\mathrm{RSH}]_0 \left(\frac{2k_t}{R_i} \right)^{1/2} \tag{28b}$$

This expression is basically a rearranged form of eqn (12b) with steady-state concentration of thiyl radicals included (eqn (2b)). Even though $k_{\mathrm{add1,2}}$ in eqn (28b) is dependent on the concentration of thiol functional groups from the original expression (eqn (12b)), its 'apparent' value and order of magnitude can be calculated using the concentration of thiol at time zero, if $1 \leq [\mathrm{RSH}]_0 < 10\,\mathrm{M}$.

TRITA-CHE Report 2013:36
ISSN 1654-1081
ISBN 978-91-7501-845-4

www.kth.se